Preparation of Ag-Based Novel Adsorbents for Environmental Remediation

by

Yijun Xie

A thesis submitted in partial fulfillment of the requirements for the degree of

Master of Science

in

Materials Engineering

Department of Chemical and Materials Engineering
University of Alberta

Abstract

With the rapid development of industry, air and water pollution has become a critical topic to the public and scientific community since the quality of air and water is essential for the prosperity of life. In this study, two novel adsorbents, Fe_3O_4@polydopamine (PDA)-Ag microspheres and SBA-15-Ag composites, have been synthesized by facile wet chemical methods. Monodisperse Ag nanoparticles (NPs) are densely deposited on the surface of PDA layers and within the mesopores of SBA-15, respectively. High catalytic activity of Fe_3O_4@PDA-Ag on the reduction of methylene blue (MB) and effective removal of Hg^0 by SBA-15-Ag have been achieved mainly due to the presence of monosized Ag NPs. The capture of Hg^0 by Ag NPs is due to the amalgamation mechanism of Ag-Hg alloy. Fe_3O_4@PDA-Ag microspheres also exhibit high adsorption rate on MB because of the electrostatic interaction between PDA layer and MB molecules. More importantly, the as-prepared Fe_3O_4@PDA-Ag microspheres demonstrate excellent reusability and cyclic stability (>27 cycles), and the regeneration process could be completed within several minutes by using $NaBH_4$ as the desorption agent via a unique catalytic desorption process. The Fe_3O_4@PDA-Ag microspheres can be easily recycled from the solution by an external magnetic field, thanks to the good magnetic performance of Fe_3O_4 cores. In addition, the Fe_3O_4@PDA-Ag microspheres show good aqueous and acid stability in aqueous solution without significant change in morphology and performance for over half a year. The new adsorbents developed in this work show important potentials in practical applications for adsorption and catalysis.

Preface

Chapter 2 of this thesis has been published as Xie, Y.; Yan, B.; Xu, H.; Chen, J.; Liu, Q.; Deng, Y.; Zeng, H., "Highly Regenerable Mussel-Inspired Fe_3O_4@Polydopamine-Ag Core–Shell Microspheres as Catalyst and Adsorbent for Methylene Blue Removal." *ACS Appl. Mater. Interfaces* **2014**, *6*, 8845-8852.

Chapter 3 of this thesis has been submitted for publication as Xie, Y.; Yan, B.; Tian, C.; Liu, Y.; Liu, Q.; Zeng, H., "Efficient Removal of Elemental Mercury (Hg^0) by SBA-15-Ag Adsorbents." *Journal of Materials Chemistry A*.

For the work of these two chapters, I was responsible for the experimental design, data collection and analysis as well as the writing of manuscripts. Dr. B. Yan assisted with the revision of the manuscripts and response to reviewers. Dr. H. Xu provided some suggestions for manuscript revision. Dr. J. Chen contributed to the transmission electron microscopy images. Dr. Y. Deng was the collaborator who gave some information on polymer synthesis. C. Tian and Y. Liu assisted for the mercury capture test. Dr. Q. Liu and H. Zeng were the supervisory authors involved with relevant concept formation. Dr. H. Zeng was the corresponding author and involved with the experiments and manuscripts.

Acknowledgements

I would like to express my sincere gratitude to my supervisor, Dr. Hongbo Zeng, for his helpful guidance and tutor in my master study. I still remembered the many moments that he showed me how to design the experiments, interpret the results, and prepare the manuscript. He witnessed my growth from a rookie to an experienced young researcher. In addition to the research work, I also learn a lot from his modest personality, amazing communication skills and optimistic attitude towards life. Most importantly, it was him who inspired me to pursue my dream of becoming a researcher. I really appreciate his invaluable guidance in these two years.

I am also very grateful to my co-supervisor, Dr. Qingxia (Chad) Liu, for his support and guidance in this work. Dr. Liu has rich research and industry experience. His precise and rigorous attitude to academic research influences me a lot in my research work as well as my personality.

Many thanks go to all of my group members, particularly to the postdoctoral fellow, Dr. Bin Yan, for his valuable suggestions and help on my research project. His insightful ideas and excellent judgments greatly broaden my vision on research. I am also very thankful to Ms. Arlene Oatway for her help on transmission electron microscope (TEM), and I really enjoy myself in every "TEM time".

The financial support from the Natural Sciences and Engineering Research Council of Canada (NSERC) and the Helmholtz-Alberta Initiative – Energy & Environment (HAI-E&E) program are highly acknowledged. I also acknowledge Alberta Centre for Surface Engineering and Science (ACSES) and National Institute for Nanotechnology (NINT) for the materials characterization work.

Last but not least, I would like to thank my parents for their consistent support and understanding on my studies for so many years. Without their full support and understanding, I could not go that far.

Table of Contents

List of Tables

List of Figures

List of Symbols

C_e	The equilibrium concentration of adsorbed materials in the solution, mg/L
C_0	The initial concentration of MB, mg/L
C_t	The concentration of MB at time t, mg/L
I_0	The intensity of absorption peak at 665 nm of MB before adsorption by Fe_3O_4@PDA-Ag
I_t	The intensity of absorption peak at 665 nm of MB after adsorption by Fe_3O_4@PDA-Ag
k	The rate constant, s^{-1}
Ms	The saturation magnetization value, emu g^{-1}
P	The equilibrium pressure of adsorbates at the temperature of adsorption, Pa
P_0	The saturation pressure of adsorbates at the temperature of adsorption, Pa
q_e	The quantities of the materials adsorbed per unit mass of adsorbent, mg/g
t	The reaction time, s
$X\%$	The removal efficiency on MB
λ_{max}	The wavelength at maximum absorbance, nm

List of Abbreviations

AAS	Atomic absorption spectroscopy
AC	Activated carbon
AOP	Advanced oxidation process
APCD	Air pollution control devices
BAC	Bead activated carbon
BET	Brunauer-Emmett-Teller
BJH	Barrett-Joyner-Halenda
BOD	Biological oxygen demanding
Br-AC	Brominated carbon
BSE	Backscattered electron
CAAA	Clean Air Act Amendments
CAMR	Clean Air Mercury Rule
CNT	Carbon nanotubes
COD	Chemical oxygen demand
COW	Colemanite ore waste
CR	Congo red
CS-ESP	Cold-side electrostatic precipitator
CVAFS	Cold Vapour Atomic Fluorescence Spectrophotometer
EAC	Extruded activated carbon
EDX	Energy dispersive X-ray spectroscopy

EG	Ethylene glycol
EPA	Environmental Protection Agency
ESP	Electrostatic precipitator
FE-SEM	Field emission scanning electron microscope
FF	Fabric filter
FGD	Flue gas desulfurization
FT-IR	Fourier transform infrared
GAC	Granular activated carbon
GB	Gold beads
GO	Graphene oxide
HRTEM	High resolution TEM
HS-ESP	Hot-side electrostatic precipitator
IUPAC	International Union of Pure and Applied Chemistry
MB	Methylene blue
MO	Methyl orange
MWNT	Multi-walled nanotubes
NBD	Nanobeam electron diffraction pattern
NPs	Nanoparticles
PDA	Polydopamine
PS	Particulate scrubber
rGO	Reduced graphene oxide
RhB	Rhodamine B

SCR	Selective catalytic reduction
SDA	Spray dryer adsorber
SDS	Sodium dodecyl sulfate
SEM	Scanning electron microscope
SMA	Surfactant-modified alumina
SWNT	Single-walled nanotubes
TEM	Transmission electron microscope
UV	Ultraviolet
XPS	X-ray photoelectron spectroscopy
XRD	X-ray diffraction

Chapter 1 Introduction

1.1 Adsorbents for dye treatment

With the fast process of industrialization and urbanization, water pollution has become a serious problem to our health. A large number of large-scale industry factories such as printing, textile, paper, pharmaceutics, petroleum and chemical plants will release huge amounts of wastewater containing organic compounds.[1] Among them, organic synthetic dyes are one group of common organic pollutants which are widely used in prints, textile and paper industries.[2] The release of the dye wastewater will cause critical environmental issues, which needs to be treated immediately.

1.1.1 Brief introduction to organic dyes

Synthetic organic dyes, a group of industry products, are extensively used in many fields of industries, such as textile, leather tanning, paper, food technology, agriculture, hair coloring, etc.[1] It is estimated that over 100,000 commercially available dyes are produced with an approximate production of over 70,000 tonnes per year.[3] In 2010, Canada imported and exported dyes and pigments with the total value of $537 and $464 MM, respectively.[4] Some of the common organic dyes are listed in Figure 1.1, and these dyes can be classified as follows:[1, 3]

Table 1.1 The classification of organic dyes.

Type of dyes	Classifications	Examples
Anionic	Direct, acid, and reactive dyes	Congo red, methyl orange,
Cationic	Basic dyes	Methylene blue, Rhodamine B
Nonionic	Disperse	Sudan I, disperse orange 37

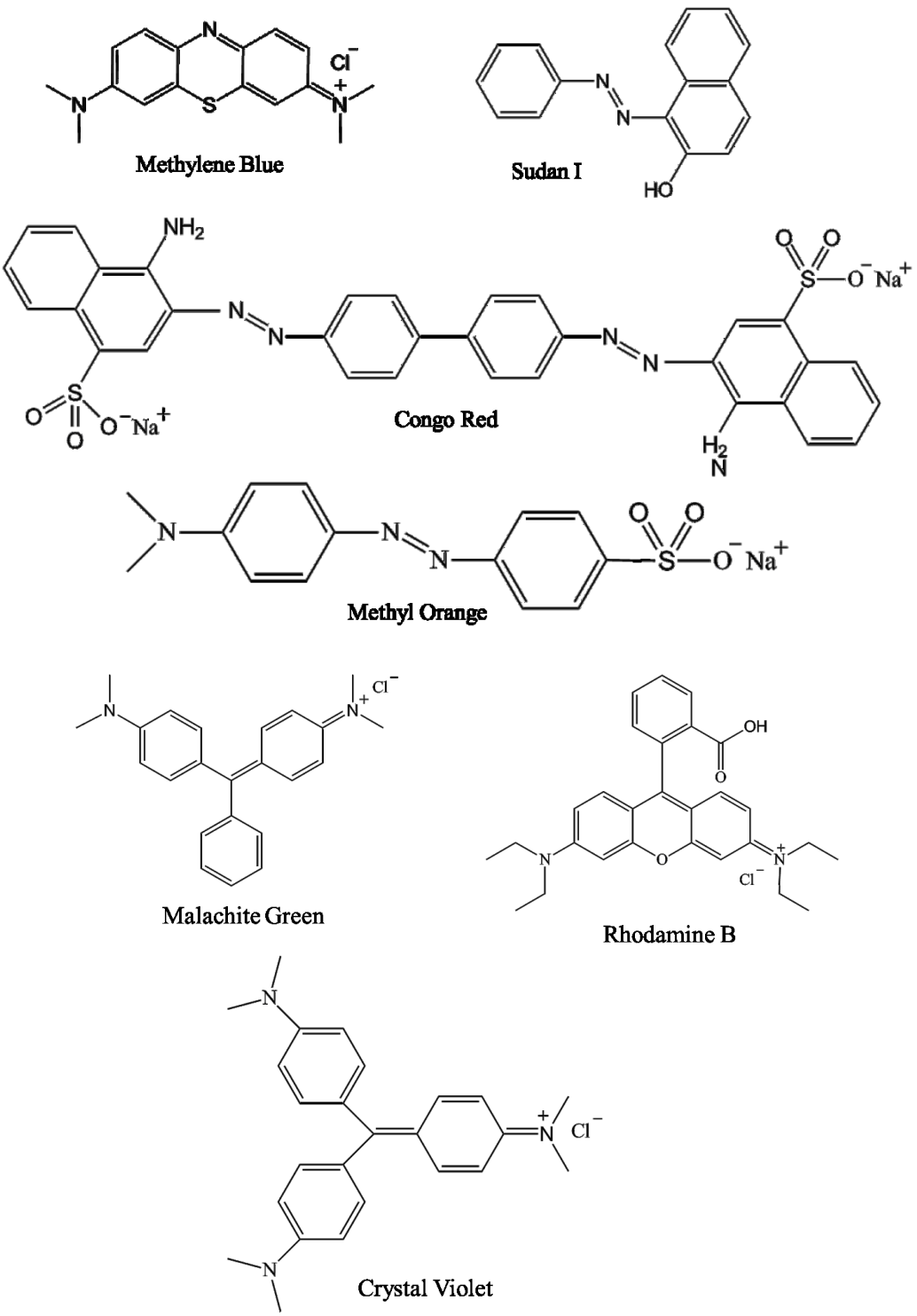

Figure 1.1 The chemical structure of common organic dyes.

Normally, dye molecules consist of two main components: the chromophores and the auxochromes.[5] The chromosphores are responsible for producing the specific color, most of which possess the azo groups or anthraquinone groups. The auxochromes are a group of atoms attached to the chromophores which can not only modify the ability of the chromophores to produce the light, but also improve the aqueous solubility of the dyes. The hydroxyl group (-OH), amino group ($-NH_2$), sulfonate group ($-SO_3^-$) and aldehyde group (-CHO) are examples of auxochromes.[6] The reductive cleavage of azo linkages should be responsible for the formation of toxic amines in the wastewater. Moreover, anthraquinone dyes are more resistant to degradation because of their stable aromatic structures and thus remain colored for a long period time in the wastewater.[1] All of these features make organic dyes with low biodegradability and hard for treatment.

Due to the low biodegradability of organic dyes, it has become a critical issue for environmental scientists to deal with water pollution caused by dye wastewater. Among the total production of organic dyes, it is reported that 10~15% of the used organic dyes are lost and have been released to water.[5, 7] In particular, large amounts of organic dyes has been consumed in textile, dyeing, cosmetic, paper, pharmaceutical, tannery and paint industries,[5] in other words, these industries are the main source of the effluents containing organic dyes with sufficient quantities. One reason why organic dyes are considered an important type of pollutant is that they are toxic to human being, and will cause severe human health disorders such as nausea, hemorrhage, irritation and ulceration of skin and eyes, mucous membranes.[5] For example, some metal complex organic dyes based on chromium will cause cancer; some azo dyes, such as benzidine-based direct dyes, tend to be reduced to colorless primary organic amines, which are more toxic compounds than their oxidized forms.[3, 8] Another reason to regard organic dyes as

major pollutants in water is that even trace concentrations of dyes in wastewater is highly visible, which affects aesthetic sense, interferes with the transmission of light to water, and influences the gas solubility in water bodies.[3, 5] Furthermore, the dyes in effluent will impede the photosynthetic activity of plants and cause microtoxicity to fish and other aquatic organisms.[5] Because of the reasons mentioned above, it is of significant importance to treat and degrade organic dyes in wastewater.

1.1.2 Current technologies for dye removal

Since the environmental consequences of dye wastewater have aroused the attention of the public, the scientists begin to take substantial measures to treat the dye wastewater during these years. Normally, the wastewater treatment process in industry consists of three steps as follows:[5]

(1) Pretreatment: The industrial wastewater is pretreated by equalization and neutralization before discharging to municipal or central sewerage systems.

(2) Primary and secondary treatment: The wastewater is directed for the removal of pollutants with the least effort. Suspended solids are eliminated by physical or chemical separation techniques and treated as concentrated solids. After the previous treatment, the wastewater is handled with the secondary treatment involving microbiological treatment, e.g. using bacteria to stabilize the waste component.

(3) Physical/chemical treatment: This process includes adsorption, chemical oxidation, chemical coagulation/flocculation, ozonation, stripping, ion exchange, irradiation, membrane separation, etc. Most of these treatment methods are more expensive than biological treatment, but they are useful for where biological treatments are ineffective.

(4) Sludge processing and disposal: The wastewater is treated with sludge processing and disposal as the final step.

Generally, the methodologies for dye wastewater treatment are classified in four categories: Physical, chemical, biological and acoustical, radiation, and electrical processes.[5] Some of the fundamental methodologies are briefly discussed in the following paragraphs:

(a) Sedimentation

Sedimentation is the basic form of primary treatment used in many municipal and industrial for dye wastewater treatment.[5] There are a lot of process options among the sedimentation process to improve the gravity settling of suspended particles in the dye wastewater, such as chemical flocculation, sedimentation basins, etc.

(b) Membrane Filtration

Membrane filtration is an integral component of drinking water and wastewater treatment system, and it could clarify, concentrate and continuously separate organic dyes from wastewater.[7] There are several types of membrane filtration processes: microfiltration, ultrafiltration and nanofiltration. Among them, microfiltration is not useful in some cases due to the large pore size of membrane, while ultrafiltration and nanofiltration processes are effective for removing almost all types of organic dyes,[8] and the reverse osmosis of the nanofiltration makes it possible to recover 97-99% of the water from the effluent streams.[7] Wu et al. reported two kinds of strong-acid cation exchange membranes for the removal of methyl violet 2B, and the membranes show good dye adsorption and desorption after three successive cycles.[9] However, the membrane filtration still suffers from some disadvantages including the clogging of the membrane pores by dye molecules, high working pressures, high cost for replacing the membrane, and disposal problems of highly concentrated residue after separation.[5, 10] Therefore, the membrane filtration technologies are suitable for water recycling with low concentration of dyes to avoid the clogging possibility and disposal problems.

(c) Coagulation/ flocculation

Coagulation/flocculation is one of the most popular methods for wastewater treatment.[11, 12] Coagulation is a complicated physical-chemical process involving a series of interactions. In general, the aluminum (Al^{3+}), calcium (Ca^{2+}), and ferric (Fe^{3+})-based salts are always used for coagulating agents to induce flocculation by forming hydroxide solids. The hydroxide solids can neutralize and adsorb particulate to achieve the removal of dyes. In addition, coagulation process would not decompose the dye compounds by chemical reactions, thus it leads to no potentially harmful or toxic products and is environmental friendly.[11] Furthermore, this process is economically feasible due to the low cost of coagulating agents, and can greatly improve the removal efficiency when combined with other techniques like adsorption.[13] However, the coagulation does not effectively remove the highly soluble, low molecular and based dyes. And the disposal of sludge produced during the coagulation process is another issue to restrict its further applications.[11]

(d) Chemical Oxidation

Chemical oxidation is a method to cleave the aromatic structure of organic dyes in effluent by oxidation with oxidizing agent. Actually the chemical oxidation is among the most commonly used technologies for dye removal due to the low quantities and high efficiency. Main oxidizing agents include hydrogen peroxide (H_2O_2), Fentons reagent (H_2O_2-Fe (II) salts), ozone, sodium hypochloride (NaOCl), chlorine, potassium permanganate ($KMnO_4$), etc.[5, 10] Some of the reagents need to be activated by ultraviolet (UV) light, for example, hydrogen peroxide. The ideal case is to reduce the organic dyes to CO_2 and H_2O, however, in most cases the oxidizing agents could only partially degrade the dyes to lower molecular weight species.[5] In addition, the

pH of the dye solution is also an important factor for the chemical oxidation. The following paragraphs will cover relevant contents of some common oxidizing agents.

Fentons reagent is a mixed solution of hydrogen peroxide and a Fe(II) catalyst that is used to treat wastewater which are resistant to conventional biological treatment.[14, 15] Fentons oxidation processes create highly reactive radical, hydroxyl radical (OH·), which is a very strong, nonselective oxidant and could oxidize almost all kinds of organic dyes.[15] Other advantages for Fentons oxidations are that the cost of Fentons oxidation is quite low, the operation is easy, and it is possible to work in a wide range of temperatures.[16, 17] The major disadvantages of this technology are narrow pH range of utilization (<3.5) and the sludge generation by the flocculation of the dye molecules and the unreacted Fentons reagent.[10, 18]

Ozonation is an effective water treatment process that is able to degrade many organic pollutants such as chlorinated hydrocarbons, phenols, and aromatic hydrocarbons through an infusion of ozone.[19, 20] Similar to the oxidation process of Fentons reagent, the ozone reacts with the organic dyes in wastewater by releasing the hydroxyl radical produced through the ozone decomposition in water or by molecular ozone itself.[19] Ozone molecule is a selective oxidizing agent and tends to attack the unsaturated bonds of organic dyes, thus the chromosphores groups with unsaturated bonds will be oxidized into smaller molecules. The reaction is very efficient. The major advantage of ozonation is the fast removal rate and does not generate extra residue or sludge. The disadvantage of onzonation is its short half-life, typically about 20 min.[10] Due to the short periods of half-life, continuous ozonation is needed and then the cost for actual applications is very high.

Sodium hypochloride (NaOCl) is another common oxidizing agent. Normally, it attacks at the amino group of the dyes by Cl^+. The generated Cl^+ initiates and accelerates the cleavage of

azo bridge.[14] In one study, Karaoğlu et al. employed UV, NaOCl and TiO_2/Sep Nanoparticles (NPs) for the photocatalytic degradation of Reactive Red 195.[21] Additionally, the decolorization rate is dependent of chlorine concentration and pH value of the dye solution. It should be mentioned that the chlorine based oxidizing agent should be restricted for utilization in the future for environmental reasons.[14]

(e) Advanced Oxidation Processes (AOPs)

Advanced oxidation processes are the processes that integrate several chemical oxidation processes together to treat the dye wastewater because a single oxidation process is not effective for the removal of dyes under different conditions. These chemical oxidation processes are always characterized with the similar chemical features including the production of hydroxyl radical (OH·) and superoxide anion (O_2^-).[22] The advantages of AOP are that they can degrade the organic dyes under ambient temperature and oxidize them directly to CO_2. Various kinds of AOP are applied for utilization such as H_2O_2-ozone, H_2O_2-UV, UV-ozone, TiO_2/ZnO photocatalysts, etc.

H_2O_2-UV radiation is using H_2O_2 as the oxidizing agent and activated by UV light at the same time. H_2O_2 and UV can react with organic dyes in aqueous solutions individually. When combined together, they could degrade the pollutants more effectively due to the strong oxidation effect of hydroxyl free radicals (OH·) generated *in situ*.[23] Some factors such as the concentration of H_2O_2, the intensity of UV irradiation, pH values, dye molecular structure will influence the removal performance of H_2O_2-UV. According to a previous report,[14] the removal is most effective at the optimal H_2O_2 concentration for different dye types, a neutral pH value (~7), high UV light intensity (1600 W). Acid dyes, reactive dyes, direct dyes as well as disperse dyes are very easy and quick to decolorize through using H_2O_2-UV radiation. The advantage of this

method is that it is the destructive method for pollution treatment and creates no sludge.[1, 23] However, it is not effective for decolorizing pigments because they tend to form a coating which is hard to remove and decompose.[14]

Photocatalysis is another effective method in AOP for dye wastewater treatment.[24, 25] The term "photocatalysis" involves the presence of photons and a photocatalyst. In the process of photocatalysis, the photocatalysts (e.g. TiO_2, ZnS, CdS, etc.) first adsorb the light radiation from the UV or visible light. Afterwards, the electrons from the valence band of the photocatalysts will be excited by the light energy to the conduction band, resulting in the production of hydroxyl radical (OH·). The as-formed hydroxyl radicals have extremely high oxidizing ability and could destruct the molecular structure of organic dyes. Various kinds of photocatalysts have been designed, such as TiO_2, ZnO, ZrO_2, CdS, ZnS and other semiconductors with the suitable band-gap energy, to treat the organic dyes in effluents. Among them, TiO_2 is one of the most widely used catalysts for water treatment due to its strong oxidizing ability, chemical stability and corrosion resistance.[26] Some recent work combined TiO_2 and magnetite together which can achieve high photocatalytic activity, fast separation and consistent recyclability. Wu et al. reported the magnetic iron oxides/TiO_2 hybrid NPs for methylene blue (MB) removal, and about 50% to 60% of MB was decomposed within 90 min illuminated under Hg lamp.[27] Linley et al. studied the novel TiO_2-magnetite rattle-type particles that achieved the complete removal of MB within approximately 5 min under UV light, which also could be recycled for 16 times.[28] In addition, modification of TiO_2 with noble metals (Ag, Pt, Au), transition metals, (Fe, Cu, V, Sr, Zn), and alkaline metals (Li, Na, K) can maximize its photocatalytic efficiency.[22] It was also shown that the photocatalytic degradation of dyes relied on many factors such as the chemical structure of dyes, pH values, concentration of catalysts, etc.[2] The main disadvantage of the

photocatalysis is that the particles of photocatalysts would be hard to separate from the wastewater if there were no integration of magnetic materials, thus result in clogging problems.

(f) Electrochemical Methods

Electrochemical method is a relatively new technology for dye removal which was developed in 1990s. In this process, the decolorization can be achieved by electro oxidation with a solid anode.[29] Gupta et al. reported that the electrochemical treatment of dyestuff using an iron cell achieved a significant reduction on chemical oxygen demand (COD) and color with high efficiency of 90%.[29] Oliveria et al. demonstrated a 100% decolorization of acid red 29 dye and 70% TOC reduction by using $Ti/Sn_{0.99}Ir_{0.01}O_2$ anode.[30] The decolorization or removal of organic dyes is strongly determined by the materials of anodes and applied potentials. This technology is very effective in decolorizing different kinds of dyes with great reduction of COD. However, the major drawback of this method is the high cost of the electricity.

(g) Ion Exchange

Ion exchange is a reversible exchange process that the ions from the aqueous solution are exchanged with the ions in the ion exchanger (polymeric or mineralic materials), which is very similar to the adsorption process in the applications of waste water treatment. Ion exchange has been widely used in the removal of organic dyes according to the previous reports.[9, 31, 32] Liu et al. studied the adsorption characteristics of two anionic reactive dyes by two types of commercial anion exchanger, strong basic (SB6407) and weak basic (DE81), and showed that strong basic ion exchanger demonstrated better adsorption capacity on the anionic dyes.[31] Wu et al. investigated the removal of basic dye, methyl violet 2B, by using two kinds of strong acid exchange membranes, ICE 450 and P81, and the results showed that P81 exhibited a greater adsorption capacity than ICE 450; the performance of both ion exchangers remained the same

during three cycles of test.[9] Although the ion exchange process could not destroy the molecular structure of organic dyes, it may provide the possibility to recover the dyes for reuse and the ion exchangers themselves can be regenerated for many times.

(h) Biological Treatment

The biological treatment is another common technology for dye removal. Generally the working conditions for biological treatment can be divided into aerobic and anaerobic conditions.[6] Bacteria and Fungi are two kinds of microorganism groups which can work under aerobic conditions. In the case of bacteria, the enzymes of aerobic bacteria could catalyze the process which includes the incorporation of oxygen from the air into the aromatic ring of organic dyes and then break down the aromatic structures.[6] Barragan et al. reported the bacteria inoculated on different solid media (kaolin, bentonite and powdered activated carbon) to attain the biodegradability of an azo dye, Acid Orange 7.[33] Their results show that the degradation of Acid Orange 7 can be facilitated by the presence of pore structures which promote the growth of aerobic microorganism, cleave the azo bond and oxidize the amine groups of Acid Orange 7. In the case of fungi strains, white-rot fungi strains, particularly for *Phanerochaete chrysosporium*, have been widely studied for decolorizing the dye wastewater.[10] This fungus strains are able to degrade many kinds of organic compounds such as dioxins, direct azo dyes, etc. Pazarlioglu et al. studied the biodegradation of nice different direct azo dyes by *Phanerochaete chrysosporium* and the results showed that it could achieve almost 100% decolorization of Direct Blue 15.[34] The advantage of this technology is that it is relatively inexpensive and the final degraded products are completely mineralized and nontoxic.[5] However, the bacteria and fungi treatments are only effective for some dyes, and many of them are hard for biological degradation under aerobic conditions.

The anaerobic treatment also reveals great potentials in dye removal due to the low redox potential (<-50 mV), which is advantageous for azo dyes reduction caused by the cleavage of azo bond.[6] Azo dye reduction can result from a biological process or a chemical reaction. In a study, Van der Zee et al. found that a combination of biotic processes and chemical reactions contributed to the reduction of two model azo dyes, Acid Orange 7 and Reactive Red 2; the presence of biotic processes is due to the enzymatic reactions while chemical reactions are stimulated by sulfide.[35] According to Delee et al.'s review, anaerobic treatment generates a smaller amount of sludge compared with aerobic treatment and no aeration is needed, providing the economic advantage of anaerobic treatment.[36] In addition, the high biological oxygen demanding (BOD) levels can be efficiently lowered down and high pH wastewater can be neutralized by including anaerobic treatment in the textile effluents treatment process according to Delee's report.[36] However, one problem for the anaerobic treatment is that it needs post-treatment process to remove the nutrients (e.g. N, P) and complete the mineralization of the pretreated dyes.

Table 1.2 Advantages and disadvantages of current technologies for the removal of organic dyes from industrial effluents

Technologies	Advantages	Disadvantages
Sedimentation	Economically available	Not effective for all dyes
Membrane filtration	Effective for most dyes	Clogging problems of dyes
Coagulation/flocculation	No harmful and toxic products	Disposal of sludge
Fentons reagent	Effective for most dyes and low cost for operation	Sludge generation
Ozonation	Fast, no sludge left	Short periods of half-life
NaOCl	Efficient for azo dyes	Not environmental friendly
H_2O_2-UV	No sludge regeneration	Not effective for pigments
Photocatalysis	Utilization of solar energy	Clogging by the particles
Electrochemical Methods	High COD reduction	High cost of electricity
Ion exchange	Recyclability	Relatively high cost
Bacteria	High COD reduction	Effective for certain dye for specific strains
Fungal strains	Completed mineralization of products	Not effective for many dyes
Anaerobic treatment	High BOD reduction	Needs post-treatment process

1.1.3 Common adsorbents for dye removal

It has long been identified that adsorption is one of the most widely used method for water treatment. According to Ali's review paper,[37] adsorption treatment has been widely used in the

removal of inorganic pollutants such as arsenic,[38] cadmium,[39] chromium,[40] cobalt,[41] copper,[42] selenium,[43] and organic pollutants such as organic dyes,[44-46] and hydrocarbons.[47, 48] Adsorption is a process that the adsorbed materials were accumulated on the surface of the solid adsorbents from liquid or gas phase. Generally, adsorption is basically dominated by two kinds of interactions: physical force or chemical bonding. If the interaction between the adsorbent and adsorbed materials is physical in nature, the adsorption is called physical adsorption (physisorption). Otherwise, if the interaction is based on the chemical bonding, it is called chemical adsorption (chemisorption). The physical adsorption is based on the van der Waals forces or electrostatic interactions, so the attraction between the adsorbent and adsorbed materials is relatively weak and the adsorption process is reversible. However, the chemical adsorption is very strong due to the high strength of the chemical bonding, so the adsorption process is irreversible and the materials is hard to desorb from the adsorbent under the room temperature, which will be shown in the following chapter.

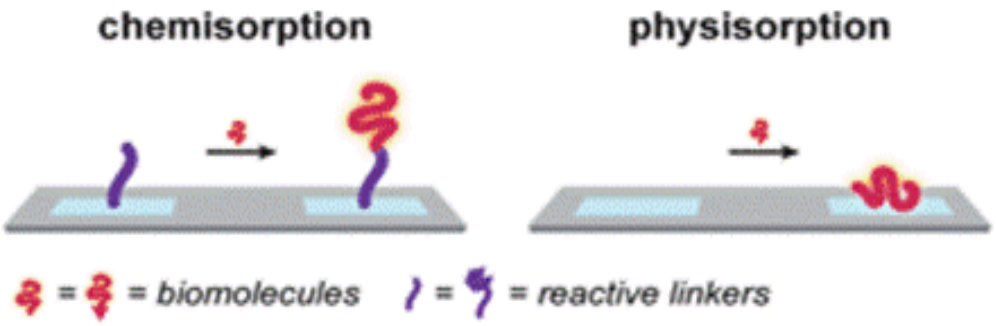

Figure 1.2 Schematics of chemisorption and physisorption.[49]

The adsorption performance of the adsorbent depends on several factors, such as the amount of adsorbent, the concentration of pollutant solution, pH value of the pollutant solution, temperature, contact time, etc. The adsorption process will finally reach equilibrium when the

concentration of pollutants in the solution keeps constant. The equilibrium curve of adsorption is called the adsorption isotherm, as is shown in Figure 1.3. The adsorption isotherms represent the relationship between the quantities of the pollutants adsorbed per unit mass of the adsorbent (q_e) and the concentration of pollutants in the solution (C_e) under constant temperature. There are some well-known models available to describe the adsorption isotherm of the adsorption results including Langmuir, Freundlich, Halsey, etc.[37] A good adsorbent should show either high adsorption capacity or short adsorption time, which requires elaborate design of adsorbent materials. Here are some common adsorbents for dye treatment.

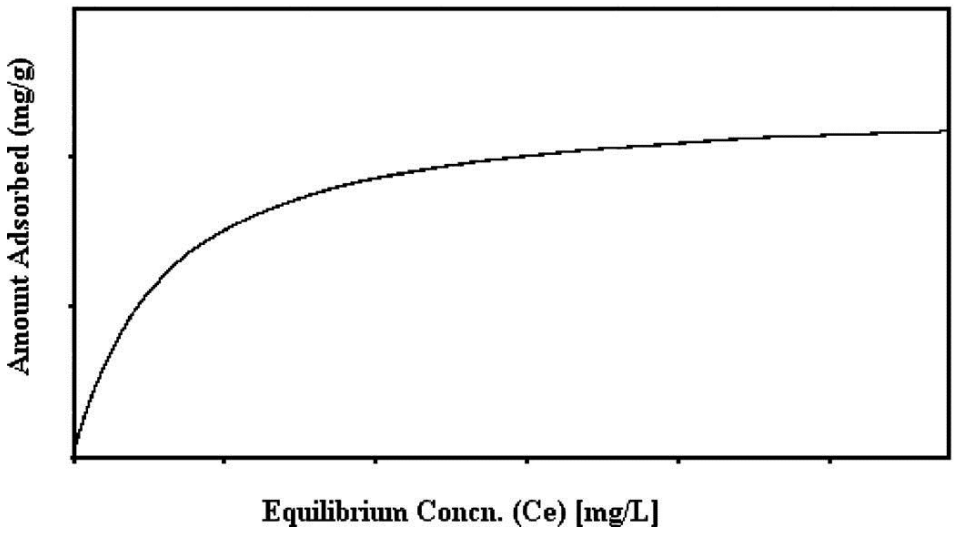

Figure 1.3 A typical example of an adsorption isotherm.[37]

(a) Metal nanoparticles (NPs)

It was reported that due to the high specific surface area and significant plasmon resonance, Ag NPs show great potentials in water treatment as efficient adsorbents and photocatalysts.[50] Yola et al. reported a facile preparation of Ag-Colemanite ore waste (COW) as adsorbents and photocatalysts to remove Reactive Yellow 86 and Reactive Red 2 in single and binary dye

solutions, and the results show that the dye solutions (100 mg L^{-1}) can be totally removed at pH 2 and Ag-COW reveals good photocatalytic activity for the degradation of two dyes under 4 cycles.[50]

(b) Metal oxides

i. Alumina and Aluminum trioxide NPs

Alumina is a synthetic porous crystalline gel with a high specific surface area of about 200 to 300 m^2/g.[5] The high specific surface area of alumina reveals the potentials to be the good adsorbent for organic dyes. Adak et al. studied a sort of surfactant-modified alumina (SMA), sodium dodecyl sulfate (SDS) modified alumina for the removal of crystal violet,[51] and it was found that SMA could remove ~99% of crystal violet in aqueous solutions even at a high concentration (200 mg L^{-1}). In another study of Adak et al., they applied a fixed bed column of SMA for the removal of crystal violet, and the SMA still shows high removal efficiency for the dye.[52] Besides alumina gel, aluminum trioxide NPs could also be a good adsorbent for dye treatment due to its high surface area, mechanical strength, high surface activity and low temperature modification.[53] Lan et al. studied hierarchical shell and hollow core structured γ-Al_2O_3 for the removal of congo red (CR) and methyl orange (MO).[54] The high specific surface area (320.6 m^2/g) of hollow structured γ-Al_2O_3 enabled the as-prepared γ-Al_2O_3 to exhibit excellent adsorption on CR with a high capacity of 835.0 mg/g.

ii. Magnesium oxide

MgO is a good candidate for adsorbent materials because it is both nontoxic and economical. Recently, there are many reports on the synthesis of MgO with high specific surface area and their applications on water treatment. For example, Tian's group reported a facile and scaled-up to synthesize porous hierarchical MgO which exhibited the very high adsorption capacity of CR

(2400 mg/g).[55] Ai et al. developed the mesoporous MgO with sacrificial template method and the as-prepared hierarchical MgO also showed great adsorption capacity (689.7 mg/g) and high adsorption rate over CR.[56] Haldorai et al. presented a multi-functional MgO immobilized chitosan composite by chemical precipitation method for the efficient removal of MO; furthermore, the same materials also display the antibacterial efficacy of 93% within 24h against a kind of bacteria, *Escherichia coli*.[57] All of these reports reveal the good potentials of hierarchical structured MgO in the applications of dye wastewater treatment.

iii. Iron oxide

Iron oxides and hydroxyl iron oxides (α-FeOOH, β-FeOOH) are always chosen as new adsorbents for dye removal due to their low cost. To improve their adsorption capacity on dyes, researchers try to modify their morphology to reach higher adsorption capacity. Zhong's group synthesized a uniform, self-assembled, 3D flowerlike structured iron oxide for Orange II removal.[58] The as-obtained α-Fe_2O_3 could remove most of Orange II with the adsorption capacity of 43.5 mg/g. In addition, the α-Fe_2O_3 could be converted to magnetic γ-Fe_2O_3 and Fe_3O_4 by a simple calcination process. The magnetic properties of these materials enable them to be easily separated via an external magnetic field. Zhu et al. reported a template-free method to obtain hierarchical flower-like α-Fe_2O_3 for the removal of CR with a high adsorption capacity of 195 mg/g.[59] In another study of α-FeOOH, Wang et al. reported uniform urchin-like α-FeOOH hollow spheres for CR removal.[60] Luo et al. synthesized magnetic flower-like γ-Fe_2O_3@NiO core-shell hierarchical structures which exhibited efficient adsorption on CR and easily for separation.[61] These studies reveal the advantages of using iron oxides as the adsorbents: low cost, high specific surface area, and easy for separation.

(c) Silica gel and silica nanomaterials

Silica gel is a granular, vitreous, porous and amorphous form of silica made from sodium silicate. It also shows a high surface area ranges from 250 to 900 m^2/g.[5] Silica gel is a good supporting material which can be modified with polymers or other organic functional groups for dye removal. Copello et al. reported Chitosan/SiO_2 hydrogel for the removal of four kinds of dyes (Remazol Black B, Erythrosine B, Neutral Red and Gentian Violet) and the hydrogel shows even higher adsorption capacity than the single chitosan sample under some conditions.[62] Yang et al. reported a hybrid hydrogel of poly(AM co DADMAC)/SiO_2 sol as the adsorbent for MO removal.[63] Besides the silica hydrogel, the silica nanomaterials like mesoporous silica could also be a supporting substrate combined with other kinds of adsorbents due to its high surface area. Nayab et al. designed a novel branched polyamine (polyethyleneimine) functionalized mesoporous silica for Alizarin red S and Xylenol Organge removal.[64] Lee et al. demonstrated the mesoporous SiO_2 and TiO_2 supraparticles with controllable pore size and particle size from micrometer to millimeter scale, which also provided good dye adsorption performance.[65] Hence, silica hydrogel and mesoporous silica are always selected as a solid surface due to its low cost, accessibility and high surface area.

(d) Zeolites

Zeolites are important microporous minerals in industrial applications. They are found naturally and can also be produced industrially on a large scale. Therefore, they are commonly used as efficient adsorbents and catalysts. For instance, Alpat et al. studied the adsorption behavior of an inexpensive natural zeolite adsorbent (Clinoptilolite) on the removal of Toluidine Blue O.[66] Yu et al. prepared the graphene oxide (GO) grafted zeolite powders functionalized by a diazonium salt, and the products show fast adsorption on rhodamine B.[67] Sapawe's group

presented a cost-effective microwave rapid synthesis of zeolite NaA for the removal of methylene (MB), which exhibited high adsorption capacity on MB.[68] Their results also confirm that the adsorption process of MB onto NaA was controlled by both physical adsorption and chemical adsorption.

(e) Carbonaceous materials

i. Activated carbon (AC)

AC is a form of carbon which are processed with physical (high temperature, long activation time) or chemical methods (chemical agents) to produce a porous structure with a high specific surface area ranging from 500 to 2000 m^2/g.[69] ACs are always classified by several types: powdered activated carbon (PAC), granular activated carbon (GAC), extruded activated carbon (EAC), bead activated carbon (BAC), impregnated carbon, and polymer coated carbon.[5] ACs are always used as efficient adsorbents for dye removal due to their high surface area. Ding et al. prepared the AC based on cheap rice husk and activated by KOH and the samples show good adsorption on RhB.[70] Al-Degs et al. investigated the effect of dye molecular charges on their adsorption from solution by using different types of ACs.[71] Their research demonstrates that cationic dyes exhibited a higher adsorption tendency towards AC over anionic dyes, which means that the surface net charge of AC will influence their adsorption performance. Despite the fact that the ACs are good materials for the removal of organic dyes, the relatively high cost of the activation process will restrict their actual applications. Furthermore, the regeneration and recyclability are also important issues for actual applications.

ii. Carbon nanotubes

Carbon nanotubes (CNTs), mainly classified as single-walled nanotubes (SWNTs) and multi-walled nanotubes (MWNTs), hold great potential applications including aerospace,

electronics, and medicine.[53] In recent years, CNTs have also been exploited in the applications of wastewater treatment, particularly for dye wastewater treatment. The characteristic structures of carbon nanotubes allow them to have strong interaction with organic molecules.[53] For example, Inyang et al. prepared a hybrid MWNTs-coated biochars, and showed that the addition of MWNTs could greatly enhance the physiochemical properties of the biochars and show good adsorption on MB.[72] Kotal's group reported a novel chemical approach to design three-dimensional MWNTs decorated rGO composites for environmental and energy applications, and the composites exhibited good adsorption for crystal violet and rhodamine 6G.[73] In another report, Cheng et al. prepared magnetic carbon nanotube–cyclodextrin composites to remove methylene blue, which can be easily separated from solution by a magnetic field.[74]

iii. Porous carbons

Porous carbons are widely used in catalysis, adsorption and energy storage. The porous structure could be produced by the template method as well as activation of carbon precursors.[75] Among the porous carbon materials, graphene and mesoporous carbon are two common materials for adsorbents. Tao et al. reported a novel monolithic porous carbon by the linkage of functionalized graphene sheets under hydrothermal method.[75] Thanks to the fully interconnected graphene network, the materials show a higher adsorption capacity for MB compared with AC. Zhang et al. prepared mesoporous carbon capsules encapsulated with magnetite NPs with high specific surface area up to 1570 m^2/g, which provides the sufficient active sites for dye removal.[76] Ma et al. fabricated the porous 3D network GO-based gels modified with sodium alginate which show high adsorption capacity on MB.[77] In addition, their results showed that electrostatic interaction between GO gel and MB contributed to the good adsorption performance. Therefore, porous carbons show great potentials in the applications of water treatment due to

their high specific surface area and 3D hierarchical structure. However, like other carbonaceous materials, one problem for their future applications is their reusability and regeneration.

1.1.4 Limitations of current adsorbents for dye removal

Although most of the current adsorbents show high adsorption capacities for organic dyes, they still suffer the problem of relatively long regeneration time and poor recyclability, and it is disadvantageous for practical applications. Therefore, it is very necessary to introduce a novel adsorbent combined with high adsorption capacities, ease of separation and good reusability.

1.2 Adsorbents for mercury removal

Mercury is a leading concern among the air pollutions addressed in the 1990 Clean Air Act Amendments (CAAA) due to its volatility, stability and ease for accumulation as methylmercury in the environment.[78] In the United States, mercury emissions from anthropogenic sources were estimated to be 158 t per year and one-third of them comes from the coal-fired utility boilers.[78-80] In Canada, mercury emissions from anthropogenic sources were estimated to be 7.84 t per year.[80] Therefore, the U.S. Environmental Protection Agency (EPA) issued the Clean Air Mercury Rule (CAMR) to reduce the mercury emissions from coal-fired utility boilers and established a mercury cap which aimed to bring about 70% reduction of mercury from 1999 emission levels.[79] Alberta government has set up a regulation implemented in 2010 to capture mercury at a minimum level of 70%.[81] Apart from the government regulations, new measures and technologies have to be taken to reduce the air pollution caused by mercury emissions.

1.2.1 Traditional technologies for mercury removal

The chemical state of mercury from the flue gas mainly displays three forms: Hg^0, Hg^{2+} and Hg (p). Among them, Hg^{2+} and Hg(p) are easy to remove from flue gas by conventional air pollution control devices (APCD).[79] Common APCDs include fabric filter (FF) bag house,

electrostatic precipitator (ESP), and wet flue gas desulfurization (FGD).[80] Hg(p) could be easily captured along with fly ash particles by ESP and/or FF bag houses, and Hg^{2+} can be removed by wet FGD equipment due to its solubility in water.[79] However, Hg^0 is the most difficult to capture according to traditional APSD because of its stability and insolubility in water. Therefore, adsorbents (e.g. AC) are needed to remove Hg^0 combined with ESP or FGD. Table 1.3 lists the mercury capture efficiency by using conventional APCD.[80]

Table 1.3 Average mercury capture by different APCD configurations.[80]

APCD configurations	Average percentage of mercury capture (%)		
	Bituminous	Subbituminous	Lignite
CS-ESP	36	3	-4
HS-ESP	9	6	N/A
FF	90	72	N/A
PS	N/A	9	N/A
SDA+ESP	N/A	35	N/A
SDA+FF	98	24	0
SDA+FF+SCR	98	N/A	N/A
PS+wet FGD	12	-8	33
CS-ESP+Wet FGD	74	29	44
HS-ESP+Wet FGD	50	29	N/A
FF+Wet FGD	98	N/A	N/A

Note: CS-ESP: cold-side ESP; HS-ESP: hot-side ESP; PS: particulate scrubber; SDA: spray dryer adsorber; SCR: selective catalytic reduction.

1.2.2 Common adsorbents for mercury removal

(a) Activated carbon (AC)

Up to now, ACs are still the most promising materials in mercury capture. For example, In Yang et al.'s review, FGD ACs are regarded as one of the most extensively used adsorbents for mercury removal.[80] The pilot-scale tests reveal that the AC injection for mercury control have achieved 25-95% removal over a C/Hg ratio 2000-15,000.[82] The equilibrium adsorption capacity of FGD AC depends on several factors such as temperature, inlet mercury concentration, flue gas components.[80] In the presence of some acidic gases, such as SO_2, HCl, NO, NO_2, the adsorbents will become less effective and rapid breakthrough and oxidation of mercury take place at 107 ºC and 163 ºC according to Yang's report.[80] This indicates the interaction of NO_2-SO_2 will affect the actual mercury control in coal-fired industry.[80] Although AC show good mercury capture capability form flue gas, the cost and their environmental impact still require careful consideration.[82]

In addition, various chemically modified AC are developed to improve the mercury capture efficiency. Brominated carbon (Br-AC) is one of the examples. The addition of bromine was in an attempt to oxidize the Hg^0 to Hg^{2+}, which could be removed by FGD or other existing devices.[83] According to the study of Liu et al., fly ash-induced oxidation by bromine played an important role in the oxidation of Hg^0,[83] and the oxidation of Hg^0 is also limited by the temperature and the compositions of flue gas. Bisson et al. reported a novel brominated biomass ash sorbent for mercury capture, and the mercury was captured by chemisorption on biomass ash sorbents.[84] The main problem for Br-AC is how to dispose of the spent adsorbents after mercury capture.

(b) Zeolites

Due to the high specific surface area and stability under harsh environments, zeolite-based adsorbents have been designed to capture Hg^0. Since mercury could amalgamate with other noble metal, including silver, gold, palladium and platinum, zeolite materials could be modified with metal NPs to capture Hg^0.[82] Liu et al. reported natural chabazite-based Ag nanocomposites for mercury capture from flue gas, and a complete mercury capture was achieved up to 250 ^oC.[85] Dong et al. synthesized the magnetite-zeolite composites encapsulated with Ag NPs which can remove Hg^0 up to 200 ^oC.[86] The advantage of the magnetite-zeolite composites is the easy separation and regeneration after use.

1.2.3 Limitations of current adsorbents for mercury capture

According to the reports of the current adsorbents like carbon nanotube and zeolites, they meet with the problem of regeneration difficulty or poor size control of Ag NPs. For example, in the case of Ag-based zeolite, most of the Ag NPs are loaded on the surface of zeolite, which tend to aggregate under high temperature. In order to use the adsorbents for real applications in flue gas, we have to solve the regeneration problem and achieve good control of Ag NPs within the substrates.

1.3 Objective and outline of the thesis

Currently most of the research on the design of adsorbents has been focused on the adsorption capacity; while there have been few studies on the adsorption rate and regeneration rate performance of adsorbents. In addition, many of the adsorbents are difficult to separate and reuse. The overall objective of this thesis is to develop novel and reusable adsorbents to address the critical environmental issues on water and air (or combustion gas) treatment.

The outline of thesis is as follows. Chapter 1 gave a brief introduction to the conventional technologies for dye and mercury removal. Chapter 2 was aimed at designing a novel adsorbent with fast adsorption ability, facile regeneration and good cyclic stability, which will be favorable for practical applications. Chapter 3 was focused on the capture of elemental mercury (Hg^0) in order to deal with the problem of air pollution by Hg^0. It should be noted that this work is the first report on the synthesis of SBA-15-Ag for the mercury capture. Chapter 4 concluded this work and made some suggestions for the future work.

1.4 References

(1) Aksu, Z. Application of biosorption for the removal of organic pollutants: a review. *Process Biochem.* **2005,** *40,* 997-1026.

(2) Forgacs, E.; Cserháti, T.; Oros, G. Removal of synthetic dyes from wastewaters: a review. *Environ. Int.* **2004,** *30,* 953-971.

(3) Fu, Y.; Viraraghavan, T. Fungal decolorization of dye wastewaters: a review. *Bioresour. Technol.* **2001,** *79,* 251-262.

(4) Canada, I. NAICS 32513 Synthetic Dyes and Pigments. http://www.ic.gc.ca/eic/site/chemicals-chimiques.nsf/eng/bt01206.html#footnote1.

(5) Gupta, V. K.; Suhas Application of low-cost adsorbents for dye removal – A review. *J. Environ. Manage.* **2009,** *90,* 2313-2342.

(6) dos Santos, A. B.; Cervantes, F. J.; van Lier, J. B. Review paper on current technologies for decolourisation of textile wastewaters: Perspectives for anaerobic biotechnology. *Bioresour. Technol.* **2007,** *98,* 2369-2385.

(7) Xu, Y.; Lebrun, R. E.; Gallo, P.-J.; Blond, P. Treatment of Textile Dye Plant Effluent by Nanofiltration Membrane. *Sep. Sci. Technol.* **1999,** *34,* 2501-2519.

(8) Marmagne, O.; Coste, C. Color Removal From Textile Plant Effluents. *Am. Dyest. Rep.* **1996,** *85,* 15-20.

(9) Wu, J.-S.; Liu, C.-H.; Chu, K. H.; Suen, S.-Y. Removal of cationic dye methyl violet 2B from water by cation exchange membranes. *J. Membr. Sci.* **2008,** *309,* 239-245.

(10) Robinson, T.; McMullan, G.; Marchant, R.; Nigam, P. Remediation of dyes in textile effluent: a critical review on current treatment technologies with a proposed alternative. *Bioresour. Technol.* **2001,** *77,* 247-255.

(11) Shi, B.; Li, G.; Wang, D.; Feng, C.; Tang, H. Removal of direct dyes by coagulation: The performance of preformed polymeric aluminum species. *J. Hazard. Mater.* **2007,** *143,* 567-574.

(12) Zhou, Y.; Liang, Z.; Wang, Y. Decolorization and COD removal of secondary yeast wastewater effluents by coagulation using aluminum sulfate. *Desalination* **2008,** *225,* 301-311.

(13) Lee, J.-W.; Choi, S.-P.; Thiruvenkatachari, R.; Shim, W.-G.; Moon, H. Submerged microfiltration membrane coupled with alum coagulation/powdered activated carbon adsorption for complete decolorization of reactive dyes. *Water Res.* **2006,** *40,* 435-444.

(14) Slokar, Y. M.; Majcen Le Marechal, A. Methods of decoloration of textile wastewaters. *Dyes Pigm.* **1998,** *37,* 335-356.

(15) Kim, T.-H.; Park, C.; Yang, J.; Kim, S. Comparison of disperse and reactive dye removals by chemical coagulation and Fenton oxidation. *J. Hazard. Mater.* **2004,** *112,* 95-103.

(16) Dutta, K.; Mukhopadhyay, S.; Bhattacharjee, S.; Chaudhuri, B. Chemical oxidation of methylene blue using a Fenton-like reaction. *J. Hazard. Mater.* **2001,** *84,* 57-71.

(17) Solozhenko, E. G.; Soboleva, N. M.; Goncharuk, V. V. Decolourization of azodye solutions by Fenton's oxidation. *Water Res.* **1995,** *29,* 2206-2210.

(18) Cheng, M.; Ma, W.; Li, J.; Huang, Y.; Zhao, J.; Wen, Y. x.; Xu, Y. Visible-Light-Assisted Degradation of Dye Pollutants over Fe(III)-Loaded Resin in the Presence of H_2O_2 at Neutral pH Values. *Environ. Sci. Technol.* **2004,** *38,* 1569-1575.

(19) Soares, O. S. G. P.; Órfão, J. J. M.; Portela, D.; Vieira, A.; Pereira, M. F. R. Ozonation of textile effluents and dye solutions under continuous operation: Influence of operating parameters. *J. Hazard. Mater.* **2006,** *137,* 1664-1673.

(20) Wu, J.; Doan, H.; Upreti, S. Decolorization of aqueous textile reactive dye by ozone. *Chem. Eng. J.* **2008,** *142,* 156-160.

(21) Karaoğlu, M. H.; Uğurlu, M. Studies on UV/NaOCl/TiO_2/Sep photocatalysed degradation of Reactive Red 195. *J. Hazard. Mater.* **2010,** *174,* 864-871.

(22) Han, F.; Kambala, V. S. R.; Srinivasan, M.; Rajarathnam, D.; Naidu, R. Tailored titanium dioxide photocatalysts for the degradation of organic dyes in wastewater treatment: A review. *Appl. Catal., A* **2009,** *359,* 25-40.

(23) Khin, M. M.; Nair, A. S.; Babu, V. J.; Murugan, R.; Ramakrishna, S. A review on nanomaterials for environmental remediation. *Energy Environ. Sci.* **2012,** *5,* 8075-8109.

(24) Aguedach, A.; Brosillon, S.; Morvan, J.; Lhadi, E. K. Photocatalytic degradation of azo-dyes reactive black 5 and reactive yellow 145 in water over a newly deposited titanium dioxide. *Appl. Catal., B* **2005,** *57,* 55-62.

(25) Gupta, V. K.; Jain, R.; Mittal, A.; Mathur, M.; Sikarwar, S. Photochemical degradation of the hazardous dye Safranin-T using TiO_2 catalyst. *J. Colloid Interface Sci.* **2007,** *309,* 464-469.

(26) Pirkanniemi, K.; Sillanpää, M. Heterogeneous water phase catalysis as an environmental application: A review. *Chemosphere* **2002,** *48,* 1047-1060.

(27) Wu, W.; Xiao, X.; Zhang, S.; Ren, F.; Jiang, C. Facile method to synthesize magnetic iron oxides/TiO2 hybrid nanoparticles and their photodegradation application of methylene blue. *Nanoscale Res. Lett.* **2011,** *6,* 533.

(28) Linley, S.; Leshuk, T.; Gu, F. X. Synthesis of Magnetic Rattle-Type Nanostructures for Use in Water Treatment. *ACS Appl. Mater. Interfaces* **2013,** *5,* 2540-2548.

(29) Gupta, V. K.; Jain, R.; Varshney, S. Electrochemical removal of the hazardous dye Reactofix Red 3 BFN from industrial effluents. *J. Colloid Interface Sci.* **2007,** *312,* 292-296.

(30) Oliveira, F.; Osugi, M.; Paschoal, F. M.; Profeti, D.; Olivi, P.; Zanoni, M. Electrochemical oxidation of an acid dye by active chlorine generated using $Ti/Sn_{(1-x)}Ir_x O_2$ electrodes. *J. Appl. Electrochem.* **2007,** *37,* 583-592.

(31) Liu, C.-H.; Wu, J.-S.; Chiu, H.-C.; Suen, S.-Y.; Chu, K. H. Removal of anionic reactive dyes from water using anion exchange membranes as adsorbers. *Water Res.* **2007,** *41,* 1491-1500.

(32) Raghu, S.; Ahmed Basha, C. Chemical or electrochemical techniques, followed by ion exchange, for recycle of textile dye wastewater. *J. Hazard. Mater.* **2007,** *149,* 324-330.

(33) Barragán, B. E.; Costa, C.; Carmen Márquez, M. Biodegradation of azo dyes by bacteria inoculated on solid media. *Dyes Pigm.* **2007,** *75,* 73-81.

(34) Pazarlioglu, N. K.; Urek, R. O.; Ergun, F. Biodecolourization of Direct Blue 15 by immobilized Phanerochaete chrysosporium. *Process Biochem.* **2005,** *40,* 1923-1929.

(35) van der Zee, F. P.; Bisschops, I. A. E.; Blanchard, V. G.; Bouwman, R. H. M.; Lettinga, G.; Field, J. A. The contribution of biotic and abiotic processes during azo dye reduction in anaerobic sludge. *Water Res.* **2003,** *37,* 3098-3109.

(36) Delée, W.; O'Neill, C.; Hawkes, F. R.; Pinheiro, H. M. Anaerobic treatment of textile effluents: A review. *J. Chem. Technol. Biotechnol.* **1998,** *73,* 323-335.

(37) Ali, I. New Generation Adsorbents for Water Treatment. *Chem. Rev.* **2012,** *112,* 5073-5091.

(38) Deliyanni, E. A.; Bakoyannakis, D. N.; Zouboulis, A. I.; Matis, K. A. Sorption of As(V) ions by akaganéite-type nanocrystals. *Chemosphere* **2003,** *50,* 155-163.

(39) Gao, Y.; Wahi, R.; Kan, A. T.; Falkner, J. C.; Colvin, V. L.; Tomson, M. B. Adsorption of Cadmium on Anatase NanoparticlesEffect of Crystal Size and pH. *Langmuir* **2004,** *20,* 9585-9593.

(40) Ponder, S. M.; Darab, J. G.; Mallouk, T. E. Remediation of Cr(VI) and Pb(II) Aqueous Solutions Using Supported, Nanoscale Zero-valent Iron. *Environ. Sci. Technol.* **2000,** *34,* 2564-2569.

(41) Uheida, A.; Salazar-Alvarez, G.; Björkman, E.; Yu, Z.; Muhammed, M. Fe3O4 and γ-Fe2O3 nanoparticles for the adsorption of Co^{2+} from aqueous solution. *J. Colloid Interface Sci.* **2006,** *298,* 501-507.

(42) Chang, Y.-C.; Chen, D.-H. Preparation and adsorption properties of monodisperse chitosan-bound Fe_3O_4 magnetic nanoparticles for removal of Cu(II) ions. *J. Colloid Interface Sci.* **2005,** *283,* 446-451.

(43) Zhang, L.; Liu, N.; Yang, L.; Lin, Q. Sorption behavior of nano-TiO_2 for the removal of selenium ions from aqueous solution. *J. Hazard. Mater.* **2009,** *170,* 1197-1203.

(44) Gao, H.; Sun, Y.; Zhou, J.; Xu, R.; Duan, H. Mussel-Inspired Synthesis of Polydopamine-Functionalized Graphene Hydrogel as Reusable Adsorbents for Water Purification. *ACS Appl. Mater. Interfaces* **2012,** *5,* 425-432.

(45) Belessi, V.; Romanos, G.; Boukos, N.; Lambropoulou, D.; Trapalis, C. Removal of Reactive Red 195 from aqueous solutions by adsorption on the surface of TiO_2 nanoparticles. *J. Hazard. Mater.* **2009,** *170,* 836-844.

(46) Moussavi, G.; Mahmoudi, M. Removal of azo and anthraquinone reactive dyes from industrial wastewaters using MgO nanoparticles. *J. Hazard. Mater.* **2009,** *168,* 806-812.

(47) Yang, K.; Xing, B. Sorption of Phenanthrene by Humic Acid-Coated Nanosized TiO_2 and ZnO. *Environ. Sci. Technol.* **2009,** *43,* 1845-1851.

(48) Wang, P.; Shi, Q.; Shi, Y.; Clark, K. K.; Stucky, G. D.; Keller, A. A. Magnetic Permanently Confined Micelle Arrays for Treating Hydrophobic Organic Compound Contamination. *J. Am. Chem. Soc.* **2008,** *131,* 182-188.

(49) Tran, H.; Killops, K. L.; Campos, L. M. Advancements and challenges of patterning biomolecules with sub-50 nm features. *Soft Matter* **2013,** *9,* 6578-6586.

(50) Yola, M. L.; Eren, T.; Atar, N.; Wang, S. Adsorptive and photocatalytic removal of reactive dyes by silver nanoparticle-colemanite ore waste. *Chem. Eng. J.* **2014,** *242,* 333-340.

(51) Adak, A.; Bandyopadhyay, M.; Pal, A. Removal of crystal violet dye from wastewater by surfactant-modified alumina. *Sep. Purif. Technol.* **2005,** *44,* 139-144.

(52) Adak, A.; Bandyopadhyay, M.; Pal, A. Fixed bed column study for the removal of crystal violet (C. I. Basic Violet 3) dye from aquatic environment by surfactant-modified alumina. *Dyes Pigm.* **2006,** *69,* 245-251.

(53) Khajeh, M.; Laurent, S.; Dastafkan, K. Nanoadsorbents: Classification, Preparation, and Applications (with Emphasis on Aqueous Media). *Chem. Rev.* **2013,** *113,* 7728-7768.

(54) Lan, S.; Guo, N.; Liu, L.; Wu, X.; Li, L.; Gan, S. Facile preparation of hierarchical hollow structure gamma alumina and a study of its adsorption capacity. *Appl. Surf. Sci.* **2013,** *283,* 1032-1040.

(55) Tian, P.; Han, X.-y.; Ning, G.-l.; Fang, H.-x.; Ye, J.-w.; Gong, W.-t.; Lin, Y. Synthesis of Porous Hierarchical MgO and Its Superb Adsorption Properties. *ACS Appl. Mater. Interfaces* **2013,** *5,* 12411-12418.

(56) Ai, L.; Yue, H.; Jiang, J. Sacrificial template-directed synthesis of mesoporous manganese oxide architectures with superior performance for organic dye adsorption. *Nanoscale* **2012,** *4,* 5401-5408.

(57) Haldorai, Y.; Shim, J.-J. An efficient removal of methyl orange dye from aqueous solution by adsorption onto chitosan/MgO composite: A novel reusable adsorbent. *Appl. Surf. Sci.* **2014,** *292,* 447-453.

(58) Zhong, L. S.; Hu, J. S.; Liang, H. P.; Cao, A. M.; Song, W. G.; Wan, L. J. Self-Assembled 3D Flowerlike Iron Oxide Nanostructures and Their Application in Water Treatment. *Adv. Mater.* **2006,** *18,* 2426-2431.

(59) Zhu, D.; Zhang, J.; Song, J.; Wang, H.; Yu, Z.; Shen, Y.; Xie, A. Efficient one-pot synthesis of hierarchical flower-like α-Fe2O3 hollow spheres with excellent adsorption performance for water treatment. *Appl. Surf. Sci.* **2013,** *284,* 855-861.

(60) Wang, B.; Wu, H.; Yu, L.; Xu, R.; Lim, T.-T.; Lou, X. W. Template-free Formation of Uniform Urchin-like α-FeOOH Hollow Spheres with Superior Capability for Water Treatment. *Adv. Mater.* **2012,** *24,* 1111-1116.

(61) Luo, S.; Chai, F.; Wang, T.; Li, L.; Zhang, L.; Wang, C.; Su, Z. Flowerlike [gamma]-Fe_2O_3@NiO hierarchical core-shell nanostructures as superb capability and magnetically separable adsorbents for water treatment. *RSC Adv.* **2013,** *3,* 12671-12677.

(62) Copello, G. J.; Mebert, A. M.; Raineri, M.; Pesenti, M. P.; Diaz, L. E. Removal of dyes from water using chitosan hydrogel/SiO_2 and chitin hydrogel/SiO_2 hybrid materials obtained by the sol–gel method. *J. Hazard. Mater.* **2011,** *186,* 932-939.

(63) Yang, X.; Ni, L. Synthesis of hybrid hydrogel of poly(AM co DADMAC)/silica sol and removal of methyl orange from aqueous solutions. *Chem. Eng. J.* **2012,** *209,* 194-200.

(64) Nayab, S.; Farrukh, A.; Oluz, Z.; Tuncel, E.; Tariq, S. R.; Rahman, H. u.; Kirchhoff, K.; Duran, H.; Yameen, B. Design and Fabrication of Branched Polyamine Functionalized Mesoporous Silica: An Efficient Absorbent for Water Remediation. *ACS Appl. Mater. Interfaces* **2014,** *6,* 4408-4417.

(65) Lee, D.-W.; Jin, M.-H.; Lee, C.-B.; Oh, D.; Ryi, S.-K.; Park, J.-S.; Bae, J.-S.; Lee, Y.-J.; Park, S.-J.; Choi, Y.-C. Facile synthesis of mesoporous silica and titania supraparticles by a meniscus templating route on a superhydrophobic surface and their application to adsorbents. *Nanoscale* **2014,** *6,* 3483-3487.

(66) Alpat, S. K.; Özbayrak, Ö.; Alpat, Ş.; Akçay, H. The adsorption kinetics and removal of cationic dye, Toluidine Blue O, from aqueous solution with Turkish zeolite. *J. Hazard. Mater.* **2008,** *151,* 213-220.

(67) Yu, Y.; Murthy, B. N.; Shapter, J. G.; Constantopoulos, K. T.; Voelcker, N. H.; Ellis, A. V. Benzene carboxylic acid derivatized graphene oxide nanosheets on natural zeolites as effective adsorbents for cationic dye removal. *J. Hazard. Mater.* **2013,** *260,* 330-338.

(68) Sapawe, N.; Jalil, A. A.; Triwahyono, S.; Shah, M. I. A.; Jusoh, R.; Salleh, N. F. M.; Hameed, B. H.; Karim, A. H. Cost-effective microwave rapid synthesis of zeolite NaA for removal of methylene blue. *Chem. Eng. J.* **2013,** *229,* 388-398.

(69) Carrott, P. J. M.; Carrott, M. M. L. R.; Roberts, R. A. Physical adsorption of gases by microporous carbons. *Colloids Surf.* **1991,** *58,* 385-400.

(70) Ding, L.; Zou, B.; Gao, W.; Liu, Q.; Wang, Z.; Guo, Y.; Wang, X.; Liu, Y. Adsorption of Rhodamine-B from aqueous solution using treated rice husk-based activated carbon. *Colloids Surf., A* **2014,** *446,* 1-7.

(71) Al-Degs, Y.; Khraisheh, M. A. M.; Allen, S. J.; Ahmad, M. N. A. Sorption behavior of cationic and anionic dyes from aqueous solution on different types of activated carbons. *Sep. Sci. Technol.* **2001,** *36,* 91-102.

(72) Inyang, M.; Gao, B.; Zimmerman, A.; Zhang, M.; Chen, H. Synthesis, characterization, and dye sorption ability of carbon nanotube–biochar nanocomposites. *Chem. Eng. J.* **2014,** *236,* 39-46.

(73) Kotal, M.; Bhowmick, A. K. Multifunctional Hybrid Materials Based on Carbon Nanotube Chemically Bonded to Reduced Graphene Oxide. *J. Phys. Chem. C* **2013,** *117,* 25865-25875.

(74) Cheng, J.; Chang, P. R.; Zheng, P.; Ma, X. Characterization of Magnetic Carbon Nanotube–Cyclodextrin Composite and Its Adsorption of Dye. *Ind. Eng. Chem. Res.* **2014,** *53,* 1415-1421.

(75) Tao, Y.; Kong, D.; Zhang, C.; Lv, W.; Wang, M.; Li, B.; Huang, Z.-H.; Kang, F.; Yang, Q.-H. Monolithic carbons with spheroidal and hierarchical pores produced by the linkage of functionalized graphene sheets. *Carbon* **2014,** *69,* 169-177.

(76) Zhang, Y.; Xu, S.; Luo, Y.; Pan, S.; Ding, H.; Li, G. Synthesis of mesoporous carbon capsules encapsulated with magnetite nanoparticles and their application in wastewater treatment. *J. Mater. Chem.* **2011,** *21,* 3664-3671.

(77) Ma, T.; Chang, P. R.; Zheng, P.; Zhao, F.; Ma, X. Fabrication of ultra-light graphene-based gels and their adsorption of methylene blue. *Chem. Eng. J.* **2014,** *240,* 595-600.

(78) Pavlish, J. H.; Sondreal, E. A.; Mann, M. D.; Olson, E. S.; Galbreath, K. C.; Laudal, D. L.; Benson, S. A. Status review of mercury control options for coal-fired power plants. *Fuel Process. Technol.* **2003,** *82,* 89-165.

(79) Presto, A. A.; Granite, E. J. Survey of Catalysts for Oxidation of Mercury in Flue Gas. *Environ. Sci. Technol.* **2006,** *40,* 5601-5609.

(80) Yang, H.; Xu, Z.; Fan, M.; Bland, A. E.; Judkins, R. R. Adsorbents for capturing mercury in coal-fired boiler flue gas. *J. Hazard. Mater.* **2007,** *146,* 1-11.

(81) Bisson, T. M.; Xu, Z.; Gupta, R.; Maham, Y.; Liu, Y.; Yang, H.; Clark, I.; Patel, M. Chemical–mechanical bromination of biomass ash for mercury removal from flue gases. *Fuel* **2013,** *108,* 54-59.

(82) Liu, Y.; Bisson, T. M.; Yang, H.; Xu, Z. Recent developments in novel sorbents for flue gas clean up. *Fuel Process. Technol.* **2010,** *91,* 1175-1197.

(83) Liu, S.-H.; Yan, N.-Q.; Liu, Z.-R.; Qu, Z.; Wang, H. P.; Chang, S.-G.; Miller, C. Using Bromine Gas To Enhance Mercury Removal from Flue Gas of Coal-Fired Power Plants. *Environ. Sci. Technol.* **2007,** *41,* 1405-1412.

(84) Bisson, T. M.; MacLean, L. C. W.; Hu, Y.; Xu, Z. Characterization of Mercury Binding onto a Novel Brominated Biomass Ash Sorbent by X-ray Absorption Spectroscopy. *Environ. Sci. Technol.* **2012,** *46,* 12186-12193.

(85) Liu, Y.; Kelly, D. J. A.; Yang, H.; Lin, C. C. H.; Kuznicki, S. M.; Xu, Z. Novel Regenerable Sorbent for Mercury Capture from Flue Gases of Coal-Fired Power Plant. *Environ. Sci. Technol.* **2008,** *42,* 6205-6210.

(86) Dong, J.; Xu, Z.; Kuznicki, S. M. Mercury Removal from Flue Gases by Novel Regenerable Magnetic Nanocomposite Sorbents. *Environ. Sci. Technol.* **2009,** *43,* 3266-3271.

Chapter 2 Highly Regenerable Mussel-Inspired Fe_3O_4@Polydopamine-Ag Core-Shell Microspheres as Catalyst and Adsorbent for Methylene Blue Removal[i]

2.1 Introduction

Water pollution by organic contaminants has become a serious environmental issue and received significant attention.[1, 2] Among many organic pollutants, it is of special importance to solve the pollution challenges with organic dyes due to their wide applications in industries such as printing, textile, paper, paints, and plastics.[3, 4] The immoderate release of wastewater containing organic dyes could impede sunlight penetration into water, thus reducing the photosynthetic reaction of plants; some synthetic dyes may cause severe health threats to human being.[5, 6] A variety of technologies have been exploited to remove these contaminants such as adsorption, photocatalytic degradation, chemical oxidation, membrane filtration, flocculation, electrooxidation.[4, 7] Adsorption is one of the most effective approaches for the treatment of organic dyes and is commonly used due to its relatively low cost and easy operation.[8, 9] Various kinds of adsorbents have been designed to remove the dyes in water with considerable adsorption capabilities, such as activated carbon,[10] carbon nanotube,[11] graphene hydrogel,[2, 12] metal oxide.[6] Inspired by the unique wet adhesion capability of marine mussels, polydopamine (PDA) has attracted strong interest as a biomimetic polymer and a universal surface modification agent for various materials with a broad range of applications.[13, 14] Recently, PDA functionalized hybrid

[i] A version of this chapter has been published in *ACS Applied Materials & Interfaces* in 2014.

nanomaterials were developed as novel nanostructured adsorbents to remove organic dyes. Duan et al. reported a free-standing PDA-modified graphene hydrogel (PDA-GH) for water treatment.[12] Priestley et al. designed a novel core-shell adsorbent by converting Fe_3O_4@PDA into Fe_3O_4@C under thermal treatment for the adsorption of rhodamine B.[15] These adsorbents demonstrated good adsorption of organic dyes with the assistance of catechol groups of PDA or hydrophobic carbon layer. Despite their considerable adsorption capabilities, many previously reported PDA-modified adsorbents and catalyst supports are limited by relatively long regeneration time or poor cyclic stability, which makes it challenging to recycle and reuse the adsorbents efficiently, further affecting their decontamination efficiencies in dye removal.

Herein, we present a facile synthetic method of *in situ* reduction to prepare core-shell Fe_3O_4@PDA-Ag microspheres, where polydopamine acts as both the reducing agent and template for the formation of Ag nanoparticles (NPs) on the dopamine surfaces in one step.[16-18] It is well-known that dopamine can spontaneously self-polymerize into polydopamine under mild solution conditions and form adhesive coating layer on various substrates, as inspired by the unique underwater adhesion properties of marine mussel foot proteins.[13, 14, 16] Additionally, dopamine can serve as a reducing and capping agent to reduce noble metallic salts into metallic NPs.[15, 16, 19, 20] Noble metal NPs are widely applied to the catalytic reduction of methylene blue (MB), a kind of common dye in dye manufacturing industry, thanks to their high catalytic activity.[21, 22] Thus, a facile route was developed in this work to synthesize novel Fe_3O_4@PDA-Ag core-shell microspheres with synergetic capabilities of high catalytic reduction activity and fast adsorption ability for MB at different pH values. The microspheres exhibit excellent cyclic performance via magnetic separation and fast regeneration rate, which can be reused for more

than 27 times by using $NaBH_4$ as the desorption agent, and each regeneration cycle requires only 6 minutes, revealing good potentials in practical applications.

2.2 Experimental Section

2.2.1 Materials

Anhydrous iron (III) chloride ($FeCl_3$) was purchased from Acros organics. Anhydrous sodium acetate (NaOAc), ethylene glycol (EG), silver nitrate ($AgNO_3$), and sodium borohydride ($NaBH_4$) were obtained from Fisher Scientific. Sodium citrate (Na_3Cit), dopamine hydrochloride, methylene blue (MB), and rhodamine B (RhB) were purchased from Sigma-Aldrich. Ultrapure water prepared with a Millipore Milli-Q water purification system (MA, USA) was used for all experiments.

2.2.2 Preparation of Fe_3O_4@Polydopamine (PDA) core-shell microspheres

The Fe_3O_4 microspheres were prepared with a modified solvothermal method.[23] $FeCl_3$ (2.6 g), Na_3Cit (1.0 g) were dissolved in EG (80 mL) to form a clear solution. Afterwards, NaOAc (4.0 g) was added to the mixture under stirring. After the mixture was fully dissolved, it was transferred and sealed into a Teflon-lined stainless-steel autoclave. The autoclave was heated at 200 ^oC for 10 h, and then cooled to room temperature (25 ^oC). The obtained black products were washed with ultrapure water and ethanol three times, and then dried in vacuum at room temperature. To coat Fe_3O_4 cores with the polydopamine shell, 80 mg of Fe_3O_4 and 80 mg dopamine hydrochloride were dissolved in 40 mL tris buffer solution (10 mM, pH=8.5). After shaking for 24 h at room temperature, the products were separated and washed with ultrapure water and ethanol several times.

2.2.3 Preparation of Fe_3O_4@PDA-Ag microspheres

For the preparation of Ag nanoparticles on PDA surfaces, Tollens' reagent (silver ammonia solution) was used as the Ag precursor solution. Silver ammonia solution was prepared by adding ammonia aqueous solution (2 wt.%) into 10 mg mL^{-1} $AgNO_3$ solution until brown precipitation was just dissolved. 80 mg of as-prepared Fe_3O_4@PDA microspheres was added to 40 mL silver ammonia solution and the mixture was shaken in a rotary shaker for 12 h at room temperature. The products were collected, washed with ultrapure water and ethanol several times, and dried under vacuum. Then, Fe_3O_4@PDA-Ag-10 microspheres were obtained.

The same sample preparation procedure was carried out to obtain the Fe_3O_4@PDA-Ag-1 and Fe_3O_4@PDA-Ag-5 microspheres by using 1 mg mL^{-1} and 5 mg mL^{-1} silver ammonia solution, respectively.

For comparison, $AgNO_3$ solution (10 mg mL^{-1}) was also used as the Ag source in place of silver ammonia solution following the same procedure.

2.2.4 Characterizations

X-ray diffraction (XRD) patterns were recorded on a Rigaku RU-200B X-ray diffractometer with a rotating anode X-ray generator, Cu Kα radiation (40 kV, 110 mA). The morphologies of microspheres were analyzed on a Philips (FEI) Morgagni 268 operated at 80 kV and JEOL JEM-2200FS transmission electron microscope (TEM) operated at 200 kV. X-ray photoelectron spectroscopy (XPS) was carried out on a Kratos Axis spectrometer with monochromatized Al Kα. C 1s peak at 284.6 eV was used to correct all XPS spectra. The UV absorption spectra of the samples were obtained on a Thermo Scientific Evolution 300 UV-Vis spectrophotometer. Zeta potentials of the microspheres were measured by using a Malvern

Zetasizer Nano. Magnetic properties were examined on a Quantum Design PPMS magnetometer with an applied field between -10000 to 10000 Oe at room temperature.

2.2.5 Catalytic reduction experiments

5 mg of Fe_3O_4@PDA-Ag microspheres were added to 10 mL of MB aqueous solution (pH=5.8, 40 mg L^{-1}). Subsequently, 0.5 mL fresh $NaBH_4$ aqueous solution (0.1 mol L^{-1}) was injected into the solution under stirring. The blue color of MB gradually vanished by catalytic reduction in the presence of reducing agents. The catalytic process was monitored by measuring the changes in the absorbance at 665 nm with a UV-vis spectrophotometer. In addition, RhB was used as another model dye for catalytic reduction test under the same procedure as MB.

2.2.6 Adsorption experiments

5 mg of Fe_3O_4@PDA-Ag microspheres were added into 2 mL of MB aqueous solution (pH=5.8, 4 mg L^{-1}) under constant stirring at room temperature. UV-vis absorption spectra of MB at different intervals were recorded to monitor the adsorption process. At the end of adsorption, the adsorbents were separated from the solution with an external magnet. The recycled adsorbents were first washed with fresh $NaBH_4$ aqueous solution (2 mL, 1.5 mmol L^{-1}), and then washed with ethanol and ultrapure water three times before the next desorption-adsorption cycle. RhB was also used as a model dye for adsorption test under the same condition as MB.

2.2.7 Stability tests

5 mg of Fe_3O_4@PDA microspheres were dispersed in 10 mL ultrapure water and stored for half a year to test the stability of PDA layer in aqueous solution. 5 mg of Fe_3O_4@PDA-Ag-10 microspheres were dispersed in 10 mL hydrochloric acid solution at pH 2 and pH 3 for 24 hours to test the acid stability of the sample. After the stability tests, the acid solution was separated

from the solid samples, and atomic absorption spectroscopy (AAS) was used to determine the concentrations of Fe^{3+}/Fe^{2+} and Ag^{+} possibly present in the acid solution.

2.3 Results and Discussions

2.3.1 Synthesis and characterizations of materials

Typically, Fe_3O_4 microspheres were first synthesized through a solvothermal method in ethylene glycol using anhydrous $FeCl_3$ as a single iron source. Afterwards, Fe_3O_4 microspheres were mixed with dopamine solution (10 mM Tris, pH 8.5), resulting in Fe_3O_4@PDA core-shell microspheres with uniform PDA thin layers outside. Tollens' reagent (silver ammonia solution) was then added to the mixture and was *in situ* reduced by PDA shell, leading to the deposition of Ag NPs on the shell surface (Figure 2.1a).

The morphology of the Fe_3O_4 core, Fe_3O_4@PDA and Fe_3O_4@PDA-Ag-10 core-shell microspheres was characterized by transmission electron microscope (TEM). The as-prepared Fe_3O_4 cores have a mean size of about 500 nm (Figure 2.1b). Thin PDA shell layers formed around the Fe_3O_4 cores show an average thickness of about 20 nm (Figure 2.1c), displaying a distinct core-shell structure. Figure 2.1d exhibits that the small Ag NPs (~25 nm) are densely and uniformly distributed on the PDA surface. It should be noted that modifying the concentrations of silver ammonia solution did not lead to any significant change of the size of Ag NPs (Figure 2.2). The high resolution TEM (HRTEM) image of the Ag NPs (Figure 2.1e) shows that the interfringe distance of Ag NPs is measured to be 0.24 nm, which could be assigned to the {111} crystal planes of fcc Ag.[18] Furthermore, the nanobeam electron diffraction pattern (NBD) confirms the crystalline nature of metallic Ag NPs (Figure 2.3). Figure 2.4a is the X-ray diffraction pattern (XRD) of the obtained product. All the diffraction peaks can be indexed to Fe_3O_4 (JCPDS 19-0629) and Ag (JCPDS 04-0783), confirming the formation of Ag NPs on the

surface of Fe_3O_4@PDA particles. Figure 2.4b depicts the Ag 3d X-ray photoelectron spectroscopy (XPS) of Fe_3O_4@PDA-Ag. The XPS peaks at 368.1 eV and 374.1 eV can be assigned to Ag $3d_{5/2}$ and Ag $3d_{3/2}$, which are close to the typical binding energy of metallic Ag, [24] confirming the formation of Ag NPs at surfaces of Fe_3O_4@PDA particles. For comparison, $AgNO_3$ solution was also used as the Ag source for the deposition of Ag NPs. Figure 2.5 reveals the low loading amount and large size of the obtained Ag NPs.

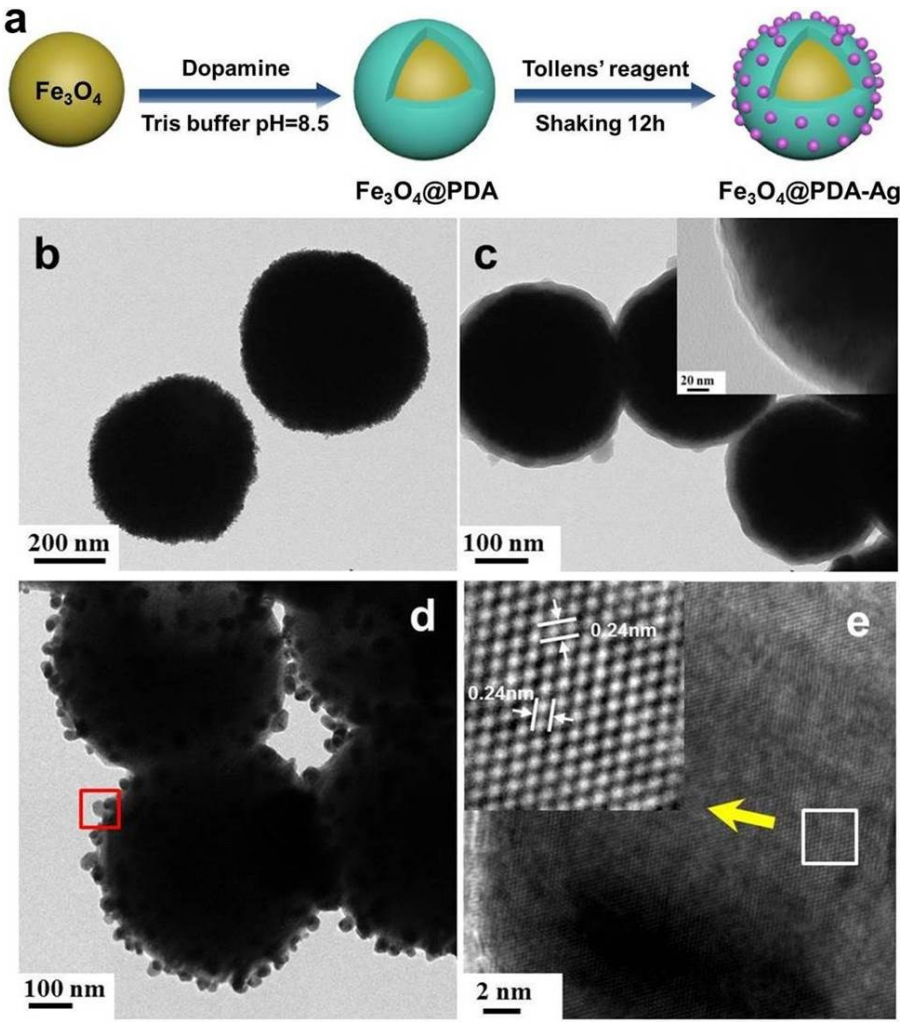

Figure 2.1 (a) Scheme of synthesis route of Fe_3O_4@PDA-Ag core-shell microspheres. TEM images of (b) Fe_3O_4 core microspheres, (c) Fe_3O_4@PDA core-shell microspheres. The inset is a higher-magnification image of dopamine shell layer of Fe_3O_4@PDA core-shell microspheres. (d)

Fe_3O_4@PDA-Ag-10 core-shell microspheres, (e) HRTEM image of Ag NPs enclosed by the red rectangular area in d. The inset is the enlarged image of the white rectangular area in e.

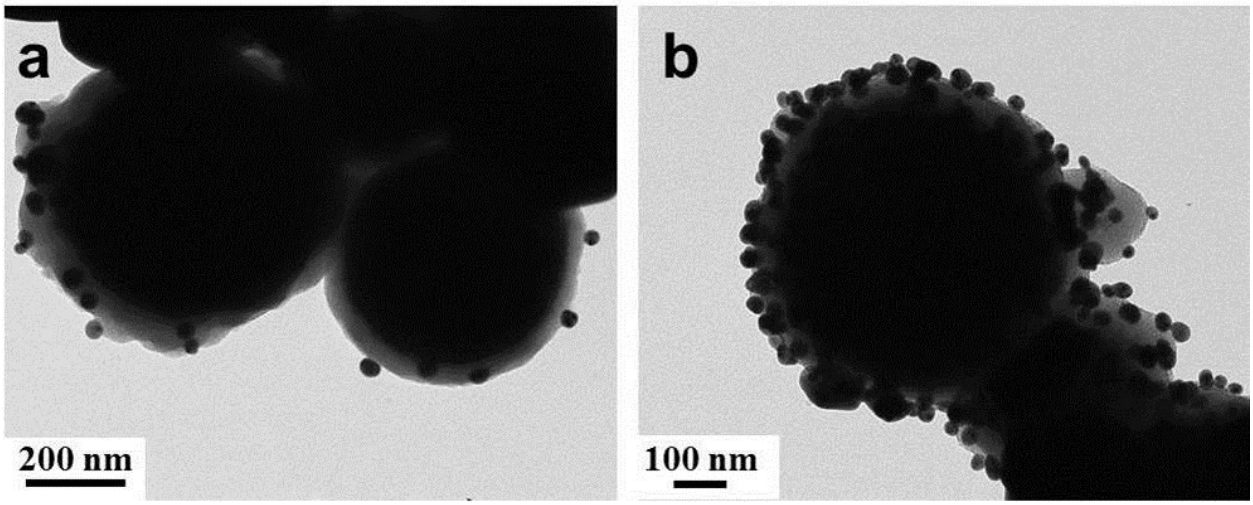

Figure 2.2 TEM images of (a) Fe_3O_4@PDA-Ag-1 (b) Fe_3O_4@PDA-Ag-5.

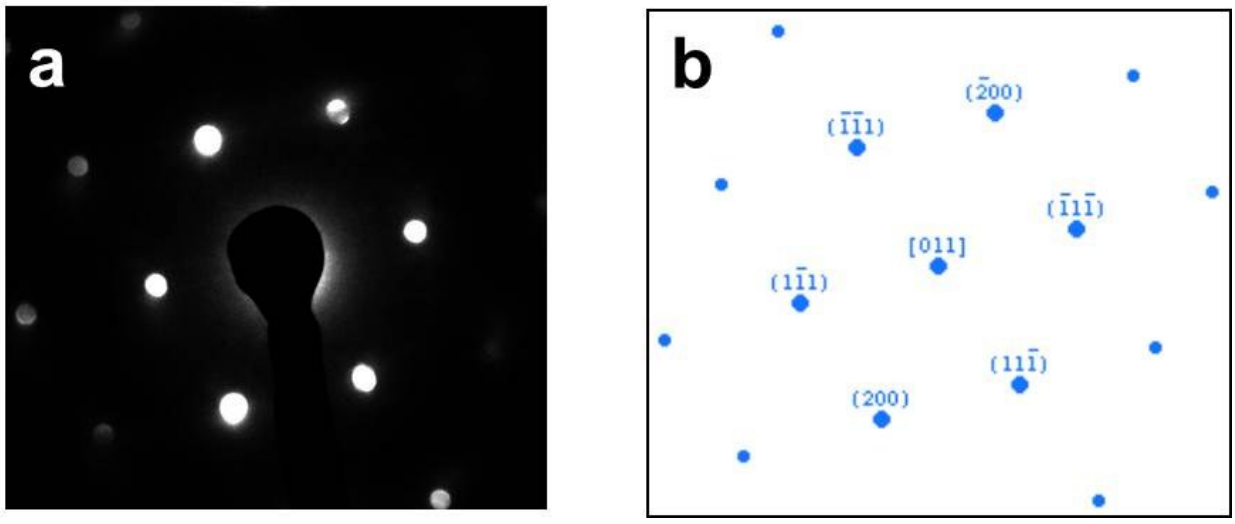

Figure 2.3 (a) NBD pattern of Ag NPs at zone axis of [011]. (b) The diffraction pattern simulation of (a).

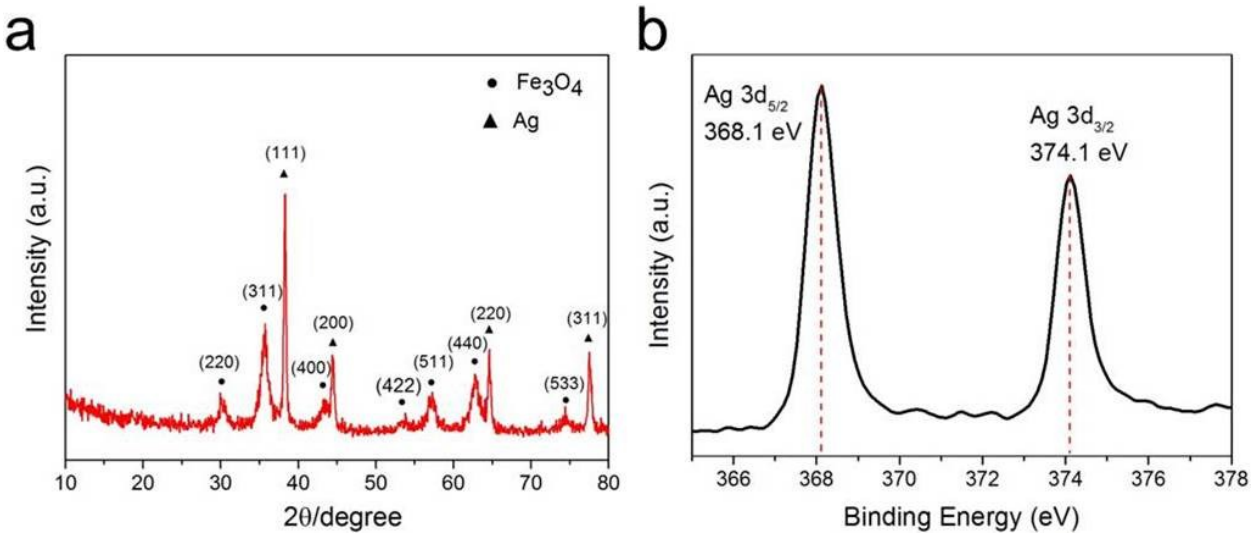

Figure 2.4 (a) XRD patterns of Fe_3O_4 core microspheres and Fe_3O_4@PDA-Ag-10 microspheres. (b) Ag 3d XPS spectra of Fe_3O_4@PDA-Ag-10 microspheres.

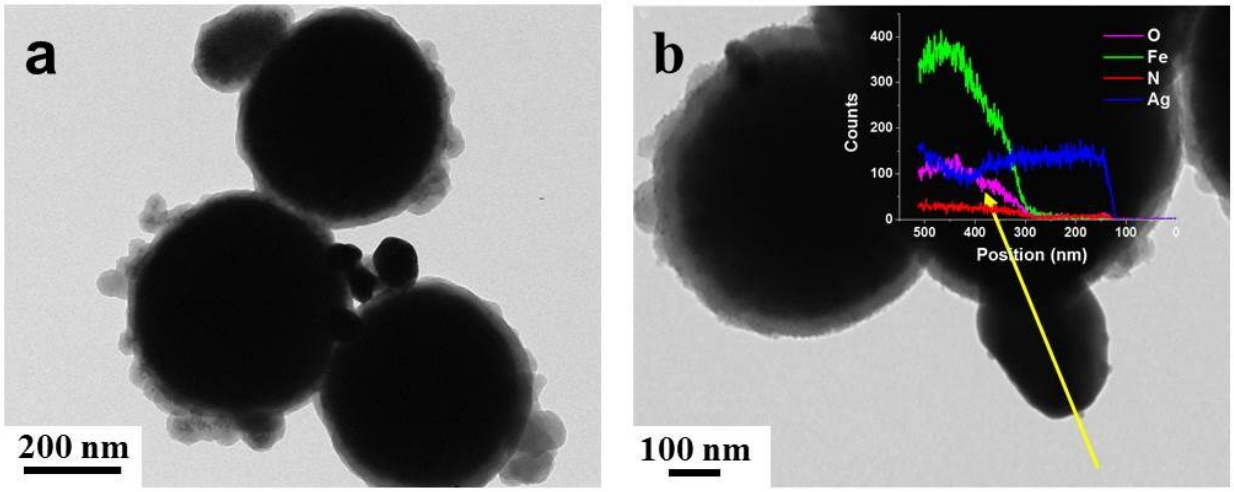

Figure 2.5 (a) Fe_3O_4@PDA-Ag core-shell microspheres prepared by using 10 mg mL^{-1} $AgNO_3$ solution as the Ag source, (b) Fe_3O_4@PDA-Ag core-shell microspheres with an EDX line-scan overlay.

Figure 2.6 shows the magnetic hysteresis loop of Fe_3O_4@PDA-Ag-10 core-shell microspheres at room temperature. The saturation magnetization value (M_s) was measured to be 45.5 emu g^{-1}. It should be noted that almost no hysteresis loops was found in the magnetization curve, suggesting the superparamagnetism of Fe_3O_4@PDA-Ag-10 core-shell microspheres. Owing to the high magnetization values and superparamagnetic characteristics, the Fe_3O_4@PDA-Ag-10 core-shell microspheres can be magnetically separated from aqueous solution within a few seconds and re-dispersed well once the magnet is removed, rendering them economic and reusable for various applications.

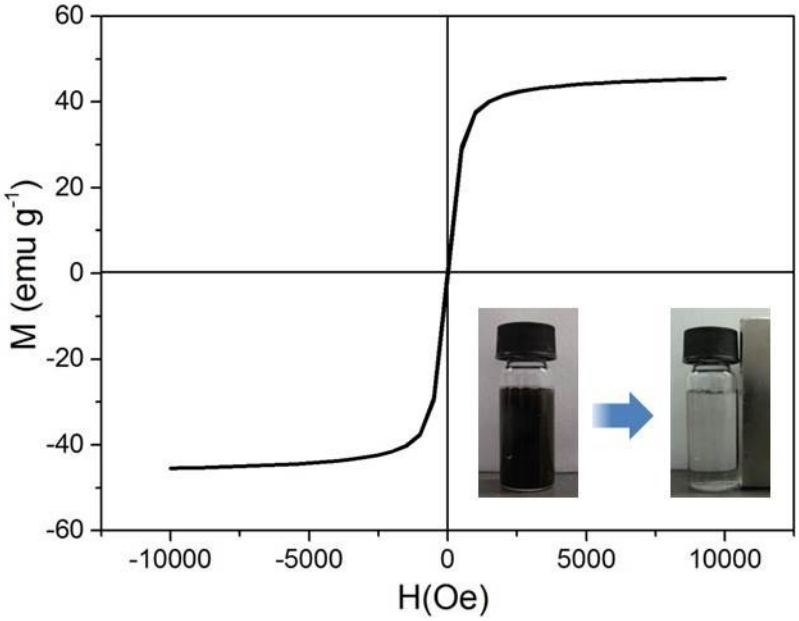

Figure 2.6 Magnetic hysteresis loop of Fe_3O_4@PDA-Ag-10 microspheres. The inset photographs: separation of Fe_3O_4@PDA-Ag-10 microspheres from aqueous dispersion using an external magnet.

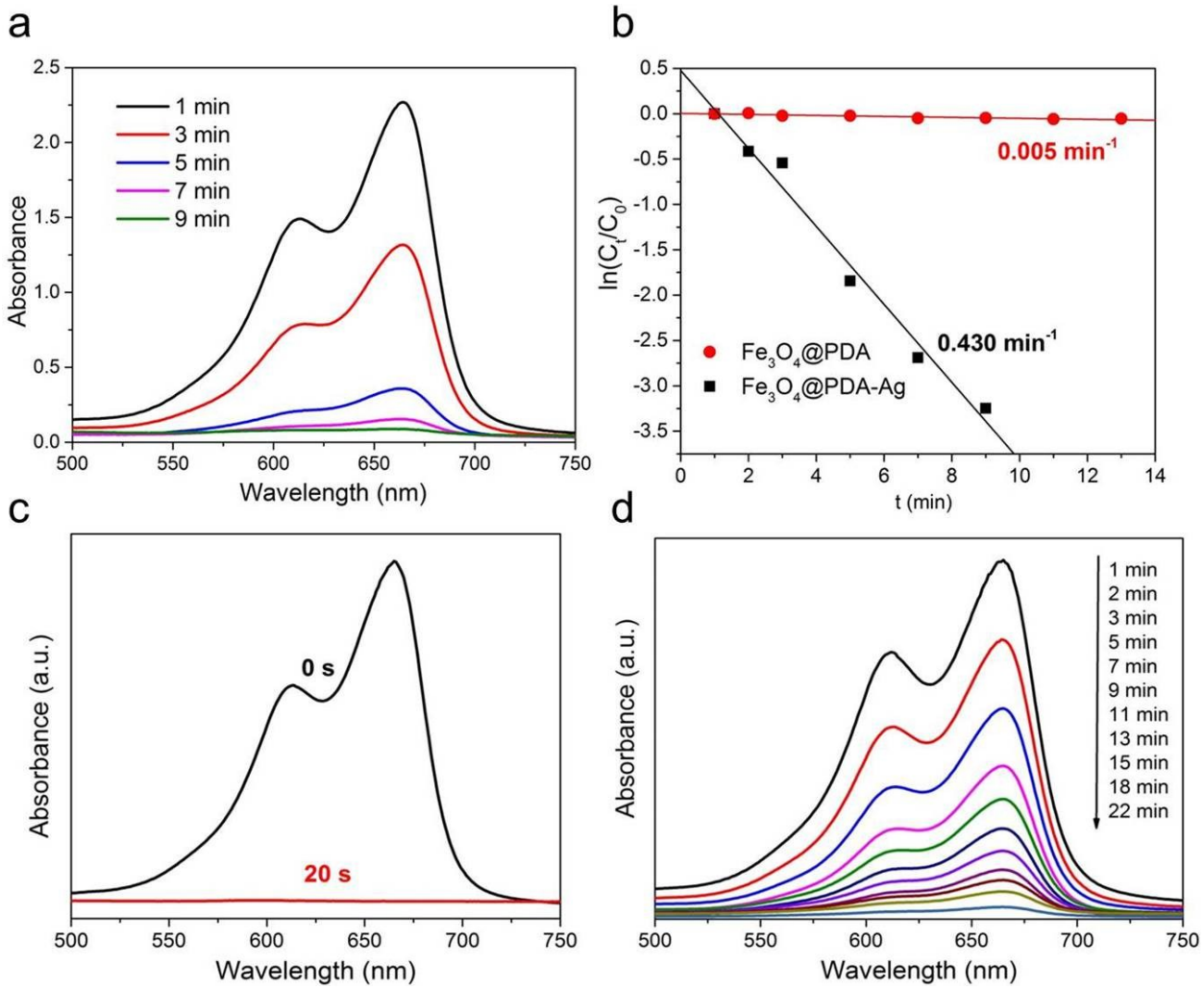

Figure 2.7 (a) Successive UV-vis spectra for catalytic reduction of MB aqueous solution (40 mg L^{-1}) by $NaBH_4$ and Fe_3O_4@PDA-Ag-10 core-shell microspheres. (b) First-order kinetics plot of catalytic reduction of MB in the presence of Fe_3O_4@PDA and Fe_3O_4@PDA-Ag-10 core-shell microspheres. Successive UV-vis spectra for MB (40 mg L^{-1}) catalytic reduction by $NaBH_4$ and Fe_3O_4@PDA-Ag core-shell microspheres prepared by using (c) 10 mg mL^{-1} silver ammonia solution and (d) 10 mg mL^{-1} $AgNO_3$ as the Ag source, respectively.

2.3.2 Catalytic reduction tests

It has been long identified that Ag NPs show excellent catalytic activity and selectivity on many catalytic reactions.[25, 26] Herein, the catalytic reduction of MB by $NaBH_4$ was used as a model reaction to investigate the catalytic performance of Fe_3O_4@PDA-Ag-10 core-shell microspheres This reaction can be monitored by the color bleaching of MB solution after the addition of the catalysts and excess amount of $NaBH_4$, as indicated by the gradual decrease in the maximum absorbance values (λ_{max}= 665 nm) with time in the UV-vis spectra. As shown in Figure 2.7a, the adsorption peak at λ_{max} gradually decreases with respect to reaction time, indicating the reduction of MB by Fe_3O_4@PDA-Ag. To clarify the catalytic effect of Ag NPs, a control experiment was conducted by using Fe_3O_4@PDA as the catalysts. To elucidate the reaction mechanism, the concentration of $NaBH_4$ could be considered as constant throughout the reaction since it was in a great excess (0.1 M). Therefore, pseudo first-order kinetics with regard to the catalytic reduction of MB, described as $\ln(C_t / C_0) = -kt$, can be applied, where C_t is concentration of MB at time t, C_0 is the initial concentration of MB and k is the rate constant.[27] Figure 2.7b reveals the linear relationship between $\ln(C_t/C_0)$ and the reaction time t (C_0=40 mg L^{-1}, V_{MB}=10 mL). The rate constant k of MB catalytic reduction is calculated to be 0.430 min^{-1} at 25°C for the case with Fe_3O_4@PDA-Ag-10 core-shell microspheres; while, as expected, Fe_3O_4@PDA has little catalytic activity with a rate constant of 0.005 min^{-1} (Figure 2.7b). When the initial amount of MB solution was reduced to half (i.e. 5 mL), the reaction could be quickly completed within 20 s with the same amount of catalyst and $NaBH_4$ (Figure 2.7c). It should be noted that despite the comparatively higher concentration of MB solution (C_0=40 mg L^{-1}) used in the current work, the bleaching rate is considerably higher than the rates reported previously

under similar experimental conditions with Ag NPs.[20, 21] This outstanding catalytic performance could be ascribed to the relatively smaller size and higher loading amount of Ag nanoparticles in our developed Fe_3O_4@PDA-Ag-10 core-shell microspheres. By delicately choosing $AgNO_3$ as the Ag source, the Fe_3O_4@PDA-Ag microspheres with larger size of Ag NPs were prepared (TEM images shown in Figure 2.5). Compared with Fe_3O_4@PDA-Ag-10 using silver ammonia as the Ag source (Figure 2.7c), it shows relatively lower catalytic activity (Figure 2.7d) mainly due to the decrease of active sites for catalytic reaction on larger Ag NPs. To investigate the impact of the content of Ag NPs on the catalytic activity of Fe_3O_4@PDA-Ag, two lower concentrations of silver ammonia solution (1 mg mL^{-1} and 5 mg mL^{-1}) were used to prepare Fe_3O_4@PDA-Ag-1 and Fe_3O_4@PDA-Ag-5, respectively. It should be noted that increasing the concentrations of silver ammonia solution did not lead to significant change in the size of Ag NPs, but could enhance the loading content of Ag NPs (Figure 2.2) resulting in better catalytic performance as shown in Figure 2.8.

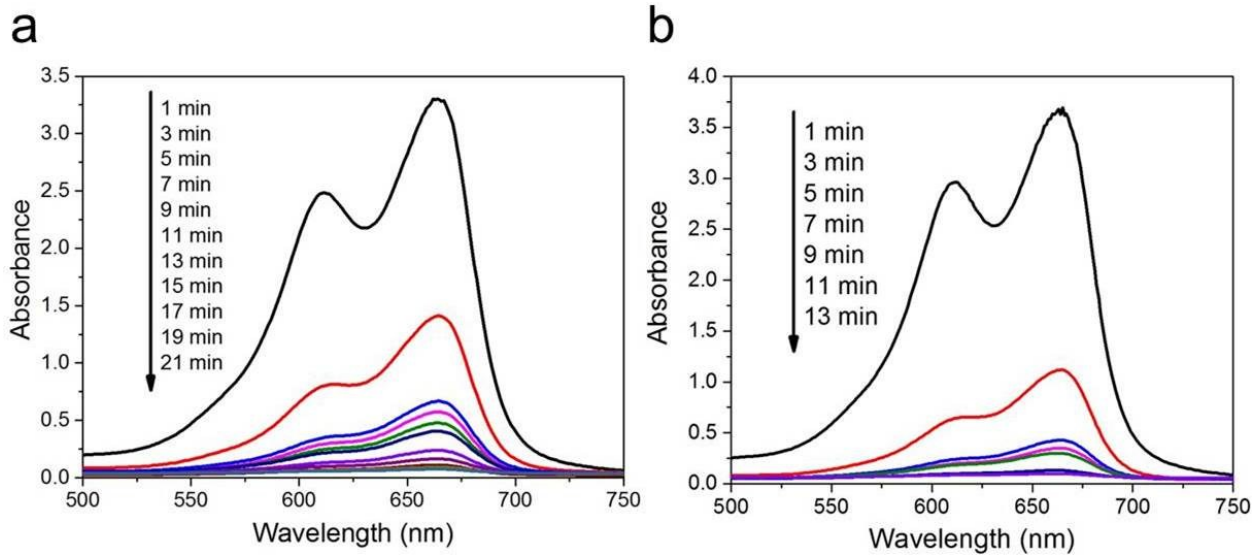

Figure 2.8 Successive UV-vis spectra for catalytic reduction of MB aqueous solution (40 mg L^{-1}) in the presence of $NaBH_4$ and (a) Fe_3O_4@PDA-Ag-1, (b) Fe_3O_4@PDA-Ag-5.

To evaluate the pH effect of the MB solution on the catalytic activity of Fe_3O_4@PDA-Ag-10 microspheres, MB solutions with three different pH values (pH 3, 7, 9) were used for the tests. Figure 2.9a-c shows that there is no significant change on the catalytic activity of Fe_3O_4@PDA-Ag-10 under different pH conditions, which implies that the high catalytic activity of the microspheres could withhold in various solution conditions of different pHs.

Additionally, the catalytic activity of Fe_3O_4@PDA-Ag-10 microspheres on another model organic dye, rhodamine B (RhB), was also tested. Figure 2.10 reveals that the maximum absorbance value at λ_{max}= 554 nm of RhB decreases with reaction time, which demonstrates that Fe_3O_4@PDA-Ag is also able to catalyze the reduction of RhB with $NaBH_4$. The catalytic reaction could be completed within 9 min, as efficient as a previous report employing Ag/SBA-15 as the catalyst [26] despite the comparatively higher concentration of RhB solution in this work. Therefore, the Fe_3O_4@PDA-Ag core-shell microspheres exhibit the potential application as an effective catalyst for the reduction of various organic dyes.

The above results reveal the high catalytic performance of Fe_3O_4@PDA-Ag core-shell microspheres, which are most likely attributed to the strong binding between the PDA layer and Ag NPs due to the strong metal coordination ability of the catechol groups in the PDA layer.[19, 28, 29]

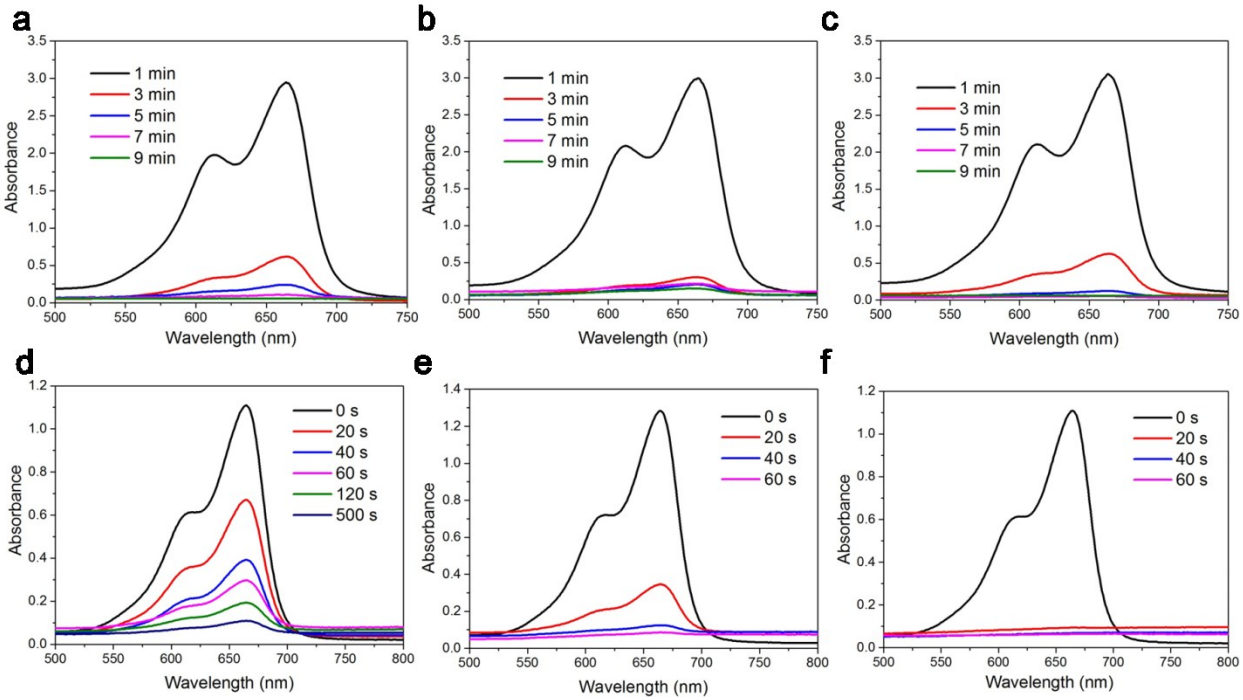

Figure 2.9 Successive UV-vis spectra for catalytic reduction of MB aqueous solution (40 mg L^{-1}) by $NaBH_4$ and Fe_3O_4@PDA-Ag-10 core-shell microspheres at (a) pH 3, (b) pH 7, (c) pH 9. Successive UV-vis spectra for the adsorption of MB aqueous solution (4 mg L^{-1}) by Fe_3O_4@PDA-Ag-10 core-shell microspheres at (d) pH 3, (e) pH 7, (f) pH 9.

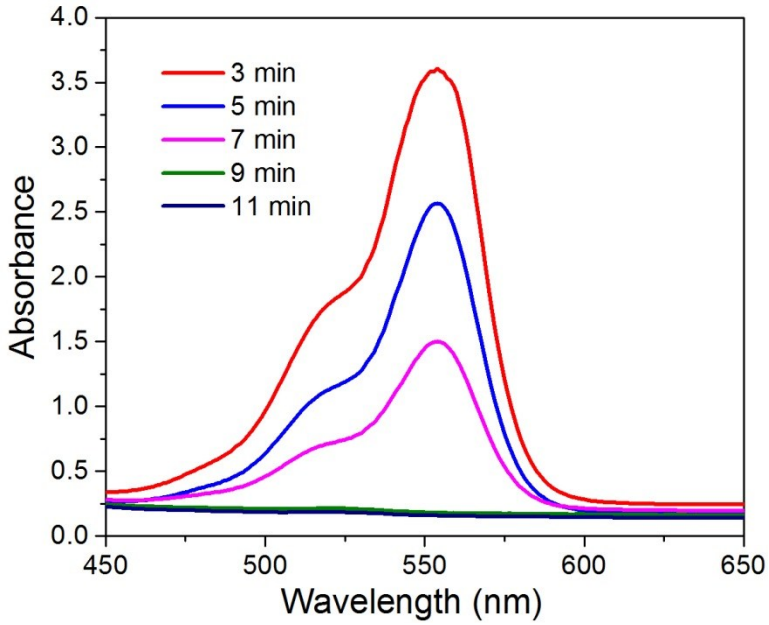

Figure 2.10 Successive UV-vis spectra for catalytic reduction of Rhodamine B aqueous solution (40 mg L^{-1}) by $NaBH_4$ and Fe_3O_4@PDA-Ag-10 core-shell microspheres.

2.3.3 Adsorption tests

Another interesting feature of Fe_3O_4@PDA-Ag microsphere is that it shows efficient adsorption of organic dyes in addition to the high catalytic activity. Again, MB was chosen as a model dye for the adsorption test. UV-vis spectroscopy was applied to monitor the adsorption process of MB after adding Fe_3O_4@PDA-Ag-10 core-shell microspheres under stirring at ambient temperature. As shown in Figure 2.11a, the intensity of the adsorption peak at λ_{max} dropped drastically within 20 s after the adsorbents were added, and the adsorption peak finally vanished after 500 s, indicating their rapid adsorption of MB. Figure 2.11b demonstrates that the adsorption performance of Fe_3O_4@PDA is similar to that of Fe_3O_4@PDA-Ag-10, while Fe_3O_4 shows much lower adsorption capability. Consequently, the remarkable adsorption rate can be

ascribed to the presence of PDA layer. Due to the well-known reducing ability of PDA to many metallic ions,[15, 16, 19, 20] a control experiment was carried out to rule out the possibility of the reduction of MB by PDA layer. The UV-vis spectra of resultant solution after adsorption by Fe_3O_4@PDA microspheres and catalytic reduction product catalyzed by Fe_3O_4@PDA-Ag microspheres were examined. The results are shown in Figure 2.12, from which it was found that the catalytic reduction product (leucomethylene blue) exhibits very strong UV-vis absorption peak at 256 nm, indicating the characteristic aromatic structure of the reduced MB,[30-32] while the UV-vis spectra of the solution after adsorption exhibit no absorption peak at 256 nm. Additionally, the Fe_3O_4@PDA-Ag-10 microspheres also exhibit some adsorption behavior on RhB with a removal efficiency of ~50% in less than 10 min, as shown in Figure 2.13.

The possible adsorption mechanism could be the synergistic effects of electrostatic interaction, π-π interaction and hydrogen bonding between PDA layers and organic dyes.[12] The zeta potential of Fe_3O_4@PDA-Ag-10 at pH 5.8 was determined to be about -45 mV (Figure 2.14), suggesting strong electrostatic interactions with positively charged MB (Figure 2.15). To confirm the presence of electrostatic interactions between PDA layer and MB, the effect of pH on the adsorption behavior of Fe_3O_4@PDA-Ag-10 was investigated. Although it was found that the catalytic activity of Fe_3O_4@PDA-Ag-10 microspheres does not change with pH, the adsorption performance of the microspheres improves with increasing solution pH (Figure 2.9d-f). Figure 2.9d-f shows that the Fe_3O_4@PDA-Ag-10 microspheres adsorb MB faster at higher pH, which is most likely attributed to the stronger electrostatic interactions between the microspheres and MB under higher pH, as confirmed by zeta potential measurement of Fe_3O_4@PDA-Ag-10 which becomes more negatively charged at higher pH (Figure 2.14). According to the previous

results, the magnetically separable Fe_3O_4@PDA-Ag microspheres can be used as a kind of promising efficient adsorbents in wastewater treatment.

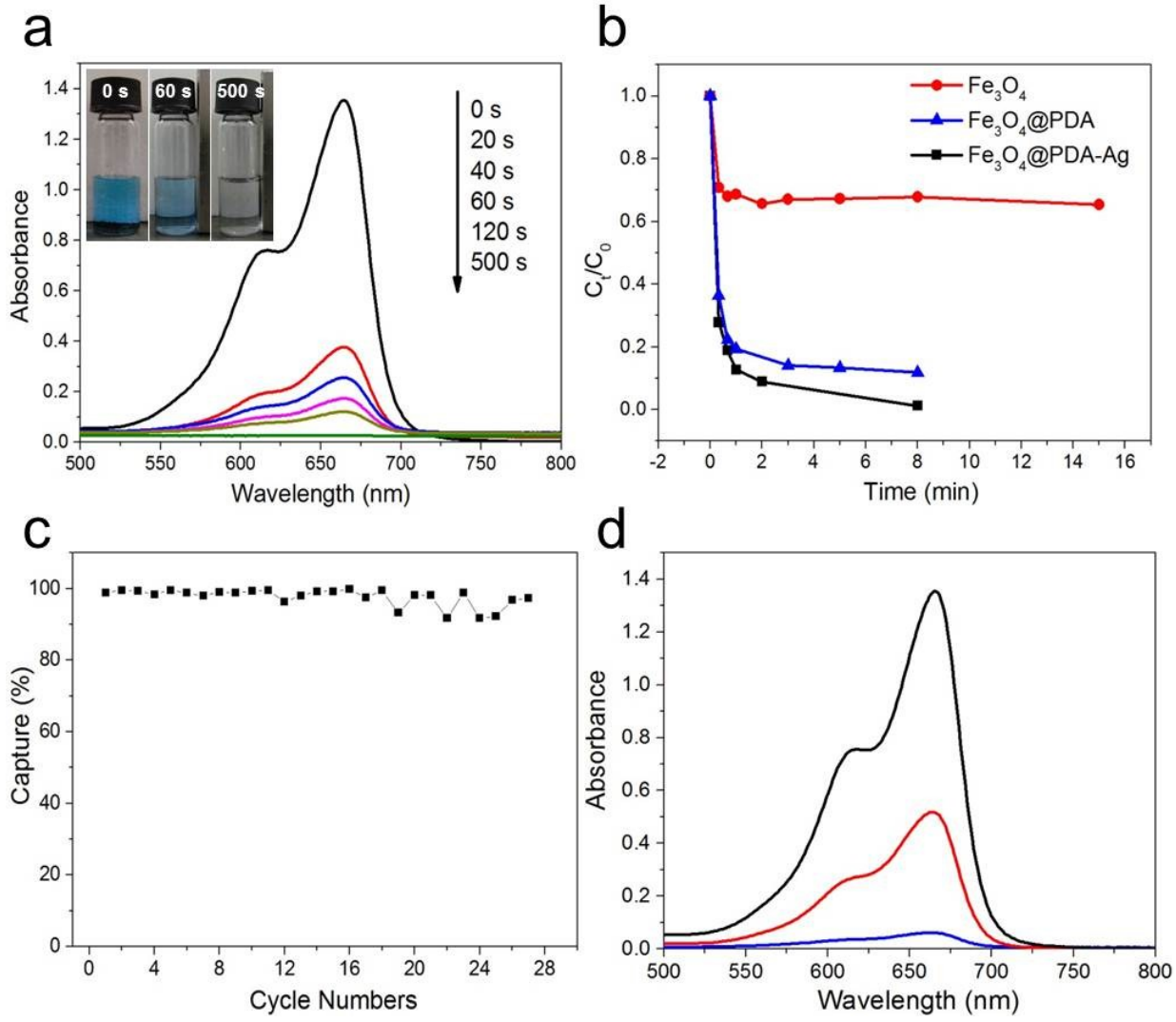

Figure 2.11 (a) Successive UV-vis absorption spectra of MB aqueous solution (4 mg L^{-1}) in the presence of Fe_3O_4@PDA-Ag-10 core-shell microspheres, (b) adsorption rate curves of MB after the addition of different adsorbents, (c) The recyclability of Fe_3O_4@PDA-Ag-10 microspheres for the adsorption of MB, and (d) UV-vis adsorption spectra of MB solution in the presence of adsorbents regenerated with different desorption agents after one cycle: $NaBH_4$ solution first, and then water and ethanol (blue curve), only with water and ethanol (red curve), initial MB

solution (black curve). Inset in (a) shows the color change of MB solution with time after the addition of Fe_3O_4@PDA-Ag-10 microspheres.

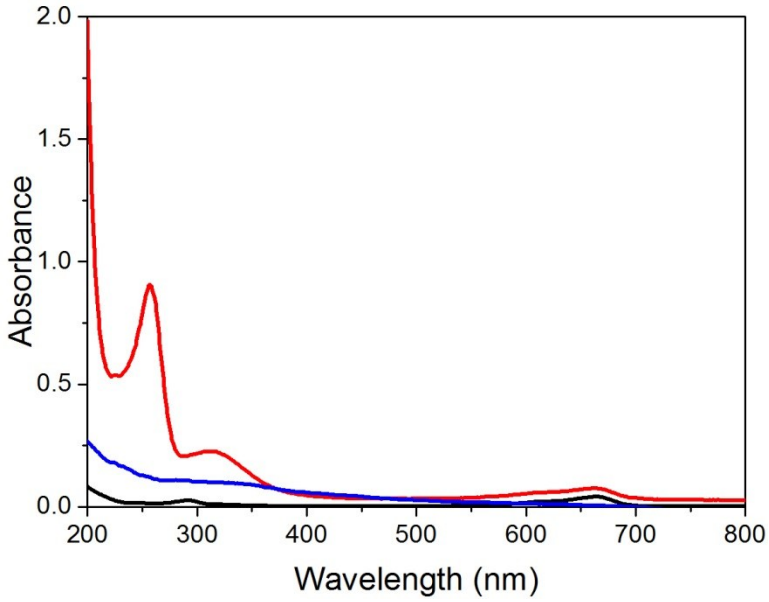

Figure 2.12 Successive UV-vis spectra for reduction product of MB (red curve) and resultant solution after adsorption by Fe_3O_4@PDA (blue curve) and Fe_3O_4@PDA-Ag-10 microspheres (black curve).

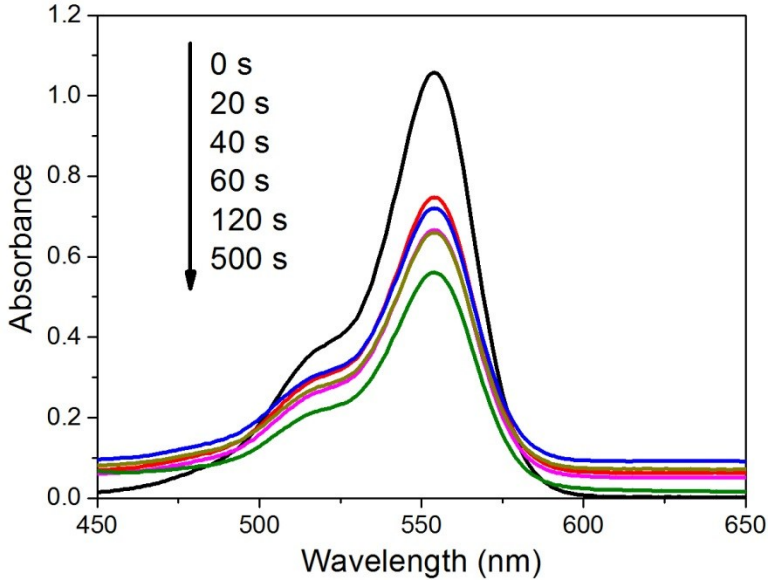

Figure 2.13 Successive UV-vis absorption spectra of rhodamine B solution (4 mg L^{-1}) in the presence of Fe_3O_4@PDA-Ag-10 core-shell microspheres.

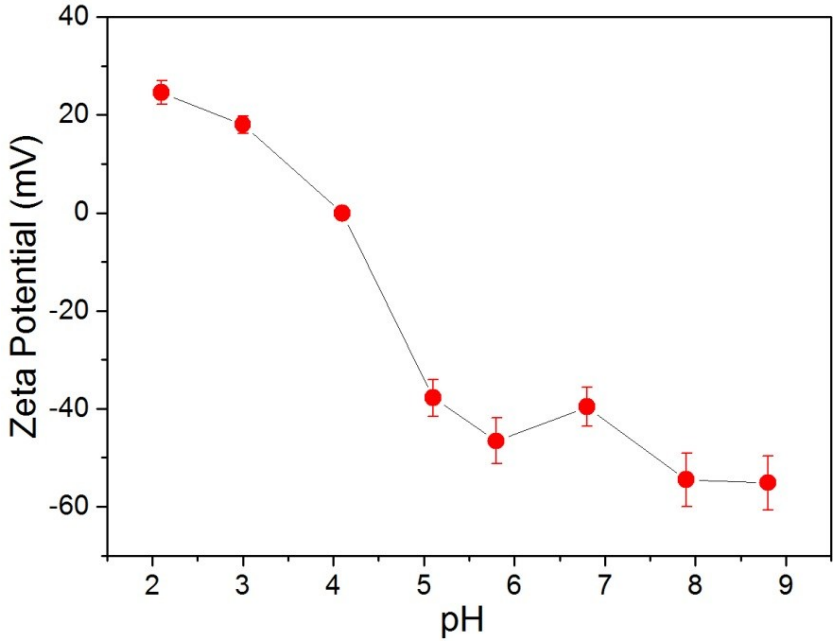

Figure 2.14 Zeta potentials of Fe_3O_4@PDA-Ag-10 under different pH values.

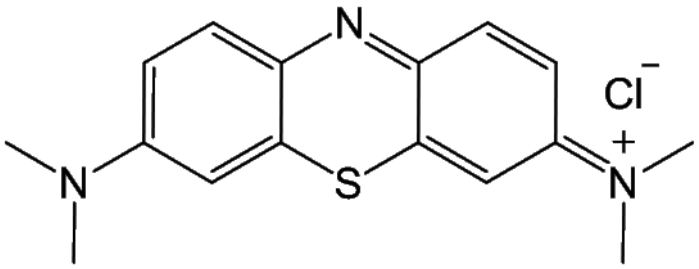

Figure 2.15 The molecular structure of MB.

The recyclability of the adsorbents was also evaluated. Figure 2.11c shows that the Fe_3O_4@PDA-Ag microspheres could be recycled and reused for at least 27 times with a stable adsorption of more than 90%, which is better than the recycle performance of Fe_3O_4@C nanocomposites[27] and graphene or graphene oxide-based hydrogel.[5, 12] Moreover, the recycle process of the novel Fe_3O_4@PDA-Ag materials can be completed in several minutes, faster than the regeneration of hydrogel reported previously which typically last more than 30 minutes.[12, 21]

According to the UV-vis absorption spectra of Figure 2.11d, It should be also noted that only 60% of the adsorbed MB can be removed from the adsorbents under the conventional regeneration procedure (viz. using water and ethanol), as compared with almost 100% removal by the addition of small amounts (2 mL) of $NaBH_4$ solution (1.5 mM) ahead of water and ethanol. The removal efficiency is described as $X\% = 1 - C_t / C_0 = 1 - I_t / I_0$, where *X%* is the removal efficiency on MB, C_0 and C_t are the concentration of MB before and after adsorption by Fe_3O_4@PDA-Ag, respectively, I_0 and I_t are the intensity of absorption peak at 665 nm of MB before and after adsorption by Fe_3O_4@PDA-Ag, respectively. The addition of small amount of $NaBH_4$ can significantly facilitate the removal of MB on Fe_3O_4@PDA-Ag microspheres via a

catalytic process, in which the Fe_3O_4@PDA-Ag microspheres perform as an electron relay system.[33, 34] Firstly, $NaBH_4$ and MB were adsorbed onto the surface of Ag NPs to initiate the catalytic reaction. When the reaction was over, the reduced MB (viz. leucomethylene blue, pK_a=5.8[30]) could be spontaneously desorbed or removed from the surface of Ag NPs and diffused into the solution due to decreased electrostatic interactions between PDA layers and reduced MB after adding $NaBH_4$ solution (pH 9.4).[27, 35] Therefore, the reduced MB could be easily washed away by the addition of ethanol and water consequentially. The presence of reduced MB solution in the catalytic reduction could be confirmed by the forementioned UV-vis spectra (Figure 2.12). The UV-vis spectra of the catalytic reduction product exhibits characteristic absorption peak at 256 nm, which corresponds to the aromatic structure of the reduced MB.[30-32] The whole regeneration process is time-efficient (~ 6 min) and the adsorbents can be easily separated from the reduced MB solution under an external magnetic field. The excellent recyclability and efficient regeneration of the adsorbents might be attributed to the stabilizations of the Ag NPs by PDA layers which prevent reduction in activity due to the coagulation of Ag NPs.[15] Our results suggest that the Fe_3O_4@PDA-Ag materials could be more favorable for practical use in wastewater treatment over conventional adsorbents in terms of long reusability and fast regeneration rate.

2.3.4 Stability tests

The good stability of Fe_3O_4@PDA-Ag microspheres is a critical factor for their practical applications. There are two possibilities that will influence the stability of our developed materials: degradability of PDA layers in the aqueous solution and acid etching of Fe_3O_4. In this work, the long-term stability of PDA films in aqueous solution was first investigated. As shown in Figure 2.16a, even after half a year of soaking in aqueous solution, the distinct PDA layers were still stably coated on the Fe_3O_4 cores with a thickness of ~20 nm and the same morphology as the fresh Fe_3O_4@PDA samples shown in Figure 2.1c, indicating the good stability of PDA layer in aqueous environment over a reasonable long period of time. Meanwhile, due to the fact that Fe_3O_4 microspheres could be easily etched under acid condition, the acid stability of Fe_3O_4@PDA-Ag-10 was also tested under strong acid environment (pH 2 and pH 3) for over 24 hours. The TEM images (Figure 2.16b-c) show that the Fe_3O_4@PDA-Ag-10 microspheres still maintain the core-shell structure under the strong acid conditions. Furthermore, the atomic absorption spectroscopy (AAS) results (Table 2.1) confirm that the Fe_3O_4@PDA-Ag-10 can withstand the strong acid condition, and there were only about 1% (w/w) of the leakage of Fe^{3+}/Fe^{2+} and almost no leakage of Ag^{+} into the solution over 24 hours. Therefore, the robust PDA layer could effectively protect the Fe_3O_4 cores and bind the Ag NPs under strong acid condition and show good stability in practical applications.

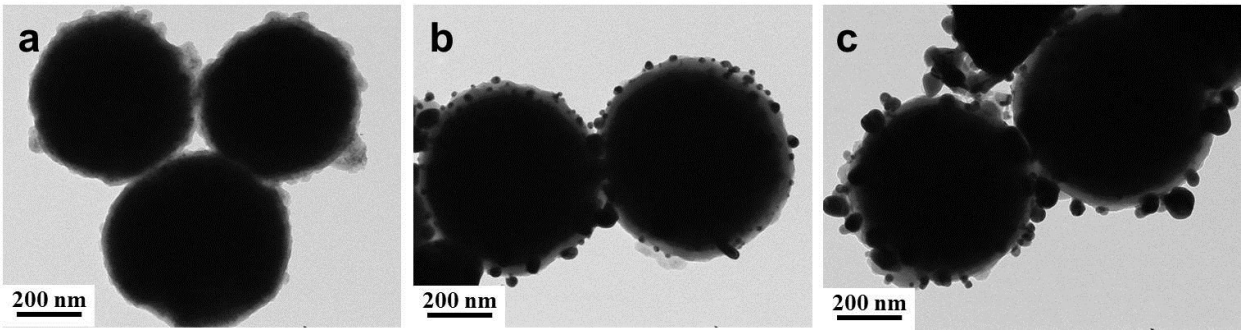

Figure 2.16 TEM images of (a) Fe_3O_4@PDA microspheres dispersed in aqueous solution for half a year, (b) Fe_3O_4@PDA-Ag-10 microspheres dispersed in acid solution with pH 2 for 24 hours, (c) Fe_3O_4@PDA-Ag-10 microspheres dispersed in acid solution with pH 3 for 24 hours.

Table 2.1 AAS results of Fe_3O_4@PDA-Ag-10 microspheres under acid condition.

Sample Name	**pH**	**$C_{Fe^{3+}/Fe^{2+}}$ (mg/L)**	**C_{Ag^+} (mg/L)**	**$W_{Fe^{3+}/Fe^{2+}}$ /W_{sample}**	**W_{Ag^+} /W_{sample}**
Fe_3O_4@PDA-Ag-10	2	5.53	0.07	1.1%	0.014%
Fe_3O_4@PDA-Ag-10	3	4.47	0.07	0.89%	0.014%

2.4 Conclusions

In conclusion, a facile, *in situ*, and efficient approach was demonstrated for the preparation of Fe_3O_4@PDA-Ag core-shell microspheres. These Ag-immobilized microspheres show excellent catalytic capabilities on the reduction of a model organic dye MB with $NaBH_4$ as well as fast adsorption/removal rate of MB from aqueous solutions at different pH values. The remarkable catalytic reduction and adsorption performance can be attributed to the monodisperse Ag NPs and mussel-inspired PDA layers coated on the magnetic microspheres. More importantly, the as-prepared Fe_3O_4@PDA-Ag microspheres exhibit excellent reusability for at least 27 cycles and fast regeneration by using $NaBH_4$ via a unique desorption mechanism of the catalytic process. The superparamagnetic properties of the Fe_3O_4@PDA-Ag microspheres enable them to be easily recovered for reuse under an external magnetic field. Additionally, the Fe_3O_4@PDA-Ag microspheres possess good stability under strong acid condition and can keep in the aqueous solution over long periods of time. The versatile mussel-inspired PDA polymer coatings on the Fe_3O_4@PDA-Ag microspheres also allow the further surface functionalization for the development of multifunctional adsorbent materials. Our results suggest that the Fe_3O_4@PDA-Ag materials developed have great potential applications in catalysis and wastewater treatment.

2.5 References

(1) Wang, P.; Shi, Q.; Shi, Y.; Clark, K. K.; Stucky, G. D.; Keller, A. A. Magnetic Permanently Confined Micelle Arrays for Treating Hydrophobic Organic Compound Contamination. *J. Am. Chem. Soc.* **2008,** *131,* 182-188.

(2) Sui, Z.; Meng, Q.; Zhang, X.; Ma, R.; Cao, B. Green synthesis of carbon nanotube-graphene hybrid aerogels and their use as versatile agents for water purification. *J. Mater. Chem.* **2012,** *22,* 8767-8771.

(3) Yu, K.; Yang, S.; Liu, C.; Chen, H.; Li, H.; Sun, C.; Boyd, S. A. Degradation of Organic Dyes via Bismuth Silver Oxide Initiated Direct Oxidation Coupled with Sodium Bismuthate Based Visible Light Photocatalysis. *Environ. Sci. Technol.* **2012,** *46,* 7318-7326.

(4) Ali, I. New Generation Adsorbents for Water Treatment. *Chem. Rev.* **2012,** *112,* 5073-5091.

(5) Tiwari, J. N.; Mahesh, K.; Le, N. H.; Kemp, K. C.; Timilsina, R.; Tiwari, R. N.; Kim, K. S. Reduced graphene oxide-based hydrogels for the efficient capture of dye pollutants from aqueous solutions. *Carbon* **2013,** *56,* 173-182.

(6) Zhu, T.; Chen, J. S.; Lou, X. W. Highly Efficient Removal of Organic Dyes from Waste Water Using Hierarchical NiO Spheres with High Surface Area. *J. Phys. Chem. C* **2012,** *116,* 6873-6878.

(7) Panizza, M.; Cerisola, G. Direct And Mediated Anodic Oxidation of Organic Pollutants. *Chem. Rev.* **2009,** *109,* 6541-6569.

(8) Moussavi, G.; Mahmoudi, M. Removal of azo and anthraquinone reactive dyes from industrial wastewaters using MgO nanoparticles. *J. Hazard. Mater.* **2009,** *168,* 806-812.

(9) Wu, J.; Wang, J.; Li, H.; Du, Y.; Huang, K.; Liu, B. Designed synthesis of hematite-based nanosorbents for dye removal. *J. Mater. Chem. A* **2013,** *1,* 9837-9847.

(10) Meshko, V.; Markovska, L.; Mincheva, M.; Rodrigues, A. E. Adsorption of basic dyes on granular acivated carbon and natural zeolite. *Water Res.* **2001,** *35,* 3357-3366.

(11) Yan, Y.; Zhang, M.; Gong, K.; Su, L.; Guo, Z.; Mao, L. Adsorption of Methylene Blue Dye onto Carbon Nanotubes: A Route to an Electrochemically Functional Nanostructure and Its Layer-by-Layer Assembled Nanocomposite. *Chem. Mater.* **2005,** *17,* 3457-3463.

(12) Gao, H.; Sun, Y.; Zhou, J.; Xu, R.; Duan, H. Mussel-Inspired Synthesis of Polydopamine-Functionalized Graphene Hydrogel as Reusable Adsorbents for Water Purification. *ACS Appl. Mater. Interfaces* **2012,** *5,* 425-432.

(13) Bandara, N.; Zeng, H.; Wu, J. Marine mussel adhesion: biochemistry, mechanisms, and biomimetics. *J. Adhes. Sci. Technol.* **2012,** *27,* 2139-2162.

(14) Zeng, H.; Hwang, D. S.; Israelachvili, J. N.; Waite, J. H. Strong reversible Fe^{3+}-mediated bridging between dopa-containing protein films in water. *Proc. Natl. Acad. Sci. U.S.A.* **2010,** *107,* 12850-12853.

(15) Liu, R.; Guo, Y.; Odusote, G.; Qu, F.; Priestley, R. D. Core–Shell Fe_3O_4 Polydopamine Nanoparticles Serve Multipurpose as Drug Carrier, Catalyst Support and Carbon Adsorbent. *ACS Appl. Mater. Interfaces* **2013,** *5,* 9167-9171.

(16) Lee, H.; Dellatore, S. M.; Miller, W. M.; Messersmith, P. B. Mussel-inspired surface chemistry for multifunctional coatings. *Science* **2007,** *318,* 426-430.

(17) Zhang, M.; He, X.; Chen, L.; Zhang, Y. Preparation of IDA-Cu functionalized core-satellite Fe_3O_4/polydopamine/Au magnetic nanocomposites and their application for depletion of abundant protein in bovine blood. *J. Mater. Chem.* **2010,** *20,* 10696-10704.

(18) Jeon, E. K.; Seo, E.; Lee, E.; Lee, W.; Um, M.-K.; Kim, B.-S. Mussel-inspired green synthesis of silver nanoparticles on graphene oxide nanosheets for enhanced catalytic applications. *Chem. Commun.* **2013,** *49,* 3392-3394.

(19) Guo, L.; Liu, Q.; Li, G.; Shi, J.; Liu, J.; Wang, T.; Jiang, G. A mussel-inspired polydopamine coating as a versatile platform for the in situ synthesis of graphene-based nanocomposites. *Nanoscale* **2012,** *4,* 5864-5867.

(20) Sureshkumar, M.; Lee, P.-N.; Lee, C.-K. Stepwise assembly of multimetallic nanoparticles via self-polymerized polydopamine. *J. Mater. Chem.* **2011,** *21,* 12316-12320.

(21) Zheng, Y.; Wang, A. Ag nanoparticle-entrapped hydrogel as promising material for catalytic reduction of organic dyes. *J. Mater. Chem.* **2012,** *22,* 16552-16559.

(22) Nadagouda, M. N.; Desai, I.; Cruz, C.; Yang, D. J. Novel Pd based catalyst for the removal of organic and emerging contaminants. *RSC Adv.* **2012,** *2,* 7540-7548.

(23) Liu, J.; Sun, Z.; Deng, Y.; Zou, Y.; Li, C.; Guo, X.; Xiong, L.; Gao, Y.; Li, F.; Zhao, D. Highly water-dispersible biocompatible magnetite particles with low cytotoxicity stabilized by citrate groups. *Angew. Chem. Int. Ed.* **2009,** *48,* 5875-5879.

(24) Guo, X.; Zhang, Q.; Sun, Y.; Zhao, Q.; Yang, J. Lateral Etching of Core–Shell Au@Metal Nanorods to Metal-Tipped Au Nanorods with Improved Catalytic Activity. *ACS Nano* **2012,** *6,* 1165-1175.

(25) Patel, A. C.; Li, S.; Wang, C.; Zhang, W.; Wei, Y. Electrospinning of Porous Silica Nanofibers Containing Silver Nanoparticles for Catalytic Applications. *Chem. Mater.* **2007,** *19,* 1231-1238.

(26) Chi, Y.; Zhao, L.; Yuan, Q.; Li, Y.; Zhang, J.; Tu, J.; Li, N.; Li, X. Facile encapsulation of monodispersed silver nanoparticles in mesoporous compounds. *Chem. Eng. J.* **2012,** *195–196,* 254-260.

(27) Zhu, M.; Wang, C.; Meng, D.; Diao, G. In situ synthesis of silver nanostructures on magnetic Fe_3O_4@C core–shell nanocomposites and their application in catalytic reduction reactions. *J. Mater. Chem. A* **2013,** *1,* 2118-2125.

(28) Zhang, M.; Zheng, J.; Zheng, Y.; Xu, J.; He, X.; Chen, L.; Fang, Q. Preparation, characterization and catalytic activity of core–satellite Au/Pdop/SiO_2/Fe_3O_4 magnetic nanocomposites. *RSC Adv.* **2013,** *3,* 13818-13824.

(29) Ryu, J.; Ku, S. H.; Lee, H.; Park, C. B. Mussel-Inspired Polydopamine Coating as a Universal Route to Hydroxyapatite Crystallization. *Adv. Funct. Mater.* **2010,** *20,* 2132-2139.

(30) Impert, O.; Katafias, A.; Kita, P.; Mills, A.; Pietkiewicz-Graczyk, A.; Wrzeszcz, G. Kinetics and mechanism of a fast leuco-Methylene Blue oxidation by copper(ii)-halide species in acidic aqueous media. *Dalton Trans.* **2003,** 348-353.

(31) Jiang, Y.; Zhang, S.; Ji, Q.; Zhang, J.; Zhang, Z.; Wang, Z. Ultrathin Cu_7S_4 nanosheets-constructed hierarchical hollow cubic cages: one-step synthesis based on Kirkendall effect and catalysis property. *J. Mater. Chem. A* **2014,** *2,* 4574-4579.

(32) Ray, C.; Dutta, S.; Sarkar, S.; Sahoo, R.; Roy, A.; Pal, T. A facile synthesis of 1D nano structured selenium and Au decorated nano selenium: catalysts for the clock reaction. *RSC Adv.* **2013,** *3,* 24313-24320.

(33) Jana, N. R.; Sau, T. K.; Pal, T. Growing Small Silver Particle as Redox Catalyst. *J. Phys. Chem. B* **1998,** *103,* 115-121.

(34) Mallick, K.; Witcomb, M.; Scurrell, M. Silver nanoparticle catalysed redox reaction: An electron relay effect. *Mater. Chem. Phys.* **2006,** *97,* 283-287.

(35) Jiang, Z.-J.; Liu, C.-Y.; Sun, L.-W. Catalytic Properties of Silver Nanoparticles Supported on Silica Spheres. *J. Phys. Chem. B* **2005,** *109,* 1730-1735.

Chapter 3 Efficient Removal of Elemental Mercury (Hg^0) by SBA-15-Ag Adsorbents[ii]

3.1 Introduction

Mercury (Hg) has become one of the most toxic elements to human beings.[1, 2] Although mercury is a trace substance in coal,[3] substantial amounts of mercury are emitted from coal-fired power plants due to the increased coal combustion.[4] Mercury from combustion flue gas commonly displays three chemical forms: elemental (Hg^0), particulate-bound (Hg_p) and oxidized (Hg^{2+}) form.[5, 6] Despite that the oxidized (Hg^{2+}) and particulate-bound (Hg_p) mercury can be relatively easily captured by conventional pollution control facilities,[7, 8] it is more challenging to remove Hg^0 than other forms of mercury because of its insolubility in water and weak interaction on conventional adsorbent particles.[1, 9] According to the previous reports, amalgamation is one of the most effective approaches for Hg^0 removal.[2, 10] In particular, noble metals, such as Au and Ag, can capture Hg^0 by forming Au-Hg or Ag-Hg amalgam. The amalgamation is more stable and stronger than relatively weaker interactions such as van der Waals force and electrostatic interactions commonly involved in physical adsorption, and the Ag-Hg amalgam tends to decompose at high temperature, which provides a potential way to recycle the adsorbent.[9, 11] To date, various strategies have been explored to deposit Ag nanoparticles (NPs) on substrates of high specific surface area.[4, 9, 11, 12] A novel magnetic zeolite-based silver nanocomposite (MgZ-Ag^0) was prepared by ion-exchange and thermal reduction for Hg^0 capture.[12] Luo et al. synthesized carbon nanotube-Ag (CNT-Ag) composite by a simple wet-chemistry and thermal reduction method for Hg^0 removal from flue gases.[9] Most previous studies focused on the

[ii] A version of this chapter has been submitted for publication in *Journal of Materials Chemistry A*.

deposition of Ag NPs on the external surface of zeolite and carbon-based materials, which could not effectively take the advantage of their high specific surface area and would possibly cause the aggregation of Ag NPs under high temperature. Due to the high cost and low specific surface area,[9] it is uneconomical to employ large quantities of pure noble metals for Hg^0 capture. Therefore, choosing suitable porous substrates encapsulating noble metallic NPs within the pores provides a feasible way to reduce the cost of adsorbents as well as enhance their capturing performance of capturing Hg^0.

Mesoporous silica (SBA-15) has been widely used as the matrix materials for loading metallic NPs owing to its high specific surface area and uniform pore size. One advantage of SBA-15 is that it is easy to load noble metallic NPs within the mesopores. For example, Han et al. reported a facile one-step method for the synthesis of Ag-loaded SBA-15 using aniline as the reductant, exhibiting fast catalytic reduction of 4-nitrophenol in the presence of $NaBH_4$.[13] Additionally, SBA-15 can stabilize the Ag NPs within the mesopores even under high temperature, which could effectively prevent the aggregation of Ag NPs. Previous studies show that spherical Ag crystallites could be homogeneously distributed on the mesopores of SBA-15 even prepared at 350 ^oC for 4 h, which displays excellent thermal stability of Ag NPs within SBA-15.[14, 15] Up to now, no study has been reported on the fabrication of SBA-15-Ag for Hg^0 capture.

Herein, we applied a two-step method to incorporate Ag NPs within mesoporous silica (SBA-15) as a novel sorbent of Hg^0 for the first time. $Ag(NH_3)_2^+$ ions were first adsorbed on the surface of SBA-15, and then reduced by trisodium citrate. The presence and distribution of Ag NPs were confirmed by transmission electron microscopy (TEM) and X-ray mapping. The

mercury cold vapour atomic fluorescence spectrophotometry (CVAFS) was applied to explore the mercury capturing efficiency of the adsorbents. The results suggest that our developed Ag-loaded SBA-15 samples exhibit excellent capability to remove Hg^0 from room temperature up to 150 ^oC, which can be regenerated under 350 ^oC for reuse, demonstrating great potential in Hg^0 capture.

3.2 Experimental Methods

3.2.1 Materials

Pluronic P-123, tetraethyl orthosilicate (TEOS), sodium citrate (Na_3Cit) were purchased from Sigma-Aldrich. Hydrochloric acid (HCl, 37%), ammonia hydroxide (28%), silver nitrate ($AgNO_3$) were obtained from Fisher Scientific. All chemicals were directly used without further purification. Ultrapure water prepared with a Millipore Milli-Q water purification system (MA, USA) was used for all experiments.

3.2.2 Synthesis of mesoporous silica (SBA-15)

2.0 g of P123 was dissolved in 62 mL of 2 M HCl at the room temperature. After P123 was completely dissolved, 4.2 g of TEOS was added to this solution and the synthesis was carried out by stirring for 24 h at 40 ^oC. Then the mixture was transferred into an autoclave and aged at 100 ^oC for 24 h. After that, the white precipitate was collected by filtration and dried at 80 ^oC. The product was obtained by removing the P123 template by calcining at 550 ^oC for 5 h.

3.2.3 Synthesis of Ag loaded mesoporous silica (SBA-15-Ag)

To prepare 10 wt% Ag loaded SBA-15, 300 mg of SBA-15 powder was soaked in 10 mL silver ammonia solution containing 52 mg $AgNO_3$ for a day. Silver ammonia solution was prepared by adding ammonia aqueous solution (2 wt.%) into $AgNO_3$ solution until brown

precipitation was just dissolved. Then, 30 mL of trisodium citrate aqueous solution containing 90 mg trisodium citrate was added to this mixture and stirred magnetically for 6 h at 80 ^{o}C. The dried solid was centrifuged with ultrapure water twice and then dried at 60 ^{o}C to obtain 10 wt% Ag loaded SBA-15 sample. 5 wt% Ag loaded SBA-15 was synthesized by using the same procedure with 26 mg $AgNO_3$ and 45 mg trisodium citrate, respectively. For comparison, $AgNO_3$ solution was also used as the Ag source in place of silver ammonia solution accordingly.

3.2.4 Characterization

Powder X-ray diffraction (XRD) patterns were recorded on a Rigaku RU-200B X-ray diffractometer with a rotating anode X-ray generator, Cu Kα radiation (40 kV, 110 mA). The transmission electron microscopy (TEM) and scanning electron microscopy (SEM) images were performed on a Philips (FEI) Morgagni 268 TEM operated at 80 kV and JEOL JAMP 9500F Auger Microscope. The samples are coated with gold film for SEM characterization. The X-ray mapping was analyzed on an energy dispersive X-ray spectroscopy (EDS) system from Oxford Instruments. X-ray photoelectron spectroscopy (XPS) was carried out on a Kratos Axis spectrometer with monochromatized Al Kα. C 1s peak at 284.6 eV was used to correct all XPS spectra. Fourier transform infrared (FT-IR) spectra were collected on Nicolet iS50 FT-IR Spectrometer (Thermo Scientific) using an ATR diamond crystal. Nitrogen adsorption/desorption isotherms were determined using a surface analysis system (iQ2MP, Quantachrome) at -196 ^{o}C. Before measurements, the samples were degassed at 3 h at 200 ^{o}C. The Brunauer-Emmett-Teller (BET) method was applied to calculate the specific surface area in a relative pressure range of 0.05 to 0.15. Pore size was obtained from the adsorption branch of N_2 adsorption-desorption isotherms. The Barrett-Joyner-Halenda (BJH) analysis provided the pore size distributions, and total pore volume was determined at $P/P_0 = 0.975$.

3.2.5 Mercury breakthrough tests

Elemental mercury (Hg^0) breakthrough test were performed on a Tekran model-2500 cold vapour atomic fluorescence spectrophotometer (CVAFS). The experimental setup was shown in Figure 3.1. In summary, 30 mg of adsorbents were loaded into a borosilicate glass u-tube with 4 mm inside diameter, held into a GC oven. The GC oven was used to control the temperature for the adsorbents to capture Hg^0. 200 μL of Hg^0 standard vapour at room temperature was injected at port 1 with an argon flow rate of 40 mL/min. The gold beads (GB) trap was used as a standard mercury preconcentration device to capture remaining Hg^0 vapour which was not adsorbed by the adsorbents. After 3 min, the gold trap was rapidly heated by the heat coil to release the Hg^0. The Hg^0 signal was further detected by CVAFS. The Hg^0 breakthrough was calculated as the ratio between the amounts of captured Hg^0 by gold trap and injected Hg^0 vapour. Regeneration of the adsorbents was achieved by heating under 350 ^oC for 10 min after capturing Hg^0 vapour.

3.2.6 Mercury breakthrough tests

In the test, 14 mg of adsorbents were exposed on continuous flue gas (flow rate: 1.2 L/min) with a composition of 4% O_2, 12% CO_2, 400 ppm SO_2, 300 ppm NO and 77.6 μg/m^3 Hg^0 under different temperature. The concentration of Hg^0 from the outlet of the flue gas was determined by the VM-3000 mercury vapour detector (Mercury Instruments, Germany).

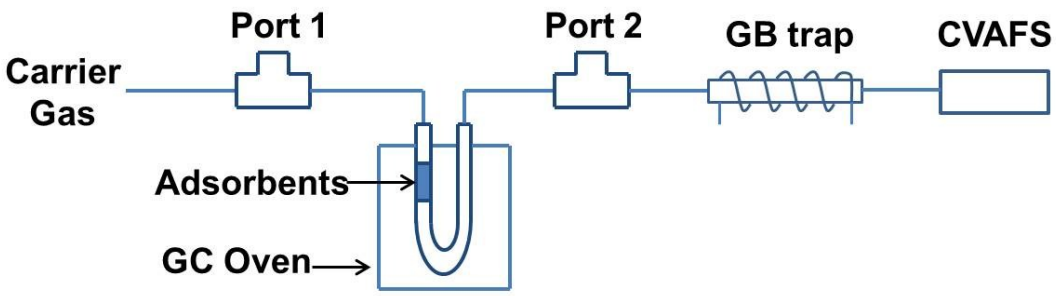

Figure 3.1 Experimental setup of mercury breakthrough test.

3.3 Results and Discussions

3.3.1 Synthesis and Characterizations of Materials

The TEM image (Figure 3.2a) shows the periodically ordered hexagonal pore structure of SBA-15 with a long channel. After soaking SBA-15 in silver ammonia solution and being reduced by trisodium citrate solution, a large number of Ag NPs with the size of 8-9 nm were embedded within the mesopores of SBA-15 as shown in Figure 3.2b-3.2c. Field emission scanning electron microscopy (FE-SEM) images (Figure 3.2d and 3.3) demonstrate that almost no aggregation of Ag NPs could be found on the surface of SBA-15-Ag. For comparison, $AgNO_3$ solution was also used as the Ag source. It was found that large spherical Ag NPs with a size of 40-200 nm were formed on the surface of SBA-15 (Figure 3.4a-b). More large-sized spherical Ag NPs are found in SBA-15 as prepared by 10% $AgNO_3$ (Figure 3.4b) than that of 5% $AgNO_3$ (Figure 3.4a), which could be attributed to the increased concentration of $AgNO_3$ solution. In particular, large Ag clusters could also be found for the sample from the 10% $AgNO_3$ case, as shown in Figure 3.5, indicating that the aggregation of Ag NPs on the exterior surface of SBA-15. Compared with $AgNO_3$ solution, silver ammonia solution serves as a more suitable Ag source for depositing uniform Ag NPs within the mesochannels of SBA-15, which is more favourable for further applications.

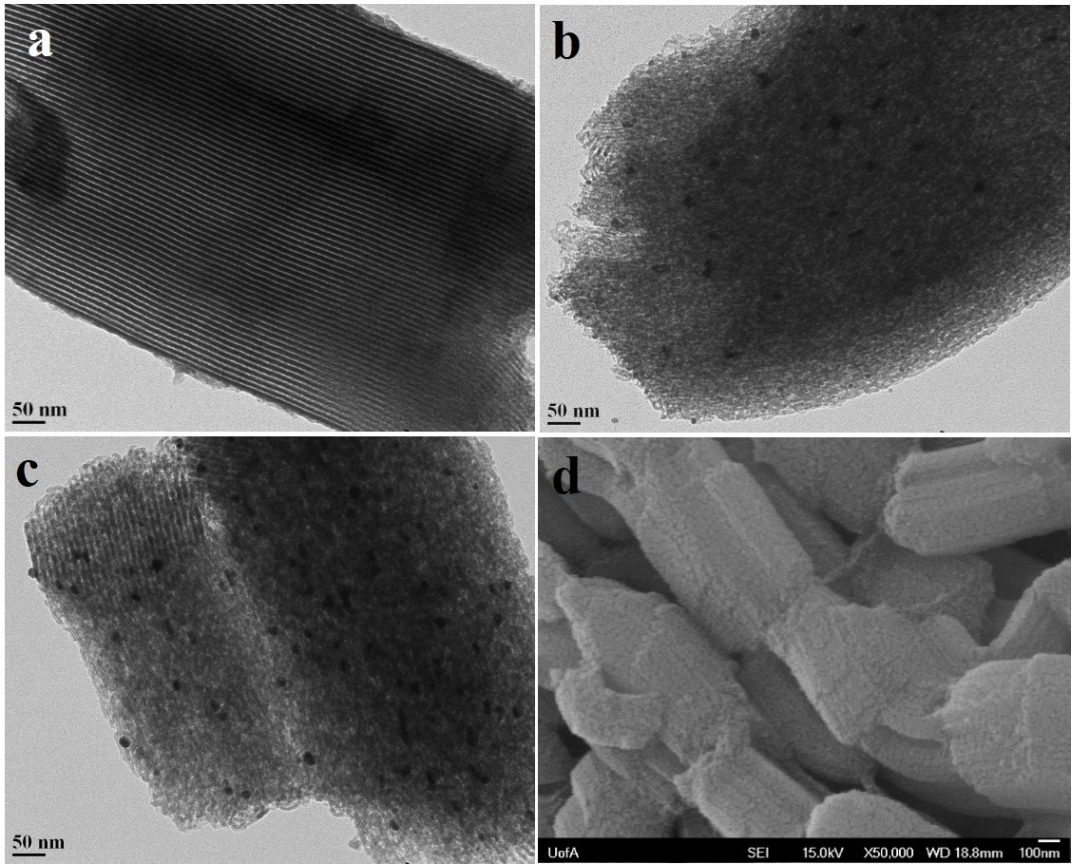

Figure 3.2 TEM images of (a) SBA-15, (b) SBA-15-5% Ag, (c) SBA-15-10% Ag. (d) FE-SEM image of SBA-15-10% Ag.

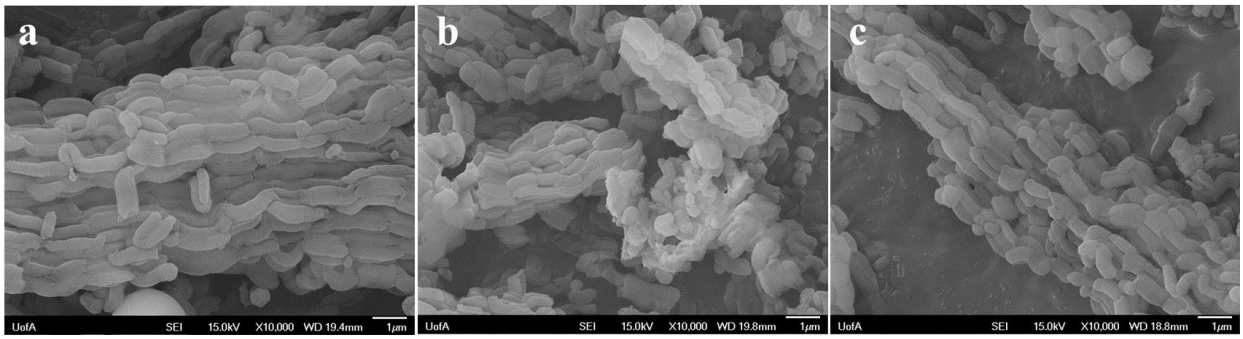

Figure 3.3 SEM images of (a) SBA-15, (b) SBA-15-5% Ag, (c) SBA-15-10% Ag when using silver ammonia solution as the Ag source.

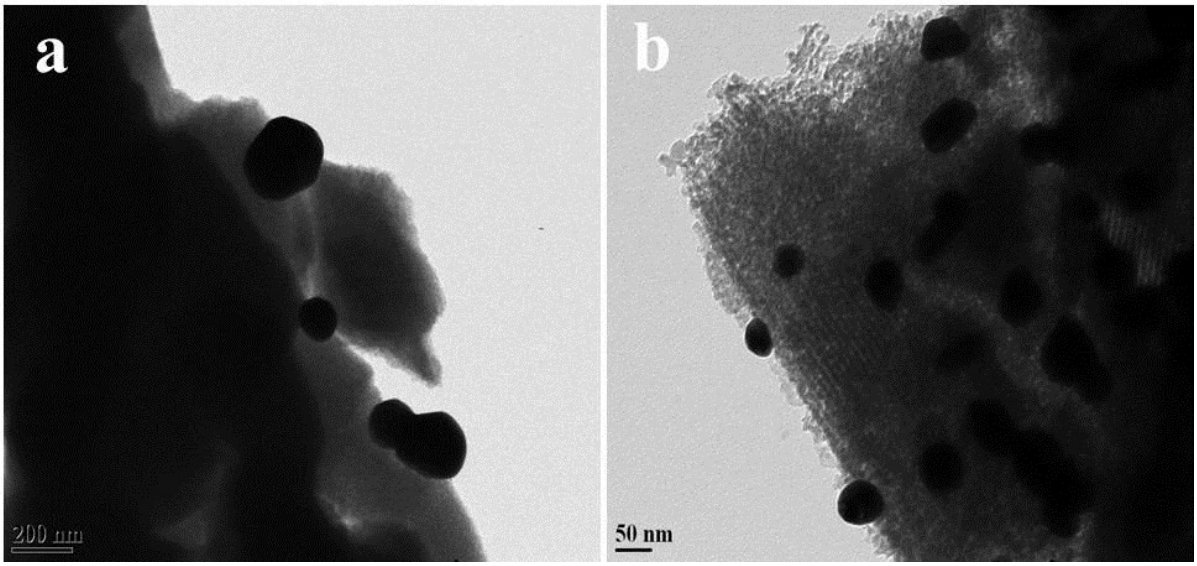

Figure 3.4 TEM images of (a) SBA-15-5% Ag, (b) SBA-15-10% Ag when using $AgNO_3$ solution as the Ag source.

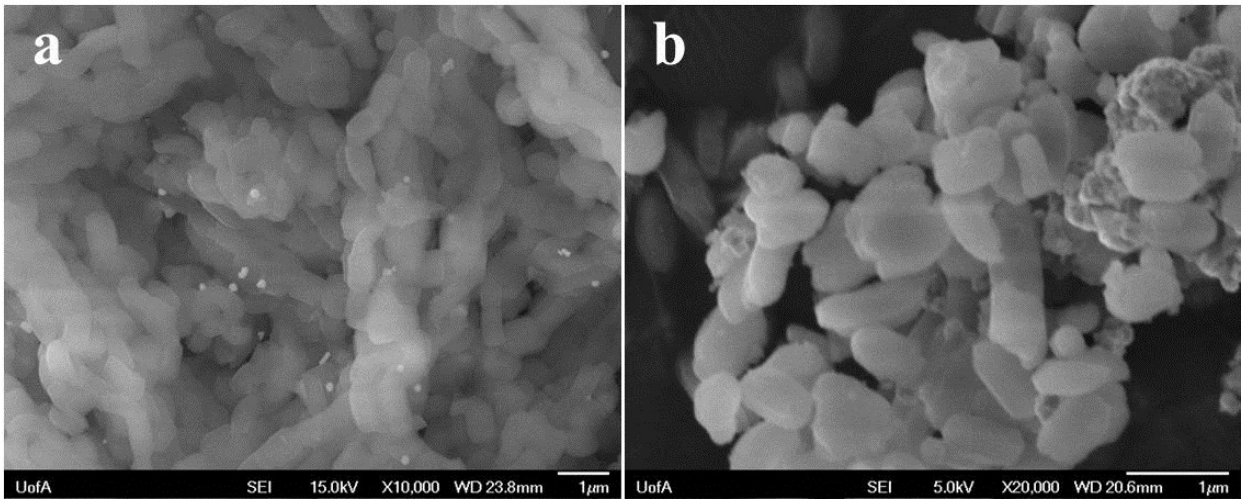

Figure 3.5 SEM images of (a) SBA-15-5% Ag, (b) SBA-15-10% Ag when using $AgNO_3$ solution as the Ag source.

The crystal structure and surface properties of the as-prepared SBA-15 and SBA-15-Ag were characterized by X-ray diffraction (XRD) and X-ray photoelectron spectroscopy (XPS), respectively. Figure 3.6a shows the broad peak in the range of 15°-30°, indicating the amorphous structure of silica. However, only SBA-15-10% Ag exhibits the characteristic peak at $2\theta = 38.0°$, which corresponds to the (111) planes of crystalline face-centered-cubic Ag (JCPDS card No. 04-0783), indicating the nano-sized of Ag NPs in SBA-15-10% Ag sample. There is no characteristic peak around 38.0°, indicating the small size of Ag NPs, which is also in good agreement with the TEM results. Figure 3.6b shows the Ag 3d XPS spectrum of SBA-15-10% Ag sample. The peaks at about 368.0 eV and 374.0 eV can be attributed to the binding energies of Ag $3d_{5/2}$ and Ag $3d_{3/2}$, which is close to the reported data of bulk Ag^0.[16]

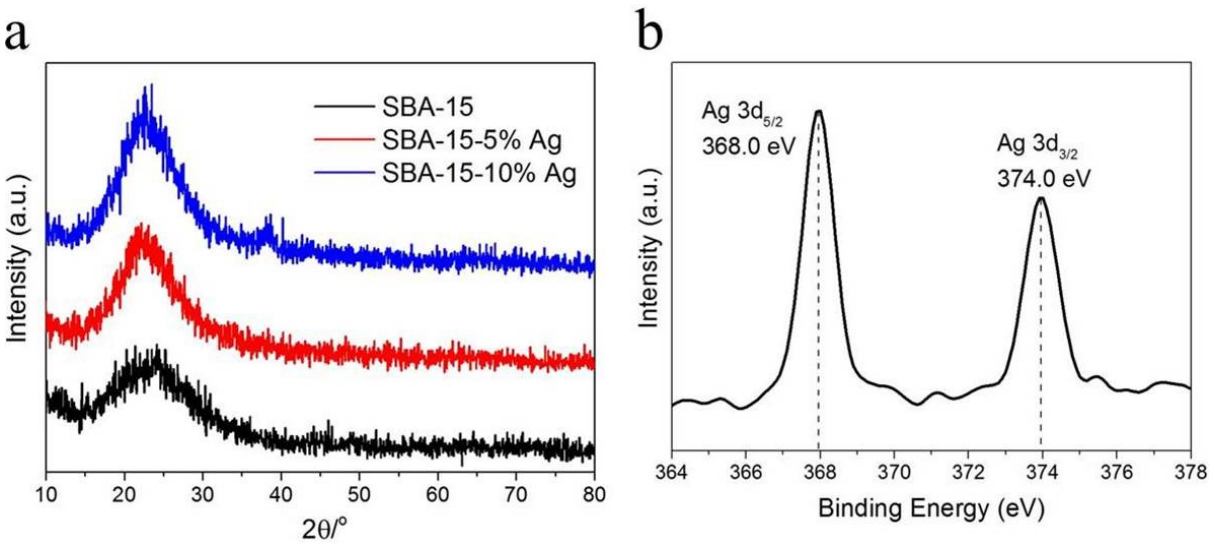

Figure 3.6 (a) Wide-angle XRD patterns of (a) SBA-15, (b) SBA-15-5% Ag. (c) SBA-15-10% Ag; (b) Ag 3d XPS spectrum of SBA-15-10% Ag.

In order to determine the elemental compositions of SBA-15-Ag and spatial distributions of different elements in the samples, SBA-15-5% Ag and SBA-15-10% Ag were analyzed with scanning electron microscopy element energy-dispersive X-ray spectroscopy (SEM-EDX). As shown in Figure. 3.7b, the characteristic peaks of Si, O and Ag confirm that the SBA-15-Ag samples are composed of Si, O and Ag elements, further validating the compositional results of XRD and XPS. The presence of Au peak is due to the gold coating in the sample preparation for SEM analysis. Furthermore, the X-ray mapping image (the inset of Figure 3.7b) demonstrates the uniform dispersion of Ag across the SBA-15-Ag sample, which agrees well with the results of TEM. The EDX results show that the Ag loading amount of SBA-15-5% Ag and SBA-15-10% Ag is 2.27% and 2.86%, respectively, indicating a slight increase of Ag loading amount when the concentration of Ag source solution increases from 5% to 10%. However, when $AgNO_3$ was used as the Ag source, distinct concentrated Ag signals can be found in the X-ray mapping image

(Figure 3.8), suggesting the aggregation of large Ag clusters. The Fourier transform infrared (FT-IR) spectra (Figure 3.9) of the SBA-15 and SBA-15-Ag show the asymmetric and symmetric stretching vibration of Si-O-Si bond at 1040 cm^{-1} and 810 cm^{-1}, respectively. There is no difference in FTIR spectra between SBA-15-Ag and SBA-15, implying that the integration of Ag NPs does not change the framework of SBA-15.

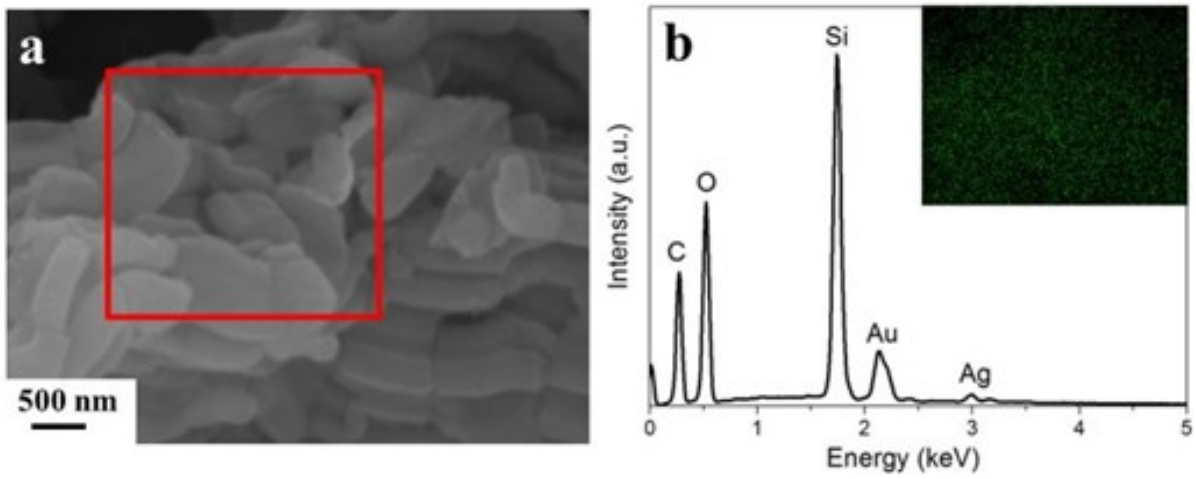

Figure 3.7 (a) The SEM image of SBA-15-10% Ag (b) EDX patterns of SBA-15-10% Ag within the red rectangular area of SEM image. The inset is X-ray mapping image of Ag element according to the SEM image.

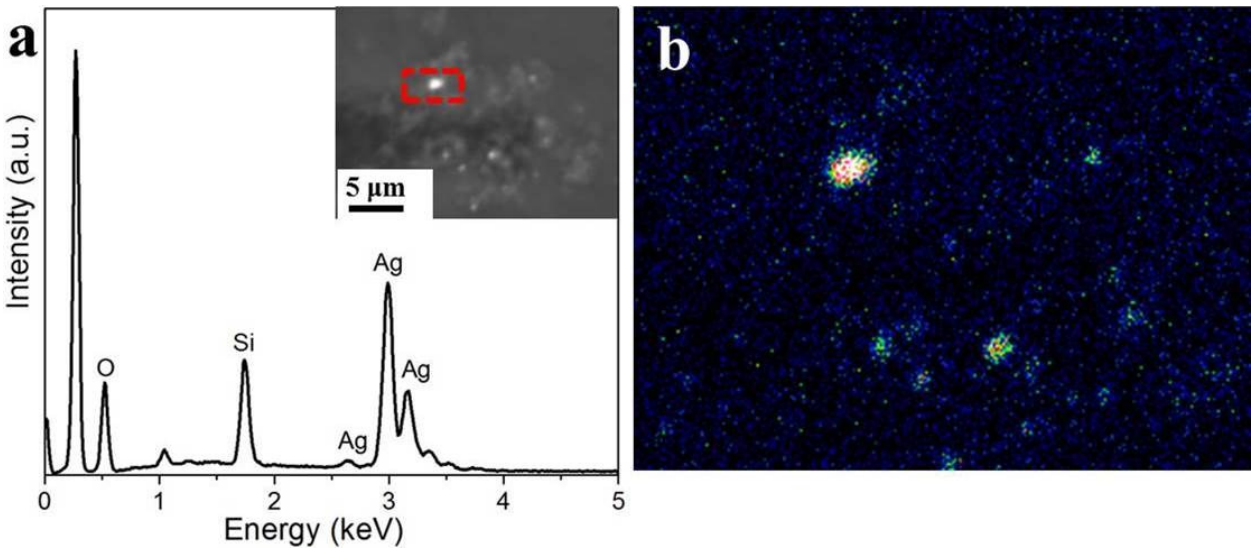

Figure 3.8 (a) The backscattered electron (BSE) image of SBA-15-10% Ag using $AgNO_3$ solution as the Ag source and its corresponding EDX pattern in the red rectangular area. (b) X-ray mapping image of Ag element according to the BSE image.

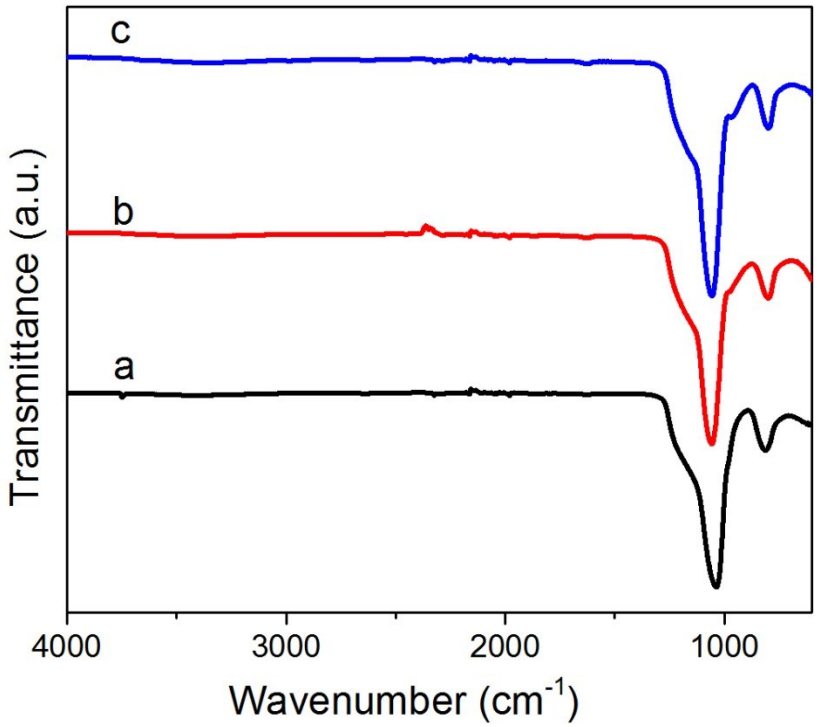

Figure 3.9 FTIR spectra of (a) SBA-15, (b) SBA-15-5% Ag, (c) SBA-15-10% Ag.

The UV-vis spectra of SBA-15 and SBA-15-Ag (Figure 3.10) show that SBA-15-5% Ag and SBA-15-10% Ag exhibit the distinct characteristic surface plasmon resonance peak of Ag NPs at 365 nm and 400 nm, respectively.[17, 18] With the increase of the concentration of Ag source solution, the surface plasmon resonance peaks of samples become broader and stronger, indicating the higher Ag loading amount.

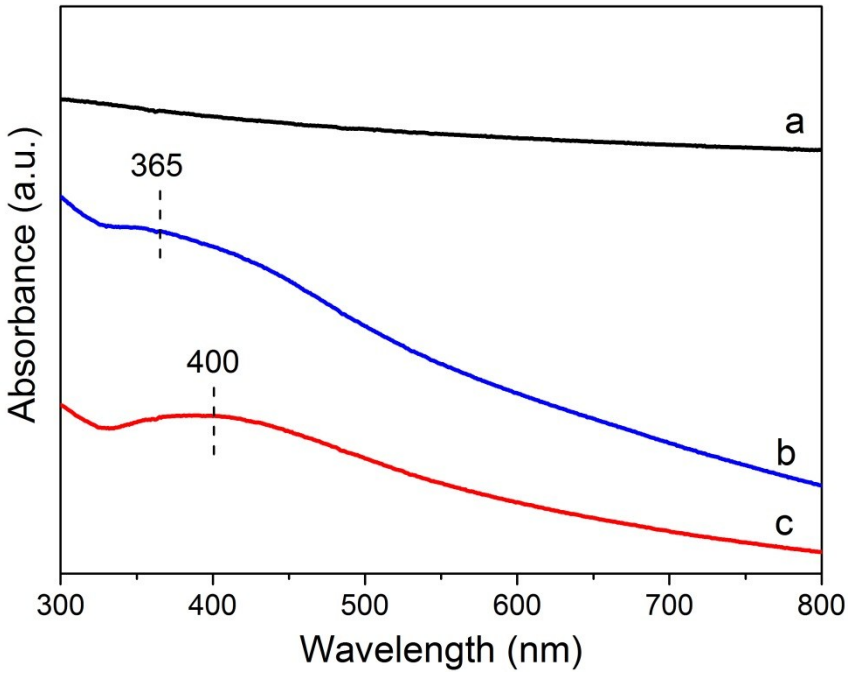

Figure 3.10 UV-vis adsorption spectra of (a) SBA-15, (b) SBA-15-5% Ag, (c) SBA-15-10% Ag.

The N_2 adsorption-desorption isotherms for SBA-15 are shown in Figure 3.11, representative of type-IV curves with H1 hysteresis loop according to the International Union of Pure and Applied Chemistry (IUPAC), suggesting the characteristics of typical mesoporous materials,[20, 21] which possesses cylindrical pores with a narrow pore size distribution at 5.7 nm (Table 3.1). Three well-distinguished regions of the adsorption isotherms were evident: (1) monolayer-multilayer adsorption (P/P_0 = 0-0.60); (2) capillary condensation (P/P_0 = 0.65-0.76); (3) multilayer adsorption on the outer surface (P/P_0 = 0.76-1.0).[22] In the case of SBA-15-5% Ag and SBA-15-10% Ag, the adsorption-desorption isotherm retains type-IV isotherm while with the combination of H1 and H3 hystersis loop. Additionally, the upper closure point of the hysteresis loop of SBA-15-Ag samples appears at a higher relative pressure (P/P_0 =0.95) than

that of SBA-15 samples (P/P_0 =0.76). The increase of P/P_0 is due to the presence of Ag NPs within the mesopores of SBA-15 which could block and distort some of the pores, resulting in the increase of pore diameter.[19, 22, 23] The BET surface area, pore volume, and pore size were determined by N_2 adsorption-desorption isotherms (Table 3.1). As shown in Table 3.1, it should be noted that SBA-15 possesses very high surface area (815.7 m^2/g) and large pore volume (~1 cm^3/g), while after loading with Ag NPs, both the specific surface area and pore volume decrease. The obtained surface area of SBA-15-Ag is still sufficient high for mercury (Hg) capture. The drop in the surface area and increase in the pore size after loading the Ag NPs could be attributed to the deposition of Ag NPs within the pores of SBA-15 matrix which leads to the blockage of some of the pore channels.[23] Minor difference in BET surface area, pore volume and pore size was observed between SBA-15-5% Ag and SBA-15-10% Ag which might be due to the slight difference in Ag loading amount based on the EDX results.

Table 3.1 Physical parameters of pore structures and specific surface area of different adsorbents.

Sample	BET surface area (m^2/g)	Pore volume (cm^3/g)	Pore size (nm)
SBA-15	816	0.99	5.7
SBA-15- 5% Ag	355	0.86	9.6
SBA-15- 10% Ag	319	0.81	9.5

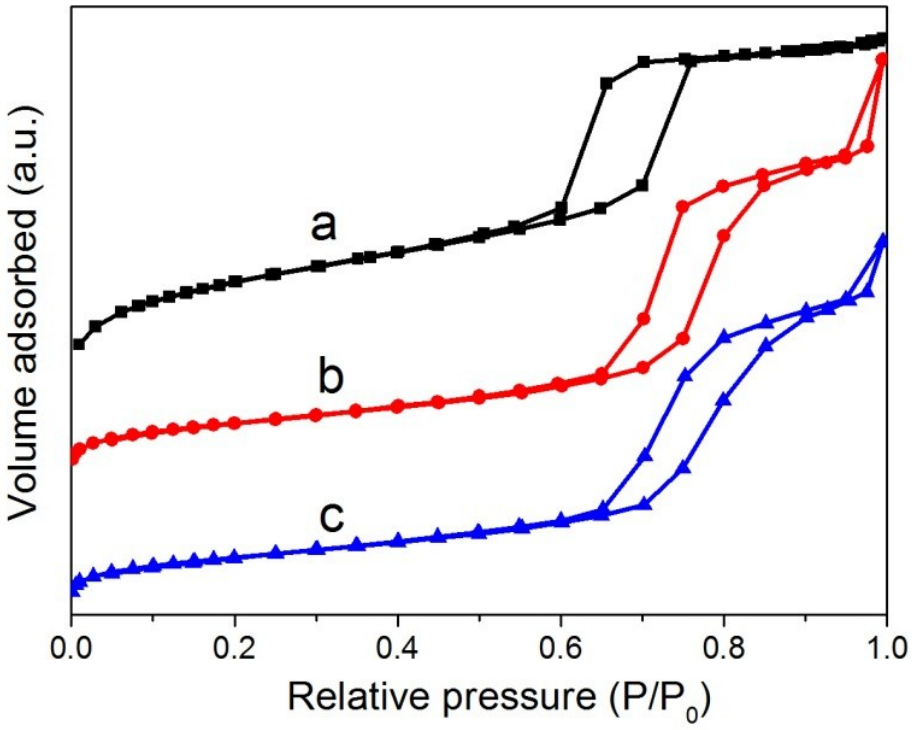

Figure 3.11 Nitrogen adsorption-desorption isotherms of (a) SBA-15, (b) SBA-15-5% Ag and (c) SBA-15-10% Ag.

3.3.2 Mercury breakthrough tests

To investigate the elemental mercury (Hg^0) capturing capability of the as-prepared SBA-15 and SBA-15-Ag, the Hg^0 breakthrough (percentage of mercury release) was examined over a wide temperature range between 25 ºC to 200 ºC. The Hg^0 breakthrough was monitored by CVAFS. The experimental setup for mercury breakthrough test was shown in Figure 3.1. Figure 3.12 shows the Hg^0 breakthrough as a function of temperature for SBA-15, SBA-15-5% Ag and SBA-15-10% Ag. As expected, the pure SBA-15 samples exhibit almost negligible Hg^0 capturing capability, showing a Hg^0 breakthrough above 70% even at room temperature. Therefore, it is obvious that the pure SBA-15 materials are not effective for mercury emission

control. The limited Hg^0 capturing capability of SBA-15 at room temperature could be contributed to the physical adsorption of Hg^0 on the surface of SBA-15.[9] However, the physical adsorption is no longer effective at higher temperature, so SBA-15 cannot capture Hg^0 at temperature higher than 50 ^oC. Therefore, further functionalization on SBA-15 such as encapsulation of noble metallic NPs is needed to improve the Hg^0 capturing capability.

After the deposition of Ag NPs on SBA-15, both 5% Ag and 10% Ag samples (30 mg) can capture more than 90% of the injected mercury (200 μL Hg^0 vapour mixed with the Ar carrier gas at a flow rate of 40 mL/min) up to 150 ^oC (Fig. 3.12), indicating promising potential applications on mercury emission control in Rankine cycle coal-fired power plants, of which the flue gas temperature could reach 150 ^oC.[12, 24] It should also be noted that the Hg^0 breakthrough of two SBA-15-Ag samples increases at higher temperature and reach 100% above 200 ^oC, revealing a complete release of Hg^0 that was initially adsorbed by SBA-15-Ag, so it is feasible to regenerate the adsorbents above this temperature. Compared with the results of Hg^0 capture performance of pure SBA-15 samples, it can be concluded that the significant improvement in Hg^0 capture by SBA-15-Ag is attributed to the presence of Ag NPs. The possible adsorption mechanism could be the amalgamation of Hg^0 with Ag NP, which is more stable than physical adsorption.[11, 12] Similar results in other Ag-based adsorbents, such as Ag-CNT[9] and MagZ-Ag,[4, 12] also suggest the effect of Ag NPs on Hg^0 capture via the amalgamation mechanism. Considering the good Hg^0 capturing performance and relatively low loading amount of Ag, it is advantageous to use SBA-15-Ag as the adsorbents for Hg^0 capture due to the relatively lower cost of SBA-15-Ag than pure Ag nanopowders.

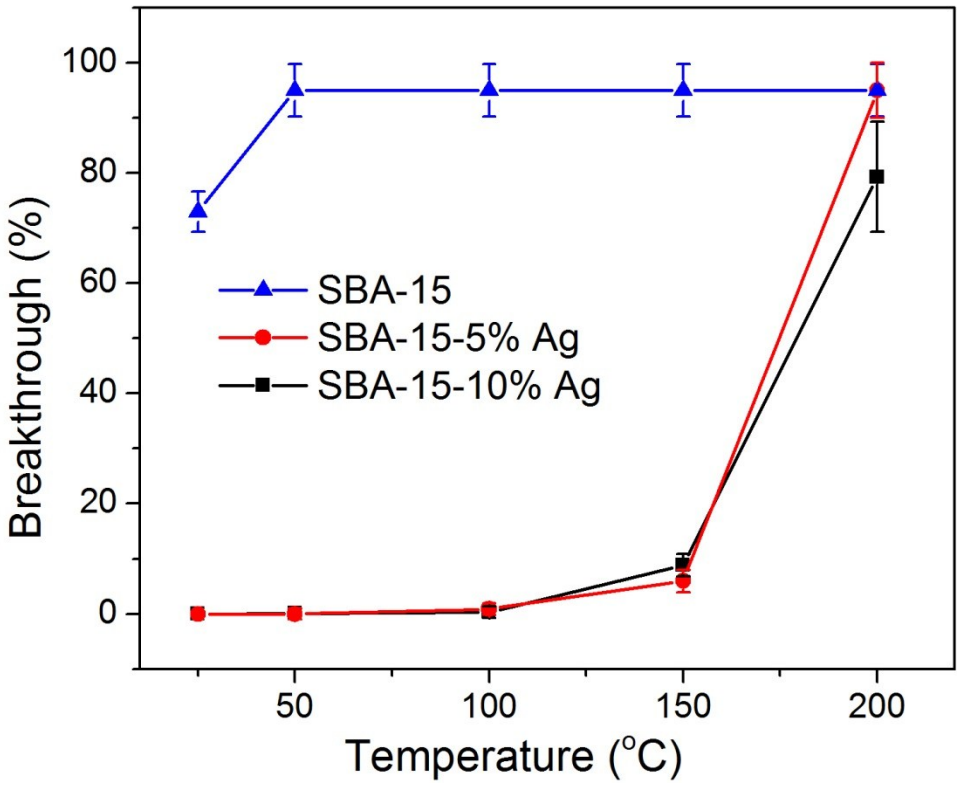

Figure 3.12 Mercury breakthrough results as a functional of capture temperature for the samples.

It should be noted that there is no significant difference in Hg^0 breakthrough for SBA-15-5% Ag and SBA-15-10% Ag under the range of 25 ºC~150 ºC, which could be due to the similar Ag loading amount according to the EDX results. The good performance of Hg^0 capture by SBA-15-Ag adsorbents from 25 ºC to 150 ºC in this study is comparable with the previous reports on MagZ-Ag[12] and Ag-CNT[9]. In addition, it could be observed from the TEM image (Fig. 3.13) that most of Ag NPs still keep their morphology even treated under 200 ºC for 2 h, indicating good stability of Ag NPs and the composite adsorbents under high temperature.

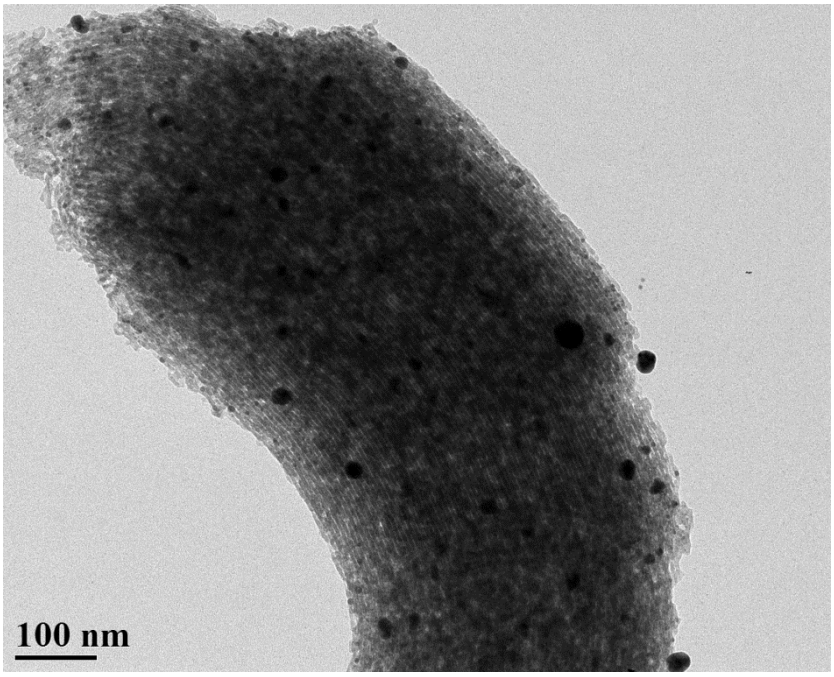

Figure 3.13 TEM image of SBA-15-10% Ag sample treated at 200 ºC for 2h.

The stability of SBA-15-10% Ag was further explored by regenerating the adsorbents at 350 ºC and cool to room temperature for reuse. Fig. 3.14 shows that SBA-15-10 % Ag could be reused for at least five successive adsorption-desorption cycles without any significant loss in capturing performance, indicating good stability of the adsorbents under heat treatment which is highly recoverable and provides great advantages in practical applications.

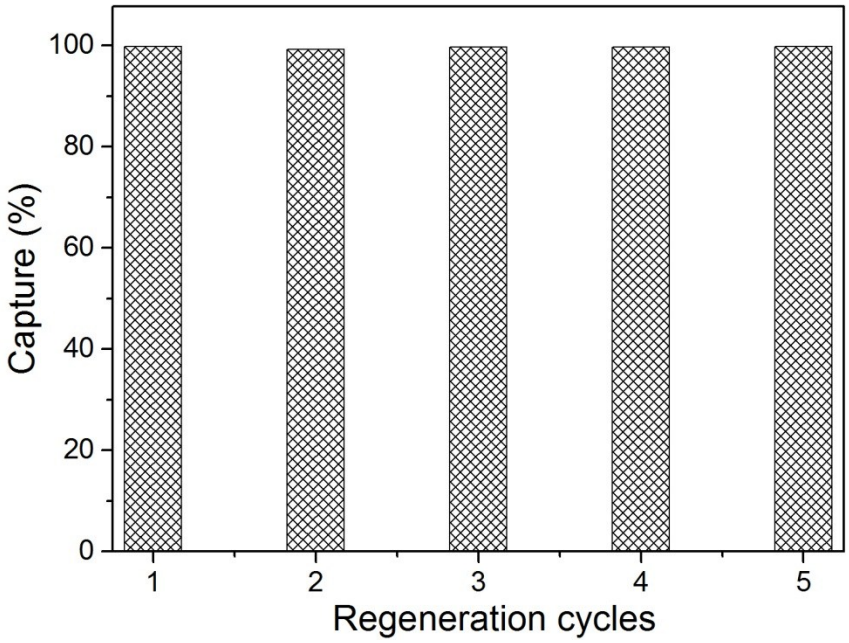

Figure 3.14 Mercury capture of SBA-15-10% Ag over five cycles of regeneration.

The adsorbent, SBA-15-10% Ag, was also exposed to the continuous flue gas flow to evaluate the mercury capture in practical flue gas environment. The components of the flue gases in this study are: 4% O_2, 12% CO_2. 400 ppm SO_2, 300 ppm NO and 77.6 μg/m^3 Hg^0 (concentration of Hg^0 in this study is two times higher than the reported value in industry[4]), and the concentration of Hg^0 in the flue gas was monitored by VM-3000 Mercury Vapor Detector (see Supporting Information). The Hg^0 capture capacity of SBA-15-10% Ag was tested by continuous flue gas exposure at the flow rate of 1.2 L/min for 1 h. Fig. 3.15 shows that the Hg^0 capture capacity of SBA-15-10% Ag was determined to be 60 μg/g at 150 ^oC, which is much higher than the Hg^0 capture capacity of Ag-/Au- beads (~3 μg/g)[9] and Ag-based zeolite (~13.3 μg/g)[4] in the previous reports. Additionally, as shown in Fig. 3.16, the net mercury capture in 5 min by 14 mg of SBA-15-10% Ag was about 5.7 ppm by weight (w/w, adsorbed

mercury/adsorbent) at 150 ºC, which is significantly higher than the previous studies by the Ag-based zeolite (40~140 ppb),[4, 11] indicating the fast Hg^0 capture by SBA-15-10 % Ag in the first 5 min. Therefore, our adsorbents demonstrate high Hg^0 capture capacity and fast Hg^0 capture rate, which clearly indicates that our Ag-loaded SBA-15 composites could be used as potential adsorbents for mercury emission control in coal-fired power plants.

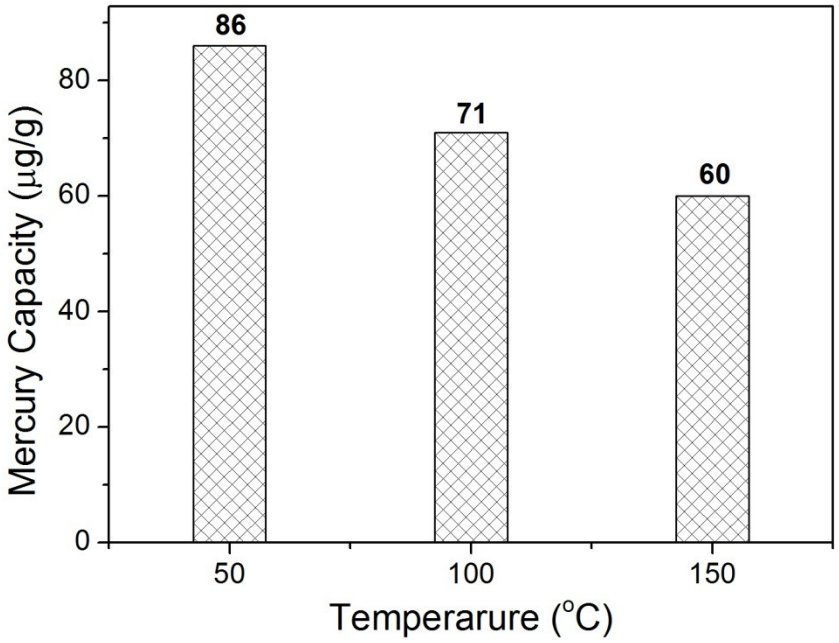

Figure 3.15 Mercury capture capacity by SBA-15-10% Ag at different temperatures measured by continuous flue gas exposure for 1 h.

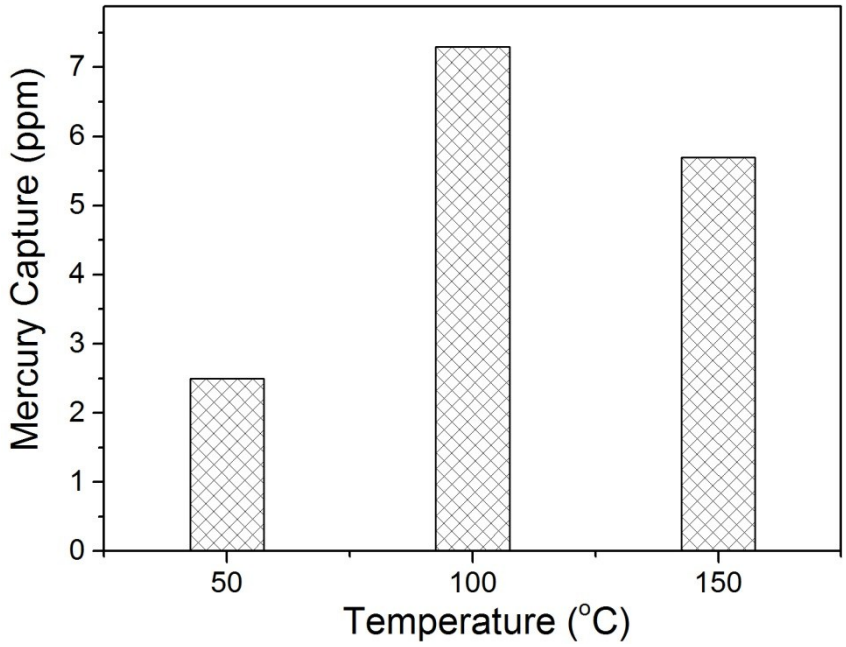

Figure 3.16 Mercury capture by SBA-15-10% Ag over a 5-min exposure in the flue gas under different temperature.

3.4 Conclusions

In summary, a facile wet chemical method was developed to synthesize SBA-15-Ag. Uniform distributions of spherical Ag NPs (8-9 nm) was deposited within the mesopores of SBA-15 according to the TEM and X-ray mapping results. The adsorbents are able to effectively capture Hg^0 up to 150 °C, around the temperature of practical flue gas in coal-fired power plants, as well as can be effectively recycled and reuse, which also show excellent thermal stability. Ag NPs within the mesopores of SBA-15-Ag are the active components for Hg^0 capture through the amalgamation mechanism, which is much more stable and effective than physical adsorption. The SBA-15-Ag samples also show great potential for Hg^0 removal in practical flue gases environment. Furthermore, the uniform dispersion of Ag NPs within SBA-15-Ag samples

provides important implications for other possible applications such as catalysis and antimicrobial agents.

3.5 References

(1) Bisson, T. M.; MacLean, L. C. W.; Hu, Y.; Xu, Z. Characterization of Mercury Binding onto a Novel Brominated Biomass Ash Sorbent by X-ray Absorption Spectroscopy. *Environ. Sci. Technol.* **2012,** *46,* 12186-12193.

(2) Liu, Y.; Bisson, T. M.; Yang, H.; Xu, Z. Recent developments in novel sorbents for flue gas clean up. *Fuel Process. Technol.* **2010,** *91,* 1175-1197.

(3) Hsi, H.-C.; Chen, S.; Rostam-Abadi, M.; Rood, M. J.; Richardson, C. F.; Carey, T. R.; Chang, R. Preparation and Evaluation of Coal-Derived Activated Carbons for Removal of Mercury Vapor from Simulated Coal Combustion Flue Gases. *Energy Fuels* **1998,** *12,* 1061-1070.

(4) Dong, J.; Xu, Z.; Kuznicki, S. M. Mercury Removal from Flue Gases by Novel Regenerable Magnetic Nanocomposite Sorbents. *Environ. Sci. Technol.* **2009,** *43,* 3266-3271.

(5) Galbreath, K. C.; Zygarlicke, C. J. Mercury transformations in coal combustion flue gas. *Fuel Process. Technol.* **2000,** *65–66,* 289-310.

(6) Guo, Y.; Yan, N.; Yang, S.; Liu, P.; Wang, J.; Qu, Z.; Jia, J. Conversion of elemental mercury with a novel membrane catalytic system at low temperature. *J Hazard Mater* **2012,** *213-214,* 62-70.

(7) Chang, J. C. S.; Ghorishi, S. B. Simulation and Evaluation of Elemental Mercury Concentration Increase in Flue Gas Across a Wet Scrubber. *Environ. Sci. Technol.* **2003,** *37,* 5763-5766.

(8) Yang, H.; Xu, Z.; Fan, M.; Bland, A. E.; Judkins, R. R. Adsorbents for capturing mercury in coal-fired boiler flue gas. *J. Hazard. Mater.* **2007,** *146,* 1-11.

(9) Luo, G.; Yao, H.; Xu, M.; Cui, X.; Chen, W.; Gupta, R.; Xu, Z. Carbon Nanotube-Silver Composite for Mercury Capture and Analysis. *Energy Fuels* **2009,** *24,* 419-426.

(10) Izquierdo, M. T.; Ballestero, D.; Juan, R.; García-Díez, E.; Rubio, B.; Ruiz, C.; Pino, M. R., Tail-end Hg capture on Au/carbon-monolith regenerable sorbents. *J. Hazard. Mater.* **2011**, *193*, 304-310.

(11) Liu, Y.; Kelly, D. J. A.; Yang, H.; Lin, C. C. H.; Kuznicki, S. M.; Xu, Z. Novel Regenerable Sorbent for Mercury Capture from Flue Gases of Coal-Fired Power Plant. *Environ. Sci. Technol.* **2008,** *42,* 6205-6210.

(12) Dong, J.; Xu, Z.; Kuznicki, S. M. Magnetic Multi-Functional Nano Composites for Environmental Applications. *Adv. Funct. Mater.* **2009,** *19,* 1268-1275.

(13) Han, J.; Fang, P.; Jiang, W.; Li, L.; Guo, R. Ag-Nanoparticle-Loaded Mesoporous Silica: Spontaneous Formation of Ag Nanoparticles and Mesoporous Silica SBA-15 by a One-Pot Strategy and Their Catalytic Applications. *Langmuir* **2012,** *28,* 4768-4775.

(14) Zheng, J.; Lin, H.; Zheng, X.; Duan, X.; Yuan, Y., Highly efficient mesostructured Ag/SBA-15 catalysts for the chemoselective synthesis of methyl glycolate by dimethyl oxalate hydrogenation. *Catal. Commun*. **2013**, *40*, 129-133.

(15) Zheng, J.; Lin, H.; Wang, Y.-n.; Zheng, X.; Duan, X.; Yuan, Y., Efficient low-temperature selective hydrogenation of esters on bimetallic Au–Ag/SBA-15 catalyst. *J. Catal.* **2013**, *297*, 110-118.

(16) Liu, J.; Zhao, Z.; Feng, H.; Cui, F. One-pot synthesis of Ag–Fe_3O_4 nanocomposites in the absence of additional reductant and its potent antibacterial properties. *J. Mater. Chem.* **2012,** *22,* 13891.

(17) Chi, Y.; Zhao, L.; Yuan, Q.; Li, Y.; Zhang, J.; Tu, J.; Li, N.; Li, X. Facile encapsulation of monodispersed silver nanoparticles in mesoporous compounds. *Chem. Eng. J.* **2012,** *195–196,* 254-260.

(18) Sureshkumar, M.; Lee, P.-N.; Lee, C.-K. Stepwise assembly of multimetallic nanoparticles via self-polymerized polydopamine. *J. Mater. Chem.* **2011,** *21,* 12316-12320.

(19) Naik, B.; Hazra, S.; Prasad, V. S.; Ghosh, N. N. Synthesis of Ag nanoparticles within the pores of SBA-15: An efficient catalyst for reduction of 4-nitrophenol. *Catal. Commun.* **2011,** *12,* 1104-1108.

(20) Sing, K. S. W.; Everett, D. H.; Haul, R. A. W.; Moscou, L.; Pierotti, R. A.; Rouquerol, J.; Siemieniewska, T. Reporting physisorption data for gas/solid systems with special reference to the determination of surface area and porosity. *Int. Union Pure Appl. Chem.* **1985,** *54,* 603-619.

(21) Zhu, W.; Han, Y.; An, L. Silver nanoparticles synthesized from mesoporous Ag/SBA-15 composites. *Microporous Mesoporous Mater.* **2005,** *80,* 221-226.

(22) Cejka, J.; Zilkova, N.; Rathousky, J.; Zukal, A. Nitrogen adsorption study of organised mesoporous alumina. *Phys. Chem. Chem. Phys.* **2001,** *3,* 5076-5081.

(23) Gürbüz, N.; Vural, S.; Yaşar, S.; Özdemir, I.; Seçkin, T. Pd functionalized MCM-41 catalysts for suzuki reactions. *J. Inorg. Organomet. Polym. Mater.* **2010,** *20,* 19-25.

(24) Guo, X.; Zheng, C.-G.; Xu, M. Characterization of Mercury Emissions from a Coal-Fired Power Plant. *Energy Fuels* **2007,** *21,* 898-902.

Chapter 4 Conclusions and Future Work

4.1 Conclusions

Due to the severe environmental crisis of air and water pollution that threatens the health of human being, new adsorbents based on magnetic-polymer composites and mesoporous materials were proposed to address this environmental issue. Two major work was contributed to this thesis: The preparation of novel musseled-inspired magnetic Fe_3O_4@PDA-Ag core-shell microspheres for dye removal (MB) and Ag-loaded mesoporous silica (SBA-15-Ag) for elemental mercury (Hg^0) capture. The major findings and conclusions of this work are shown as follows:

(1) A facile and *in situ* method was demonstrated to synthesize Fe_3O_4@PDA-Ag core-shell microspheres. This method combined with hydrothermal treatment and *in situ* reduction achieves the dense deposition of monodisperse Ag NPs on PDA surfaces. Ag NPs with uniform size were also loaded within the mesopores of SBA-15 by using siliver ammonia solution and sodium citrate.

(2) Two model organic dyes, MB and RhB, were successfully catalytically reduced by $NaBH_4$ and Fe_3O_4@PDA-Ag microspheres. The excellent catalytic performance of Fe_3O_4@PDA-Ag microspheres can be achieved under different pH values. The remarkable catalytic reduction performance can be attributed to the strong binding between the PDA layers and monodisperse Ag NPs.

(3) The as-prepared Fe_3O_4@PDA-Ag microspheres and SBA-15-Ag show good adsorption capability on MB and Hg^0 under different pHs and temperature, respectively. The good adsorption performance of two adsorbents, Fe_3O_4@PDA-Ag

and SBA-15-Ag, could be attributed to the electrostatic interactions between PDA layers and MB molecules and amalgamation of Ag-Hg, respectively.

(4) Good stability of Fe_3O_4@PDA-Ag microspheres and SBA-15-Ag is beneficial to the actual applications of the adsorbents in industry.

(5) Excellent reusability and fast regeneration of Fe_3O_4@PDA-Ag microspheres could be realized by using $NaBH_4$ via a unique desorption mechanism through the catalytic process. The superparamagnetism of Fe_3O_4@PDA-Ag makes them easily separated and reused by an external magnet.

(6) The convenient further modifications of organic functionl groups and metal NPs on Fe_3O_4@PDA and SBA-15 provide great potentials in many other applications.

4.2 Contributions to the original knowledge

Although the preparation of different adsorbents has been reported in many previous studies, few reports were found on the performance of adsorption and regeneration rate of the adsorbents. The first part of this work was proposed to design a new adsorbent (Fe_3O_4@PDA-Ag) with fast adsorption and regeneration rate. A novel desorption mechanism based on catalytic reduction by $NaBH_4$ was presented to accelerate the desorption rate of adsorbent, and the adsorbent can be separated and collected via an external magnetic field. Furthermore, the utilization of mussel-inspired polydopamine (PDA) layer presents a new way for *in situ* reduction of metal ions. In the second part of this work, SBA-15-Ag was applied to the removal of Hg^0 for the first time and it can adsorb Hg^0 up to 150 ^oC. In addition, it could also be used in the practical flue gas environment, which could be integrated with conventional pollution control facilities such as ESP and wet scrubber. Therefore, both of the adsorbents reveal great potentials in real industrial applications.

4.3 Suggestions on future work

In the present study, the adsorption capacity of the adsorbents is not exceptionally high due to the large size of Fe_3O_4 cores; therefore, porous, hierarchical structured Fe_3O_4 microspheres are suggested to replace the Fe_3O_4 cores in the current study due to the advantage that the high specific surface area and porous structure of Fe_3O_4 will facilitate the access of organic dyes to the adsorbents. The following work could be performed:

(1) The porous Fe_3O_4 microspheres could be easily synthesized by conventional wet chemical method. Some functionalization layers could also be coated on Fe_3O_4 cores.

(2) The morphology of the microspheres could be controlled by changing the experimental parameter and the characterization work could be finished.

(3) The dye removal performance of porous Fe_3O_4 microspheres on different organic dyes could be tested.

(4) Other type of environmental pollutions could also be tested by using this sample.

Bibliography

(1) Aksu, Z. Application of biosorption for the removal of organic pollutants: a review. *Process Biochem.* **2005,** *40,* 997-1026.

(2) Forgacs, E.; Cserháti, T.; Oros, G. Removal of synthetic dyes from wastewaters: a review. *Environ. Int.* **2004,** *30,* 953-971.

(3) Fu, Y.; Viraraghavan, T. Fungal decolorization of dye wastewaters: a review. *Bioresour. Technol.* **2001,** *79,* 251-262.

(4) Canada, I. NAICS 32513 Synthetic Dyes and Pigments. http://www.ic.gc.ca/eic/site/chemicals-chimiques.nsf/eng/bt01206.html#footnote1.

(5) Gupta, V. K.; Suhas Application of low-cost adsorbents for dye removal – A review. *J. Environ. Manage.* **2009,** *90,* 2313-2342.

(6) dos Santos, A. B.; Cervantes, F. J.; van Lier, J. B. Review paper on current technologies for decolourisation of textile wastewaters: Perspectives for anaerobic biotechnology. *Bioresour. Technol.* **2007,** *98,* 2369-2385.

(7) Xu, Y.; Lebrun, R. E.; Gallo, P.-J.; Blond, P. Treatment of Textile Dye Plant Effluent by Nanofiltration Membrane. *Sep. Sci. Technol.* **1999,** *34,* 2501-2519.

(8) Marmagne, O.; Coste, C. Color Removal From Textile Plant Effluents. *Am. Dyest. Rep.* **1996,** *85,* 15-20.

(9) Wu, J.-S.; Liu, C.-H.; Chu, K. H.; Suen, S.-Y. Removal of cationic dye methyl violet 2B from water by cation exchange membranes. *J. Membr. Sci.* **2008,** *309,* 239-245.

(10) Robinson, T.; McMullan, G.; Marchant, R.; Nigam, P. Remediation of dyes in textile effluent: a critical review on current treatment technologies with a proposed alternative. *Bioresour. Technol.* **2001,** *77,* 247-255.

(11) Shi, B.; Li, G.; Wang, D.; Feng, C.; Tang, H. Removal of direct dyes by coagulation: The performance of preformed polymeric aluminum species. *J. Hazard. Mater.* **2007,** *143,* 567-574.

(12) Zhou, Y.; Liang, Z.; Wang, Y. Decolorization and COD removal of secondary yeast wastewater effluents by coagulation using aluminum sulfate. *Desalination* **2008,** *225,* 301-311.

(13) Lee, J.-W.; Choi, S.-P.; Thiruvenkatachari, R.; Shim, W.-G.; Moon, H. Submerged microfiltration membrane coupled with alum coagulation/powdered activated carbon adsorption for complete decolorization of reactive dyes. *Water Res.* **2006,** *40,* 435-444.

(14) Slokar, Y. M.; Majcen Le Marechal, A. Methods of decoloration of textile wastewaters. *Dyes Pigm.* **1998,** *37,* 335-356.

(15) Kim, T.-H.; Park, C.; Yang, J.; Kim, S. Comparison of disperse and reactive dye removals by chemical coagulation and Fenton oxidation. *J. Hazard. Mater.* **2004,** *112,* 95-103.

(16) Dutta, K.; Mukhopadhyay, S.; Bhattacharjee, S.; Chaudhuri, B. Chemical oxidation of methylene blue using a Fenton-like reaction. *J. Hazard. Mater.* **2001,** *84,* 57-71.

(17) Solozhenko, E. G.; Soboleva, N. M.; Goncharuk, V. V. Decolourization of azodye solutions by Fenton's oxidation. *Water Res.* **1995,** *29,* 2206-2210.

(18) Cheng, M.; Ma, W.; Li, J.; Huang, Y.; Zhao, J.; Wen, Y. x.; Xu, Y. Visible-Light-Assisted Degradation of Dye Pollutants over Fe(III)-Loaded Resin in the Presence of H_2O_2 at Neutral pH Values. *Environ. Sci. Technol.* **2004,** *38,* 1569-1575.

(19) Soares, O. S. G. P.; Órfão, J. J. M.; Portela, D.; Vieira, A.; Pereira, M. F. R. Ozonation of textile effluents and dye solutions under continuous operation: Influence of operating parameters. *J. Hazard. Mater.* **2006,** *137,* 1664-1673.

(20) Wu, J.; Doan, H.; Upreti, S. Decolorization of aqueous textile reactive dye by ozone. *Chem. Eng. J.* **2008,** *142,* 156-160.

(21) Karaoğlu, M. H.; Uğurlu, M. Studies on UV/NaOCl/TiO_2/Sep photocatalysed degradation of Reactive Red 195. *J. Hazard. Mater.* **2010,** *174,* 864-871.

(22) Han, F.; Kambala, V. S. R.; Srinivasan, M.; Rajarathnam, D.; Naidu, R. Tailored titanium dioxide photocatalysts for the degradation of organic dyes in wastewater treatment: A review. *Appl. Catal., A* **2009,** *359,* 25-40.

(23) Khin, M. M.; Nair, A. S.; Babu, V. J.; Murugan, R.; Ramakrishna, S. A review on nanomaterials for environmental remediation. *Energy Environ. Sci.* **2012,** *5,* 8075-8109.

(24) Aguedach, A.; Brosillon, S.; Morvan, J.; Lhadi, E. K. Photocatalytic degradation of azo-dyes reactive black 5 and reactive yellow 145 in water over a newly deposited titanium dioxide. *Appl. Catal., B* **2005,** *57,* 55-62.

(25) Gupta, V. K.; Jain, R.; Mittal, A.; Mathur, M.; Sikarwar, S. Photochemical degradation of the hazardous dye Safranin-T using TiO_2 catalyst. *J. Colloid Interface Sci.* **2007,** *309,* 464-469.

(26) Pirkanniemi, K.; Sillanpää, M. Heterogeneous water phase catalysis as an environmental application: A review. *Chemosphere* **2002,** *48,* 1047-1060.

(27) Wu, W.; Xiao, X.; Zhang, S.; Ren, F.; Jiang, C. Facile method to synthesize magnetic iron oxides/TiO_2 hybrid nanoparticles and their photodegradation application of methylene blue. *Nanoscale Res. Lett.* **2011,** *6,* 533.

(28) Linley, S.; Leshuk, T.; Gu, F. X. Synthesis of Magnetic Rattle-Type Nanostructures for Use in Water Treatment. *ACS Appl. Mater. Interfaces* **2013,** *5,* 2540-2548.

(29) Gupta, V. K.; Jain, R.; Varshney, S. Electrochemical removal of the hazardous dye Reactofix Red 3 BFN from industrial effluents. *J. Colloid Interface Sci.* **2007,** *312,* 292-296.

(30) Oliveira, F.; Osugi, M.; Paschoal, F. M.; Profeti, D.; Olivi, P.; Zanoni, M. Electrochemical oxidation of an acid dye by active chlorine generated using $Ti/Sn_{(1-x)}Ir_x O_2$ electrodes. *J. Appl. Electrochem.* **2007,** *37,* 583-592.

(31) Liu, C.-H.; Wu, J.-S.; Chiu, H.-C.; Suen, S.-Y.; Chu, K. H. Removal of anionic reactive dyes from water using anion exchange membranes as adsorbers. *Water Res.* **2007,** *41,* 1491-1500.

(32) Raghu, S.; Ahmed Basha, C. Chemical or electrochemical techniques, followed by ion exchange, for recycle of textile dye wastewater. *J. Hazard. Mater.* **2007,** *149,* 324-330.

(33) Barragán, B. E.; Costa, C.; Carmen Márquez, M. Biodegradation of azo dyes by bacteria inoculated on solid media. *Dyes Pigm.* **2007,** *75,* 73-81.

(34) Pazarlioglu, N. K.; Urek, R. O.; Ergun, F. Biodecolourization of Direct Blue 15 by immobilized Phanerochaete chrysosporium. *Process Biochem.* **2005,** *40,* 1923-1929.

(35) van der Zee, F. P.; Bisschops, I. A. E.; Blanchard, V. G.; Bouwman, R. H. M.; Lettinga, G.; Field, J. A. The contribution of biotic and abiotic processes during azo dye reduction in anaerobic sludge. *Water Res.* **2003,** *37,* 3098-3109.

(36) Delée, W.; O'Neill, C.; Hawkes, F. R.; Pinheiro, H. M. Anaerobic treatment of textile effluents: A review. *J. Chem. Technol. Biotechnol.* **1998,** *73,* 323-335.

(37) Ali, I. New Generation Adsorbents for Water Treatment. *Chem. Rev.* **2012,** *112,* 5073-5091.

(38) Deliyanni, E. A.; Bakoyannakis, D. N.; Zouboulis, A. I.; Matis, K. A. Sorption of As(V) ions by akaganéite-type nanocrystals. *Chemosphere* **2003,** *50,* 155-163.

(39) Gao, Y.; Wahi, R.; Kan, A. T.; Falkner, J. C.; Colvin, V. L.; Tomson, M. B. Adsorption of Cadmium on Anatase Nanoparticles-Effect of Crystal Size and pH. *Langmuir* **2004,** *20,* 9585-9593.

(40) Ponder, S. M.; Darab, J. G.; Mallouk, T. E. Remediation of Cr(VI) and Pb(II) Aqueous Solutions Using Supported, Nanoscale Zero-valent Iron. *Environ. Sci. Technol.* **2000,** *34,* 2564-2569.

(41) Uheida, A.; Salazar-Alvarez, G.; Björkman, E.; Yu, Z.; Muhammed, M. Fe_3O_4 and γ-Fe_2O_3 nanoparticles for the adsorption of Co^{2+} from aqueous solution. *J. Colloid Interface Sci.* **2006,** *298,* 501-507.

(42) Chang, Y.-C.; Chen, D.-H. Preparation and adsorption properties of monodisperse chitosan-bound Fe_3O_4 magnetic nanoparticles for removal of Cu(II) ions. *J. Colloid Interface Sci.* **2005,** *283,* 446-451.

(43) Zhang, L.; Liu, N.; Yang, L.; Lin, Q. Sorption behavior of nano-TiO_2 for the removal of selenium ions from aqueous solution. *J. Hazard. Mater.* **2009,** *170,* 1197-1203.

(44) Gao, H.; Sun, Y.; Zhou, J.; Xu, R.; Duan, H. Mussel-Inspired Synthesis of Polydopamine-Functionalized Graphene Hydrogel as Reusable Adsorbents for Water Purification. *ACS Appl. Mater. Interfaces* **2012,** *5,* 425-432.

(45) Belessi, V.; Romanos, G.; Boukos, N.; Lambropoulou, D.; Trapalis, C. Removal of Reactive Red 195 from aqueous solutions by adsorption on the surface of TiO_2 nanoparticles. *J. Hazard. Mater.* **2009,** *170,* 836-844.

(46) Moussavi, G.; Mahmoudi, M. Removal of azo and anthraquinone reactive dyes from industrial wastewaters using MgO nanoparticles. *J. Hazard. Mater.* **2009,** *168,* 806-812.

(47) Yang, K.; Xing, B. Sorption of Phenanthrene by Humic Acid-Coated Nanosized TiO_2 and ZnO. *Environ. Sci. Technol.* **2009,** *43,* 1845-1851.

(48) Wang, P.; Shi, Q.; Shi, Y.; Clark, K. K.; Stucky, G. D.; Keller, A. A. Magnetic Permanently Confined Micelle Arrays for Treating Hydrophobic Organic Compound Contamination. *J. Am. Chem. Soc.* **2008,** *131,* 182-188.

(49) Tran, H.; Killops, K. L.; Campos, L. M. Advancements and challenges of patterning biomolecules with sub-50 nm features. *Soft Matter* **2013,** *9,* 6578-6586.

(50) Yola, M. L.; Eren, T.; Atar, N.; Wang, S. Adsorptive and photocatalytic removal of reactive dyes by silver nanoparticle-colemanite ore waste. *Chem. Eng. J.* **2014,** *242,* 333-340.

(51) Adak, A.; Bandyopadhyay, M.; Pal, A. Removal of crystal violet dye from wastewater by surfactant-modified alumina. *Sep. Purif. Technol.* **2005,** *44,* 139-144.

(52) Adak, A.; Bandyopadhyay, M.; Pal, A. Fixed bed column study for the removal of crystal violet (C. I. Basic Violet 3) dye from aquatic environment by surfactant-modified alumina. *Dyes Pigm.* **2006,** *69,* 245-251.

(53) Khajeh, M.; Laurent, S.; Dastafkan, K. Nanoadsorbents: Classification, Preparation, and Applications (with Emphasis on Aqueous Media). *Chem. Rev.* **2013,** *113,* 7728-7768.

(54) Lan, S.; Guo, N.; Liu, L.; Wu, X.; Li, L.; Gan, S. Facile preparation of hierarchical hollow structure gamma alumina and a study of its adsorption capacity. *Appl. Surf. Sci.* **2013,** *283,* 1032-1040.

(55) Tian, P.; Han, X.-y.; Ning, G.-l.; Fang, H.-x.; Ye, J.-w.; Gong, W.-t.; Lin, Y. Synthesis of Porous Hierarchical MgO and Its Superb Adsorption Properties. *ACS Appl. Mater. Interfaces* **2013,** *5,* 12411-12418.

(56) Ai, L.; Yue, H.; Jiang, J. Sacrificial template-directed synthesis of mesoporous manganese oxide architectures with superior performance for organic dye adsorption. *Nanoscale* **2012,** *4,* 5401-5408.

(57) Haldorai, Y.; Shim, J.-J. An efficient removal of methyl orange dye from aqueous solution by adsorption onto chitosan/MgO composite: A novel reusable adsorbent. *Appl. Surf. Sci.* **2014,** *292,* 447-453.

(58) Zhong, L. S.; Hu, J. S.; Liang, H. P.; Cao, A. M.; Song, W. G.; Wan, L. J. Self-Assembled 3D Flowerlike Iron Oxide Nanostructures and Their Application in Water Treatment. *Adv. Mater.* **2006,** *18,* 2426-2431.

(59) Zhu, D.; Zhang, J.; Song, J.; Wang, H.; Yu, Z.; Shen, Y.; Xie, A. Efficient one-pot synthesis of hierarchical flower-like α-Fe_2O_3 hollow spheres with excellent adsorption performance for water treatment. *Appl. Surf. Sci.* **2013,** *284,* 855-861.

(60) Wang, B.; Wu, H.; Yu, L.; Xu, R.; Lim, T.-T.; Lou, X. W. Template-free Formation of Uniform Urchin-like α-FeOOH Hollow Spheres with Superior Capability for Water Treatment. *Adv. Mater.* **2012,** *24,* 1111-1116.

(61) Luo, S.; Chai, F.; Wang, T.; Li, L.; Zhang, L.; Wang, C.; Su, Z. Flowerlike [gamma]-Fe_2O_3@NiO hierarchical core-shell nanostructures as superb capability and magnetically separable adsorbents for water treatment. *RSC Adv.* **2013,** *3,* 12671-12677.

(62) Copello, G. J.; Mebert, A. M.; Raineri, M.; Pesenti, M. P.; Diaz, L. E. Removal of dyes from water using chitosan hydrogel/SiO_2 and chitin hydrogel/SiO ⩵ hybrid materials obtained by the sol–gel method. *J. Hazard. Mater.* **2011,** *186,* 932-939.

(63) Yang, X.; Ni, L. Synthesis of hybrid hydrogel of poly(AM co DADMAC)/silica sol and removal of methyl orange from aqueous solutions. *Chem. Eng. J.* **2012,** *209,* 194-200.

(64) Nayab, S.; Farrukh, A.; Oluz, Z.; Tuncel, E.; Tariq, S. R.; Rahman, H. u.; Kirchhoff, K.; Duran, H.; Yameen, B. Design and Fabrication of Branched Polyamine Functionalized

Mesoporous Silica: An Efficient Absorbent for Water Remediation. *ACS Appl. Mater. Interfaces* **2014,** *6,* 4408-4417.

(65) Lee, D.-W.; Jin, M.-H.; Lee, C.-B.; Oh, D.; Ryi, S.-K.; Park, J.-S.; Bae, J.-S.; Lee, Y.-J.; Park, S.-J.; Choi, Y.-C. Facile synthesis of mesoporous silica and titania supraparticles by a meniscus templating route on a superhydrophobic surface and their application to adsorbents. *Nanoscale* **2014,** *6,* 3483-3487.

(66) Alpat, S. K.; Özbayrak, Ö.; Alpat, Ş.; Akçay, H. The adsorption kinetics and removal of cationic dye, Toluidine Blue O, from aqueous solution with Turkish zeolite. *J. Hazard. Mater.* **2008,** *151,* 213-220.

(67) Yu, Y.; Murthy, B. N.; Shapter, J. G.; Constantopoulos, K. T.; Voelcker, N. H.; Ellis, A. V. Benzene carboxylic acid derivatized graphene oxide nanosheets on natural zeolites as effective adsorbents for cationic dye removal. *J. Hazard. Mater.* **2013,** *260,* 330-338.

(68) Sapawe, N.; Jalil, A. A.; Triwahyono, S.; Shah, M. I. A.; Jusoh, R.; Salleh, N. F. M.; Hameed, B. H.; Karim, A. H. Cost-effective microwave rapid synthesis of zeolite NaA for removal of methylene blue. *Chem. Eng. J.* **2013,** *229,* 388-398.

(69) Carrott, P. J. M.; Carrott, M. M. L. R.; Roberts, R. A. Physical adsorption of gases by microporous carbons. *Colloids Surf.* **1991,** *58,* 385-400.

(70) Ding, L.; Zou, B.; Gao, W.; Liu, Q.; Wang, Z.; Guo, Y.; Wang, X.; Liu, Y. Adsorption of Rhodamine-B from aqueous solution using treated rice husk-based activated carbon. *Colloids Surf., A* **2014,** *446,* 1-7.

(71) Al-Degs, Y.; Khraisheh, M. A. M.; Allen, S. J.; Ahmad, M. N. A. Sorption behavior of cationic and anionic dyes from aqueous solution on different types of activated carbons. *Sep. Sci. Technol.* **2001,** *36,* 91-102.

(72) Inyang, M.; Gao, B.; Zimmerman, A.; Zhang, M.; Chen, H. Synthesis, characterization, and dye sorption ability of carbon nanotube–biochar nanocomposites. *Chem. Eng. J.* **2014,** *236,* 39-46.

(73) Kotal, M.; Bhowmick, A. K. Multifunctional Hybrid Materials Based on Carbon Nanotube Chemically Bonded to Reduced Graphene Oxide. *J. Phys. Chem. C* **2013,** *117,* 25865-25875.

(74) Cheng, J.; Chang, P. R.; Zheng, P.; Ma, X. Characterization of Magnetic Carbon Nanotube–Cyclodextrin Composite and Its Adsorption of Dye. *Ind. Eng. Chem. Res.* **2014,** *53,* 1415-1421.

(75) Tao, Y.; Kong, D.; Zhang, C.; Lv, W.; Wang, M.; Li, B.; Huang, Z.-H.; Kang, F.; Yang, Q.-H. Monolithic carbons with spheroidal and hierarchical pores produced by the linkage of functionalized graphene sheets. *Carbon* **2014,** *69,* 169-177.

(76) Zhang, Y.; Xu, S.; Luo, Y.; Pan, S.; Ding, H.; Li, G. Synthesis of mesoporous carbon capsules encapsulated with magnetite nanoparticles and their application in wastewater treatment. *J. Mater. Chem.* **2011,** *21,* 3664-3671.

(77) Ma, T.; Chang, P. R.; Zheng, P.; Zhao, F.; Ma, X. Fabrication of ultra-light graphene-based gels and their adsorption of methylene blue. *Chem. Eng. J.* **2014,** *240,* 595-600.

(78) Pavlish, J. H.; Sondreal, E. A.; Mann, M. D.; Olson, E. S.; Galbreath, K. C.; Laudal, D. L.; Benson, S. A. Status review of mercury control options for coal-fired power plants. *Fuel Process. Technol.* **2003,** *82,* 89-165.

(79) Presto, A. A.; Granite, E. J. Survey of Catalysts for Oxidation of Mercury in Flue Gas. *Environ. Sci. Technol.* **2006,** *40,* 5601-5609.

(80) Yang, H.; Xu, Z.; Fan, M.; Bland, A. E.; Judkins, R. R. Adsorbents for capturing mercury in coal-fired boiler flue gas. *J. Hazard. Mater.* **2007,** *146,* 1-11.

(81) Bisson, T. M.; Xu, Z.; Gupta, R.; Maham, Y.; Liu, Y.; Yang, H.; Clark, I.; Patel, M. Chemical–mechanical bromination of biomass ash for mercury removal from flue gases. *Fuel* **2013,** *108,* 54-59.

(82) Liu, Y.; Bisson, T. M.; Yang, H.; Xu, Z. Recent developments in novel sorbents for flue gas clean up. *Fuel Process. Technol.* **2010,** *91,* 1175-1197.

(83) Liu, S.-H.; Yan, N.-Q.; Liu, Z.-R.; Qu, Z.; Wang, H. P.; Chang, S.-G.; Miller, C. Using Bromine Gas To Enhance Mercury Removal from Flue Gas of Coal-Fired Power Plants. *Environ. Sci. Technol.* **2007,** *41,* 1405-1412.

(84) Bisson, T. M.; MacLean, L. C. W.; Hu, Y.; Xu, Z. Characterization of Mercury Binding onto a Novel Brominated Biomass Ash Sorbent by X-ray Absorption Spectroscopy. *Environ. Sci. Technol.* **2012,** *46,* 12186-12193.

(85) Liu, Y.; Kelly, D. J. A.; Yang, H.; Lin, C. C. H.; Kuznicki, S. M.; Xu, Z. Novel Regenerable Sorbent for Mercury Capture from Flue Gases of Coal-Fired Power Plant. *Environ. Sci. Technol.* **2008,** *42,* 6205-6210.

(86) Dong, J.; Xu, Z.; Kuznicki, S. M. Mercury Removal from Flue Gases by Novel Regenerable Magnetic Nanocomposite Sorbents. *Environ. Sci. Technol.* **2009,** *43,* 3266-3271.

(87) Sui, Z.; Meng, Q.; Zhang, X.; Ma, R.; Cao, B. Green synthesis of carbon nanotube-graphene hybrid aerogels and their use as versatile agents for water purification. *J. Mater. Chem.* **2012,** *22,* 8767-8771.

(88) Yu, K.; Yang, S.; Liu, C.; Chen, H.; Li, H.; Sun, C.; Boyd, S. A. Degradation of Organic Dyes via Bismuth Silver Oxide Initiated Direct Oxidation Coupled with Sodium Bismuthate Based Visible Light Photocatalysis. *Environ. Sci. Technol.* **2012,** *46,* 7318-7326.

(89) Tiwari, J. N.; Mahesh, K.; Le, N. H.; Kemp, K. C.; Timilsina, R.; Tiwari, R. N.; Kim, K. S. Reduced graphene oxide-based hydrogels for the efficient capture of dye pollutants from aqueous solutions. *Carbon* **2013,** *56,* 173-182.

(90) Zhu, T.; Chen, J. S.; Lou, X. W. Highly Efficient Removal of Organic Dyes from Waste Water Using Hierarchical NiO Spheres with High Surface Area. *J. Phys. Chem. C* **2012,** *116,* 6873-6878.

(91) Panizza, M.; Cerisola, G. Direct And Mediated Anodic Oxidation of Organic Pollutants. *Chem. Rev.* **2009,** *109,* 6541-6569.

(92) Wu, J.; Wang, J.; Li, H.; Du, Y.; Huang, K.; Liu, B. Designed synthesis of hematite-based nanosorbents for dye removal. *J. Mater. Chem. A* **2013,** *1,* 9837-9847.

(93) Meshko, V.; Markovska, L.; Mincheva, M.; Rodrigues, A. E. Adsorption of basic dyes on granular acivated carbon and natural zeolite. *Water Res.* **2001,** *35,* 3357-3366.

(94) Yan, Y.; Zhang, M.; Gong, K.; Su, L.; Guo, Z.; Mao, L. Adsorption of Methylene Blue Dye onto Carbon Nanotubes: A Route to an Electrochemically Functional Nanostructure and Its Layer-by-Layer Assembled Nanocomposite. *Chem. Mater.* **2005,** *17,* 3457-3463.

(95) Bandara, N.; Zeng, H.; Wu, J. Marine mussel adhesion: biochemistry, mechanisms, and biomimetics. *J. Adhes. Sci. Technol.* **2012,** *27,* 2139-2162.

(96) Zeng, H.; Hwang, D. S.; Israelachvili, J. N.; Waite, J. H. Strong reversible Fe^{3+}-mediated bridging between dopa-containing protein films in water. *Proc. Natl. Acad. Sci. U.S.A.* **2010,** *107,* 12850-12853.

(97) Liu, R.; Guo, Y.; Odusote, G.; Qu, F.; Priestley, R. D. Core–Shell Fe_3O_4 Polydopamine Nanoparticles Serve Multipurpose as Drug Carrier, Catalyst Support and Carbon Adsorbent. *ACS Appl. Mater. Interfaces* **2013,** *5,* 9167-9171.

(98) Lee, H.; Dellatore, S. M.; Miller, W. M.; Messersmith, P. B. Mussel-inspired surface chemistry for multifunctional coatings. *Science* **2007,** *318,* 426-430.

(99) Zhang, M.; He, X.; Chen, L.; Zhang, Y. Preparation of IDA-Cu functionalized core-satellite Fe_3O_4/polydopamine/Au magnetic nanocomposites and their application for depletion of abundant protein in bovine blood. *J. Mater. Chem.* **2010,** *20,* 10696-10704.

(100) Jeon, E. K.; Seo, E.; Lee, E.; Lee, W.; Um, M.-K.; Kim, B.-S. Mussel-inspired green synthesis of silver nanoparticles on graphene oxide nanosheets for enhanced catalytic applications. *Chem. Commun.* **2013,** *49,* 3392-3394.

(101) Guo, L.; Liu, Q.; Li, G.; Shi, J.; Liu, J.; Wang, T.; Jiang, G. A mussel-inspired polydopamine coating as a versatile platform for the in situ synthesis of graphene-based nanocomposites. *Nanoscale* **2012,** *4,* 5864-5867.

(102) Sureshkumar, M.; Lee, P.-N.; Lee, C.-K. Stepwise assembly of multimetallic nanoparticles via self-polymerized polydopamine. *J. Mater. Chem.* **2011,** *21,* 12316-12320.

(103) Zheng, Y.; Wang, A. Ag nanoparticle-entrapped hydrogel as promising material for catalytic reduction of organic dyes. *J. Mater. Chem.* **2012,** *22,* 16552-16559.

(104) Nadagouda, M. N.; Desai, I.; Cruz, C.; Yang, D. J. Novel Pd based catalyst for the removal of organic and emerging contaminants. *RSC Adv.* **2012,** *2,* 7540-7548.

(105) Liu, J.; Sun, Z.; Deng, Y.; Zou, Y.; Li, C.; Guo, X.; Xiong, L.; Gao, Y.; Li, F.; Zhao, D. Highly water-dispersible biocompatible magnetite particles with low cytotoxicity stabilized by citrate groups. *Angew. Chem. Int. Ed.* **2009,** *48,* 5875-5879.

(106) Guo, X.; Zhang, Q.; Sun, Y.; Zhao, Q.; Yang, J. Lateral Etching of Core–Shell Au@Metal Nanorods to Metal-Tipped Au Nanorods with Improved Catalytic Activity. *ACS Nano* **2012,** *6,* 1165-1175.

(107) Patel, A. C.; Li, S.; Wang, C.; Zhang, W.; Wei, Y. Electrospinning of Porous Silica Nanofibers Containing Silver Nanoparticles for Catalytic Applications. *Chem. Mater.* **2007,** *19,* 1231-1238.

(108) Chi, Y.; Zhao, L.; Yuan, Q.; Li, Y.; Zhang, J.; Tu, J.; Li, N.; Li, X. Facile encapsulation of monodispersed silver nanoparticles in mesoporous compounds. *Chem. Eng. J.* **2012,** *195–196,* 254-260.

(109) Zhu, M.; Wang, C.; Meng, D.; Diao, G. In situ synthesis of silver nanostructures on magnetic Fe_3O_4@C core–shell nanocomposites and their application in catalytic reduction reactions. *J. Mater. Chem. A* **2013,** *1,* 2118-2125.

(110) Zhang, M.; Zheng, J.; Zheng, Y.; Xu, J.; He, X.; Chen, L.; Fang, Q. Preparation, characterization and catalytic activity of core–satellite Au/Pdop/SiO_2/Fe_3O_4 magnetic nanocomposites. *RSC Adv.* **2013,** *3,* 13818-13824.

(111) Ryu, J.; Ku, S. H.; Lee, H.; Park, C. B. Mussel-Inspired Polydopamine Coating as a Universal Route to Hydroxyapatite Crystallization. *Adv. Funct. Mater.* **2010,** *20,* 2132-2139.

(112) Impert, O.; Katafias, A.; Kita, P.; Mills, A.; Pietkiewicz-Graczyk, A.; Wrzeszcz, G. Kinetics and mechanism of a fast leuco-Methylene Blue oxidation by copper(ii)-halide species in acidic aqueous media. *Dalton Trans.* **2003,** 348-353.

(113) Jiang, Y.; Zhang, S.; Ji, Q.; Zhang, J.; Zhang, Z.; Wang, Z. Ultrathin Cu_7S_4 nanosheets-constructed hierarchical hollow cubic cages: one-step synthesis based on Kirkendall effect and catalysis property. *J. Mater. Chem. A* **2014,** *2,* 4574-4579.

(114) Ray, C.; Dutta, S.; Sarkar, S.; Sahoo, R.; Roy, A.; Pal, T. A facile synthesis of 1D nano structured selenium and Au decorated nano selenium: catalysts for the clock reaction. *RSC Adv.* **2013,** *3,* 24313-24320.

(115) Jana, N. R.; Sau, T. K.; Pal, T. Growing Small Silver Particle as Redox Catalyst. *J. Phys. Chem. B* **1998,** *103,* 115-121.

(116) Mallick, K.; Witcomb, M.; Scurrell, M. Silver nanoparticle catalysed redox reaction: An electron relay effect. *Mater. Chem. Phys.* **2006,** *97,* 283-287.

(117) Jiang, Z.-J.; Liu, C.-Y.; Sun, L.-W. Catalytic Properties of Silver Nanoparticles Supported on Silica Spheres. *J. Phys. Chem. B* **2005,** *109,* 1730-1735.

(118) Hsi, H.-C.; Chen, S.; Rostam-Abadi, M.; Rood, M. J.; Richardson, C. F.; Carey, T. R.; Chang, R. Preparation and Evaluation of Coal-Derived Activated Carbons for Removal of Mercury Vapor from Simulated Coal Combustion Flue Gases. *Energy Fuels* **1998,** *12,* 1061-1070.

(119) Galbreath, K. C.; Zygarlicke, C. J. Mercury transformations in coal combustion flue gas. *Fuel Process. Technol.* **2000,** *65–66,* 289-310.

(120) Guo, Y.; Yan, N.; Yang, S.; Liu, P.; Wang, J.; Qu, Z.; Jia, J. Conversion of elemental mercury with a novel membrane catalytic system at low temperature. *J Hazard Mater* **2012,** *213-214,* 62-70.

(121) Chang, J. C. S.; Ghorishi, S. B. Simulation and Evaluation of Elemental Mercury Concentration Increase in Flue Gas Across a Wet Scrubber. *Environ. Sci. Technol.* **2003,** *37,* 5763-5766.

(122) Luo, G.; Yao, H.; Xu, M.; Cui, X.; Chen, W.; Gupta, R.; Xu, Z. Carbon Nanotube-Silver Composite for Mercury Capture and Analysis. *Energy Fuels* **2009,** *24,* 419-426.

(123) Izquierdo, M. T.; Ballestero, D.; Juan, R.; García-Díez, E.; Rubio, B.; Ruiz, C.; Pino, M. R., Tail-end Hg capture on Au/carbon-monolith regenerable sorbents. *J. Hazard. Mater.* **2011**, *193*, 304-310.

(124) Dong, J.; Xu, Z.; Kuznicki, S. M. Magnetic Multi-Functional Nano Composites for Environmental Applications. *Adv. Funct. Mater.* **2009,** *19,* 1268-1275.

(125) Han, J.; Fang, P.; Jiang, W.; Li, L.; Guo, R. Ag-Nanoparticle-Loaded Mesoporous Silica: Spontaneous Formation of Ag Nanoparticles and Mesoporous Silica SBA-15 by a One-Pot Strategy and Their Catalytic Applications. *Langmuir* **2012,** *28,* 4768-4775.

(126) Zheng, J.; Lin, H.; Zheng, X.; Duan, X.; Yuan, Y., Highly efficient mesostructured Ag/SBA-15 catalysts for the chemoselective synthesis of methyl glycolate by dimethyl oxalate hydrogenation. *Catal. Commun.* **2013**, *40*, 129-133.

(127) Zheng, J.; Lin, H.; Wang, Y.-n.; Zheng, X.; Duan, X.; Yuan, Y. Efficient low-temperature selective hydrogenation of esters on bimetallic Au–Ag/SBA-15 catalyst. *J. Catal.* **2013,** *297,* 110-118.

(128) Liu, J.; Zhao, Z.; Feng, H.; Cui, F. One-pot synthesis of Ag–Fe_3O_4 nanocomposites in the absence of additional reductant and its potent antibacterial properties. *J. Mater. Chem.* **2012,** *22,* 13891.

(129) Naik, B.; Hazra, S.; Prasad, V. S.; Ghosh, N. N. Synthesis of Ag nanoparticles within the pores of SBA-15: An efficient catalyst for reduction of 4-nitrophenol. *Catal. Commun.* **2011,** *12,* 1104-1108.

(130) Sing, K. S. W.; Everett, D. H.; Haul, R. A. W.; Moscou, L.; Pierotti, R. A.; Rouquerol, J.; Siemieniewska, T. Reporting physisorption data for gas/solid systems with special reference to the determination of surface area and porosity. *Int. Union Pure Appl. Chem.* **1985,** *54,* 603-619.

(131) Zhu, W.; Han, Y.; An, L. Silver nanoparticles synthesized from mesoporous Ag/SBA-15 composites. *Microporous Mesoporous Mater.* **2005,** *80,* 221-226.

(132) Cejka, J.; Zilkova, N.; Rathousky, J.; Zukal, A. Nitrogen adsorption study of organised mesoporous alumina. *Phys. Chem. Chem. Phys.* **2001,** *3,* 5076-5081.

(133) Gürbüz, N.; Vural, S.; Yaşar, S.; Özdemir, I.; Seçkin, T. Pd functionalized MCM-41 catalysts for suzuki reactions. *J. Inorg. Organomet. Polym. Mater.* **2010,** *20,* 19-25.

(134) Guo, X.; Zheng, C.-G.; Xu, M. Characterization of Mercury Emissions from a Coal-Fired Power Plant. *Energy Fuels* **2007,** *21,* 898-902.